

รายงานวิจัยฉบับสมบูรณ์

โครงการ: การแก้ปัญหาย้อนกลับสำหรับข้อมูล
Magnetotelluric ในสามมิติบน Data Space โดยใช้วิธี
Conjugate Gradient
(Data Space Conjugate Gradient Inversion for 3-D
Magnetotelluric Data)

โดย ผศ. ดร. วีระชัย สิริพันธ์วราภรณ์ ภาควิชาฟิสิกส์ คณะวิทยาศาสตร์ มหาวิทยาลัยมหิดล

สิงหาคม 2550

รายงานวิจัยฉบับสมบูรณ์

โครงการ: การแก้ปัญหาย้อนกลับสำหรับข้อมูล
Magnetotelluric ในสามมิติบน Data Space โดยใช้วิธี
Conjugate Gradient
(Data Space Conjugate Gradient Inversion for 3-D
Magnetotelluric Data)

ผศ. ดร. วีระชัย สิริพันธ์วราภรณ์ ภาควิชาฟิสิกส์ คณะวิทยาศาสตร์ มหาวิทยาลัยมหิดล

สนับสนุนโดยสำนักงานกองทุนสนับสนุนการวิจัย

(ความเห็นในรายงานนี้เป็นของผู้วิจัย สกว. ไม่จำเป็นต้องเห็นด้วยเสมอไป)

1

บทคัดย่อ

การแก้ปัญหาย้อนกลับ (inverse problem) ของข้อมูล Magnetotelluric (MT) ใน data space ช่วยให้ ระบบของสมการที่ต้องแก้ลดลงจากเดิมที่มีขนาด M x M ที่ทำใน model space เป็น N x N ใน data space เมื่อ M คือจำนวนพารามิเตอร์ของแบบจำลอง และ N คือจำนวนพารามิเตอร์ของข้อมูล ซึ่งส่วน ใหญ่แล้ว N จะมีค่าน้อยกว่า M มากๆ การแก้ปัญหาย้อนกลับใน data space นี้สามารถทำให้การ แก้ปัญหาย้อนกลับของข้อมูล MT ในสามมิติ (3-D) เป็นไปได้บนเครื่องคอมพิวเตอร์ธรรมดา (Siripunvaraporn et al., 2005) อย่างไรก็ตาม วิธีนี้ก็ยังมีความจำเป็นที่ต้องเก็บข้อมูล sensitivity matrix (**J**) ที่มีขนาด *N x M* ลงในหน่วยความจำของคอมพิวเตอร์ซึ่งทำให้เกิดข้อจำกัดของการนำไปใช้ ในที่นี้ เราได้ประยุกต์เอาวิธี conjugate gradient มาใช้ในการแก้ระบบของสมการใน data space ด้วย วิธีนี้เมตริก **J** จะไม่ถูกสร้างขึ้นมาทำให้ไม่ต้องเก็บข้อมูลลงในหน่วยความจำ สิ่งที่เราทำคือเรา คำนวณหาผลคูณของเมตริก J กับเวกเตอร์ใดๆ โดยการแก้ปัญหาไปข้างหน้า (forward problem) หนึ่ง ครั้งเท่านั้นเอง เพื่อประเมินประสิทธิภาพของการคำนวณระหว่างวิธีใหม่ซึ่งก็คือ data space conjugate gradient (DCG) สำหรับทั้ง สองมิติ (2-D) และ 3-D ของข้อมูล MT กับวิธีเดิมซึ่งก็คือ data space Occam's method (DASOCC) เราใช้วิธีนับจำนวนครั้งของการแก้ปัญหาไปข้างหน้า จากการทดลองกับ ข้อมูลจำลอง เราพบว่าแม้ว่า DCG จะช่วยลดปริมาณการใช้หน่วยความจำของเครื่องคอมพิวเตอร์ลงได้ อย่างมาก แต่กลายเป็นว่ามันต้องใช้จำนวนครั้งของการแก้ปัญหาไปข้างหน้าที่มากกว่า นั่นหมายถึง เวลาที่ใช้ในการคำนวณจะมากกว่าวิธีอย่าง DASOCC ซึ่งใช้หน่วยความจำมาก ดังนั้นผลสรุป คือ มันมี trade-off ระหว่างหน่วยความจำกับเวลาที่ใช้ในการคำนวณ และการจะเลือกว่าจะใช้วิธี DASOCC หรือ DCG ก็ขึ้นอยู่กับผู้ใช้และข้อมูลที่นำไปใช้

Abstract

A data space approach to magnetotelluric (MT) inversion reduces the size of the system of equations that must be solved from $M \times M$, as required for a model space approach, to only N \times N, where M is the number of model parameter and N is the number of data. This reduction makes 3-D MT inversion on a personal computer possible for modest values of M and N (Siripunvaraporn et al. 2005). However the need to store the $N \times M$ sensitivity matrix **J** remains a serious limitation. Here, we consider application of conjugate gradient (CG) methods to solve the system of data space Gauss-Newton equations. With this approach J is not explicitly formed and stored, but instead the product of J with an arbitrary vector is computed by solving one forward problem. To assess the computational efficiency we test our data space conjugate gradient (DCG) algorithm for the 2-D and 3-D MT inverse problem, and compare the results with those from the data space Occam's (DASOCC for 2-D; WSINV3DMT for 3-D) inversion by counting the number of forward modeling calls. Experiments with synthetic data show that although DCG requires significantly less memory, it generally requires more forward problem solutions than a scheme such as DASOCC and WSINV3DMT, which is based on a full computation of J. We therefore conclude that there is a trade-off between memory used and cpu run time, and the choice between DASOCC (WSINV3DMT) and DCG will depend on the application and users.

กิตติกรรมประกาศ

ข้าพเจ้าขอขอบคุณ สกว. ที่ให้โอกาสข้าพเจ้าได้ทำวิจัยในเรื่องที่ข้าพเจ้าถนัดมาเป็นเวลา ต่อเนื่อง เพราะทุนวิจัยนี้ทำให้ข้าพเจ้าไม่ต้องไปรับงานสอนพิเศษ ทำให้ข้าพเจ้าสามารถใช้เวลาเต็มที่ใน การทำงานวิจัยให้ได้มีคุณภาพเป็นที่ยอมรับในกลุ่มคนทำวิจัยเรื่องเดียวกัน ทุนวิจัยนี้ยังสามารถทำให้ ข้าพเจ้าได้ใช้เวลาเต็มที่ในการเตรียมบุคลากรและนักศึกษาในการทำวิจัยในอนาคตเพื่อเป็นประโยชน์ต่อ ประเทศ

นอกจากนี้ ข้าพเจ้าต้องขอขอบคุณ Prof. Dr. Gary Egbert ที่ยอมสละเวลาส่วนตัวในการ discuss งานวิจัยต่างๆ รวมทั้ง review manuscripts พร้อมทั้งวางแผนในเรื่องของ future research and collaboration พร้อมทั้งยอมให้ข้าพเจ้าใช้คอมพิวเตอร์สมรรถนะสูงอีกด้วย รวมทั้ง Associate Professor Makoto Uyeshima และ Professor Hisashi Utada จาก Earthquake Research Institute (ERI), University of Tokyo ผู้คอยสนับสนุนในเรื่องต่างๆ รวมทั้งยอมให้ข้าพเจ้าใช้คอมพิวเตอร์สมรถ นะสูงของ ERI อีกด้วย สำหรับอีกคนที่คอยกระตุ้นและชักจูงข้าพเจ้าเข้ามาในวงการวิจัยหลังจากจบ ปริญญาเอก คือ ศาสตราจารย์ ดร. ยงค์วิมล เลณบุรี ปราศจากท่าน ข้าพเจ้าก็คงหลงไปกับงานวิชาการ และบริการวิชาการต่างๆ รวมทั้งสอนพิเศษ ซึ่งอาจทำให้ข้าพเจ้าละทิ้งและไม่สนใจงานวิจัยเลยก็ได้ นอกจากนี้แล้วความสำเร็จของท่านในเรื่องต่างๆ ยังได้เป็นแบบอย่างให้ข้าพเจ้าได้เดินตามอีกด้วย

ข้าพเจ้าต้องขอขอบคุณบุคลากร คณาจารย์ และนักศึกษาของภาควิชาฟิสิกส์ คณะวิทยาศาสตร์ มหาวิทยาลัยมหิดลทุกท่าน ที่คอยสนับสนุนการทำงานของข้าพเจ้าให้บรรลุถึงเป้าหมายได้อย่างสมบูรณ์ นอกจากนี้แล้วยังมีเพื่อนๆ จากภาควิชาอื่นๆ อีกด้วย รวมทั้งท่านคณบดีและทีมงาน คณะวิทยาศาสตร์ มหาวิทยาลัยมหิดล ที่คอยกระตุ้นและสนับสนุนงานวิจัยมาตลอด

อีกกลุ่มหนึ่งที่ข้าพเจ้าจะไม่ขอบคุณไม่ได้ คือ บุคลากรของสกว. ฝ่ายวิชาการที่เป็นมิตรอันดี และคอยช่วยเหลือในเรื่องต่างๆ เป็นอย่างดี โดยเฉพาะคุณบุ๋ม ชลนภา

สุดท้ายนี้ ข้าพเจ้าต้องขอขอบคุณบุคคลที่คอยเป็นกำลังใจ เข้าใจในทุกสิ่งทุกอย่าง บุคคลเหล่านี้ คือคุณแม่และครอบครัวของข้าพเจ้า ขอบคุณมากครับ

ผศ. ดร. วีระชัย สิริพันธ์วราภรณ์

เนื้อหางานวิจัย

บทน้ำ

การแก้ปัญหาย้อนกลับ (Inversion) ในทางธรณีฟิสิกส์ (Geophysics) คือกระบวนการที่จะได้มาซึ่ง แบบจำลอง (model) ของโลกที่สามารถอธิบายถึงข้อมูลที่ได้มาจากการเก็บที่บริเวณพื้นผิวของโลก ข้อมูลในทางธรณีฟิสิกส์นั้นเป็นไปได้ในหลายรูปแบบ ไม่ว่าจะเป็นคลื่นแผ่นดินไหว คลื่นแม่เหล็กไฟฟ้า แรงโน้มถ่วงของโลก ความร้อนใต้พื้นดิน หรือว่าสนามแม่เหล็ก ข้อมูลเหล่านี้มีประโยชน์อย่างมากในการ บ่งบอกว่าใต้พื้นโลกของเรานั้นประกอบไปด้วยอะไรบ้าง และยังมีประโยชน์ทั้งทางตรงและทางอ้อมต่อ เศรษฐกิจและสิ่งแวดล้อมของประเทศ

ในโครงการนี้เราเน้นข้อมูลทางธรณีฟิสิกส์ที่เรียกว่า Magnetotelluric data ซึ่งเป็นข้อมูลที่ได้มา จากการวัดสนามแม่เหล็กและสนามไฟฟ้าที่บริเวณพื้นผิวของโลกเรา อัตราส่วนของสนามแม่เหล็กและสนามไฟฟ้าที่บริเวณพื้นผิวของโลกเรา อัตราส่วนของสนามแม่เหล็กและสนามไฟฟ้าสามารถนำมาใช้เป็นตัวบ่งบอกถึงความต้านทานไฟฟ้า (electrical resistivity) หรือความสามารถในการนำไฟฟ้า (electrical conductivity) ภายใต้พื้นโลกที่ความลึกต่างๆ ได้ เราสามารถนำข้อมูล electrical resistivity นี้ไปใช้ในการอธิบายโครงสร้างของโลกเพื่ออธิบายการเกิดแผ่นดินไหว (Unsworth et al., 2000; Siripunvaraporn et al., 1998) การศึกษาเทคโทนิคของพื้นที่ (Jones, 1992) หรือใช้ในการสำรวจหาทรัพยากรธรรมชาติ (Tuncer et al., 2006; Orange, 1989; Vozoff, 1972 และอื่นๆ)

ข้อมูลที่ได้มาจากการสำรวจจะเป็นข้อมูลดิบที่ต้องนำมาผ่าน data processing เพื่อให้ได้ apparent resistivity และ phase หรือ impedance tensor ซึ่งเป็นฟังก์ชันของความถี่หรือว่าคาบ เพื่อ นำไปใช้ในการตีความหมายต่อไป การตีความหมายจากข้อมูลโดยตรงนั้นเป็นไปได้ยาก เนื่องจากข้อมูล ที่ได้มาไม่ได้เป็นฟังก์ชันของความลึก ดังนั้น inversion คือกระบวนการที่นำเอาค่า apparent resistivity และ phase ที่เป็นฟังก์ชันของความถี่หรือคาบ ไปแปลงให้เป็นค่า electrical resistivity กับความลึก โดย ผ่านกระบวนการทางคณิตศาสตร์ที่สลับซับซ้อน

ในอดีต การตีความหมายมักจำกัดอยู่ในหนึ่งมิติ เนื่องจากข้อจำกัดของคอมพิวเตอร์เทคโนโลยี และซอฟท์แวร์ และความง่ายในการประยุกต์ใช้ ทั้งทฤษฎี และวิธีการแก้ปัญหาย้อนกลับ ต่อมาเมื่อ คอมพิวเตอร์เทคโนโลยีได้กล่าวหน้าขึ้นมาก การพัฒนา 2-D และ 3-D inversion codes ได้ก้าวหน้าขึ้นมาอย่างรวดเร็ว (see Siripunvaraporn et al., 2004, 2005; Siripunvaraporn and Egbert, 2000) โดย Siripunvaraporn et al. (2005) เป็นคนแรกที่ release 3-D code ที่เรียกว่า WSINV3DMT ที่ สามารถทำงานได้บนเครื่อง PC ทั่วไปสู่สาธารณะ เพื่อให้มีการนำไปใช้ในการตีความหมายข้อมูลเพื่อ เป็นประโยชน์ต่อโลกที่เราอาศัยอยู่ ซึ่งปัจจุบันนี้มีสมาชิกมากกว่า 20 ประเทศที่ใช้โปรแกรมนี้อยู่ ดัง รายละเอียด (http://mucc.mahidol.ac.th/~scwsp/wsinv3dmt/)

อย่างไรก็ตาม แม้ว่า WSINV3DMT จะทำงานได้บนเครื่อง PC ทั่วไป แต่ก็ยังมีปัญหาหลักๆ อยู่ คือ การใช้หน่วยความจำของเครื่องคอมพิวเตอร์ในปริมาณมาก ดังนั้นการทำงานกับข้อมูลใหญ่ๆ หรือ แบบจำลองใหญ่ๆ จึงเป็นไปไม่ได้ วิธีแก้ไขคือการสั่งให้โปรแกรมทำงานกับเครื่องคอมพิวเตอร์สมรรถนะ สูงเพียงอย่างเดียวเท่านั้น ซึ่งเครื่องคอมพิวเตอร์สมรรถนะสูงเหล่านี้มีราคาที่แพงมาก

ดังนั้นในโครงการนี้ เราต้องการแก้ไขข้อบกพร่องนี้ คือ การลดปริมาณหน่วยความจำที่ใช้ให้ น้อยที่สุดเพื่อให้ทำงานได้บนเครื่อง PC ทั่วไป แม้ว่าจะทำงานกับข้อมูลที่มีขนาดใหญ่ก็ตาม วิธีหนึ่งที่ เราเสนอก็คือ การแก้ระบบสมการด้วยวิธี conjugate gradient (CG) แทนที่จะแก้แบบโดยตรง คือใช้ Cholesky decomposition เหมือนที่ทำใน WSINV3DMT การใช้วิธี CG มาช่วยจำทำให้เราไม่ต้องเก็บ sensitivity matrix (J) ซึ่งมีขนาดใหญ่ในหน่วยความจำของคอมพิวเตอร์ซึ่งจะทำให้เราลดปริมาณการใช้ หน่วยความจำได้เป็นอย่างมาก ซึ่งโปรแกรมใหม่นี้เราจะเรียกว่า data space conjugate gradient method (DCG) ขั้นตอนในการพัฒนาโปรแกรมนี้ประกอบไปด้วยหลายขั้นตอน เราจะอธิบายขั้นตอน ต่างๆเหล่านี้ในตอนต่อไป รวมทั้งแสดงให้เห็นการเปรียบเทียบของวิธีนี้ (DCG) กับ WSINV3DMT

Overview of Inversion Method

จุดประสงค์ในการทำ inversion คือการหาแบบจำลอง (m) ที่สามารถให้ค่า model responses **F[m]** ที่ fit ข้อมูล **d** ที่มีทั้งหมด *N* ค่าได้ หรือสามารถเขียนได้ดังนี้

$$\chi^{2}_{d} = (\mathbf{d} - \mathbf{F}[\mathbf{m}])^{\mathsf{T}} \mathbf{C}_{d}^{-1} (\mathbf{d} - \mathbf{F}[\mathbf{m}]) \tag{1}$$

เมื่อ $\mathbf{C}_{\mathbf{d}}$ คือ data covariance และ ^T คือ transpose of matrix เนื่องจาก nonuniqueness of inverse problem ดังนั้นจึงมี models จำนวนมากที่สามารถ fit ข้อมูลได้อย่างดีพอๆ กัน ดังนั้นเพื่อแก้ปัญหานี้ เราจึงจำกัดการ search หา model โดยการให้ inversion คำนวณหา model ที่มีลักษณะเป็น minimum possible structure สำหรับค่า misfit ค่าหนึ่งที่กำหนดไว้ การกำหนดในลักษณะนี้ทำให้ inversion นั้น stable มากขึ้น เราสามารถเขียน model structure ในทางคณิตศาสตร์ได้ดังนี้

$$\chi_{m}^{2} = (\mathbf{m} - \mathbf{m}_{0})^{T} \mathbf{C}_{m}^{-1} (\mathbf{m} - \mathbf{m}_{0})$$
 (2)

เมื่อ **m** คือ model ที่มีทั้งหมด M ค่า ส่วน \mathbf{m}_{o} คือ base model และ \mathbf{C}_{m} คือ model covariance จาก สมการ (1) และ (2) นี้ unconstrained functional $\mathbf{U}(\mathbf{m},\lambda)$ ที่เราจะต้องทำการ minimize สามารถเขียน ได้ดังนี้

$$U(\mathbf{m}, \lambda) = (\mathbf{m} - \mathbf{m}_0)^{\mathsf{T}} \mathbf{C}_{\mathbf{m}}^{-1} (\mathbf{m} - \mathbf{m}_0) + \lambda^{-1} \{ (\mathbf{d} - \mathbf{F}[\mathbf{m}])^{\mathsf{T}} \mathbf{C}_{\mathbf{d}}^{-1} (\mathbf{d} - \mathbf{F}[\mathbf{m}]) - \chi^2 \}$$
(3)

เมื่อ λ^{-1} คือ Lagrange multiplier เราจำเป็นต้องคำนวณหา stationary point ของสมการนี้เมื่อเทียบกับ λ และ **m** ซึ่งคำนวณได้ยาก ดังนั้นวิธีหนึ่งคือการแก้สมการ penalty functional แทน ซึ่งมีลักษณะดังนี้

$$W_{\lambda} (\mathbf{m}) = (\mathbf{m} - \mathbf{m}_0)^{\mathsf{T}} \mathbf{C}_{\mathbf{m}}^{-1} (\mathbf{m} - \mathbf{m}_0) + \lambda^{-1} \{ (\mathbf{d} - \mathbf{F}[\mathbf{m}])^{\mathsf{T}} \mathbf{C}_{\mathbf{d}}^{-1} (\mathbf{d} - \mathbf{F}[\mathbf{m}]) \}$$
(4)

เนื่องจากเมื่อ λ นั้นคงที่ หรือ fixed ไว้ เราจะได้ว่า $\partial U/\partial \mathbf{m} = \partial W_{\lambda}/\partial \mathbf{m}$ ดังนั้นเราสามารถแก้สมการ (4) แทนที่สมการที่ (3) ได้แต่ต้อง vary ค่า λ ไปเรื่อยๆเพื่อให้ได้ค่า misfit ที่น้อยที่สุด

WSINV3DMT Overview

เนื่องจาก **F[m]** นั้นเป็น non-unique problem ดังนั้น iterative solutions จึงจำเป็น (Constable et al., 1987)

$$F[m_{k+1}] = F[m_k] + J_k(m_{k+1} - m_k), \tag{5}$$

เมื่อ k คือ iteration number และ $\mathbf{J}_k = [\partial \mathbf{F}/\partial \mathbf{m}]$ คือ $N \times M$ sensitivity matrix calculated at \mathbf{m}_k ซึ่งเป็น ตัวอธิบายการเปลี่ยนแปลงของข้อมูลเนื่องจากการเปลี่ยนแปลงของ model แทนที่ (5) ใน (4) เราได้ approximated penalty functional เมื่อ solve หา stationary points ของ approximated penalty functional เราได้ว่าในแต่ละ iteration จะมี solution ดังนี้

$$\mathbf{m}_{k+1}(\lambda) = [\lambda \mathbf{C}_{m}^{-1} + \Gamma_{k}^{m}]^{-1} \mathbf{J}_{k}^{\mathsf{T}} \mathbf{C}_{d}^{-1} \underline{\mathbf{d}}_{k} + \mathbf{m}_{0}$$
 (6)

เมื่อ "model space cross-product" $\Gamma_{\mathbf{k}}^{\ \mathbf{m}} = \mathbf{J}_{\mathbf{k}}^{\ \mathbf{T}} \mathbf{C}_{\mathbf{d}}^{\ \mathbf{-1}} \mathbf{J}_{\mathbf{k}}$ คือ $M \times M$ positive semi-definite symmetric matrix.

วิธีนี้เป็นการแก้สมการของระบบใน model space เพราะการคำนวณส่วนใหญ่ขึ้นกับค่า M เช่น จาก สมการที่ (6) จำเป็นต้องหา inverted matrix ที่มีขนาด $M \times M$ ซึ่งการคำนวณนี้จะใช้เวลาในการคำนวณอย่าง มาก และยังต้องการหน่วยความจำจำนวนมากอีกด้วย ทั้งนี้เพราะว่า M มักมีขนาดใหญ่ โดยเฉพาะอย่างยิ่งถ้า เราพิจารณาในกรณีที่เป็นสามมิติ การแก้สมการนี้มักเป็นไปไม่ได้ถ้าต้องการคำนวณด้วยเครื่อง PC ธรรมดา ตัวอย่างของค่า M สำหรับสามมิติที่ใช้ในการทดสอบโปรแกรม inversion ที่เขียนขึ้นคือ $M = 21 \times 28 \times 18 = 10584$ การคำนวณง่าย ๆ จากตัวเลขนี้พบว่าในการแก้สมการที่ (6) เราจำเป็นต้องใช้หน่วยความจำถึง ประมาณ 450 Mbytes เมื่อรวมกับหน่วยความจำที่ต้องการจากตัวแปรอื่น ๆ พบว่าการแก้สมการนี้บน PC ที่มี หน่วยความจำถึง 1 Gbytes นั้นเป็นไปไม่ได้

โดยปกติแล้ว N (จำนวนข้อมูล) มักน้อยกว่า M (จำนวนค่าของแบบจำลอง) หรือเขียนง่ายว่า N << M โดยเฉพาะถ้าเราพิจารณาในกรณีของสามมิติ เราพบว่า statement นี้มักถูกต้อง เช่นในกรณีข้างต้น N = 1440 ดังนั้นถ้าเราสามารถแปลงรูปการคำนวณให้เปลี่ยนจาก model space เป็น data space เราจะสามารถ ลดเวลาที่ใช้ในการคำนวณได้รวมทั้งลดหน่วยความจำที่ต้องการอีกด้วย

Parker (1994) แสดงให้เห็นว่าสำหรับ iteration k, \mathbf{m}_{k+1} สามารถเขียนได้ว่าเป็น linear combination of rows of the smoothed sensitivity matrix $\mathbf{C}_{\mathbf{m}}\mathbf{J}_{k}^{\mathsf{T}}$, หรือ

$$\mathbf{m}_{k+1} - \mathbf{m}_{0} = \mathbf{C}_{m} \mathbf{J}_{k}^{\mathsf{T}} \mathbf{\beta}_{k+1} \tag{7}$$

เมื่อ β_{k+1} คือ unknown expansion coefficient vector แทนค่า (7) ลงใน approximated penalty functional แล้วแก๊สมการเพื่อหา stationary point เทียบกับ β เราได้ว่า

$$\beta_{k+1} = [\lambda \mathbf{C}_{d} + \Gamma_{k}^{n}]^{-1} \underline{\mathbf{d}}_{k}$$
 (8)

เมื่อ "data space cross-product" $\Gamma_k^n = \mathbf{J}_k \, \mathbf{C}_m \, \mathbf{J}_k^{\mathsf{T}}$ เป็น $N \times N$ positive semi-definite symmetric matrix ใน กรณีนี้จะเห็นได้ว่าเราเพียงแก้สมการที่มีขนาดเพียง $N \times N$ เท่านั้น ไม่ใช้ $M \times M$ เหมือนในกรณีของ model space ดังนั้นในกรณีตัวอย่างข้างต้น เมตริกที่ต้องทำการ invert จะมีขนาดเพียง 1440 x 1440 เท่านั้น แทนที่ จะเป็น 10584 x 10584 เหมือนในกรณี model space และหน่วยความจำที่ต้องใช้ก็ลดเหลือเพียง 8 MByte เท่านั้นในการเก็บ representer matrix

ในกรณีการแปลงรูปการคำนวณไม่ทำให้ solution ที่ได้ผิดเพี้ยนไป ดังนั้นตราบใดที่เราใช้ค่า λ และ **C**_m เดียวกันแล้ว ทั้งการคำนวณใน model space และ data space นั้นจะให้ผลที่เหมือนกัน รายละเอียด สามารถดูได้จาก Siripunvaraporn and Egbert (2000) และ Siripunvaraporn and Egbert (2004, 2005) pseudo code สำหรับ WSINV3DMT (หรือ DASOCC สำหรับ 2-D) แสดงในรูปที่ 1

 \mathbf{d} = observed data, $\mathbf{C}_{\mathbf{d}}$ = data error, $\mathbf{m}_{\mathbf{0}}$ = initial model, $\mathbf{C}_{\mathbf{m}}$ = model covariance

Solve forward problem and compute misfit from model m_0

Start DASOCC outer loop iteration k:

For i = 1 to $N_s * N_m * N_p$

Call forward solver to form sensitivity for data i

End

Compute $\mathbf{d}_k = \mathbf{d} - \mathbf{F}[\mathbf{m}_k] + \mathbf{J}_k(\mathbf{m}_k - \mathbf{m}_0)$

Compute $\Gamma_k = \mathbf{C}_d^{-1/2} \mathbf{J}_k \mathbf{C}_m \mathbf{J}_k^T \mathbf{C}_d^{-1/2}$

For various values of λs

Use J_k to compute representer matrix $\mathbf{R}_k = [\lambda \mathbf{I} + \Gamma_k]$

Use Cholesky decomposition to solve \mathbf{m}_{k+1} - $\mathbf{m}_0 = \mathbf{C}_{\mathbf{m}} \mathbf{J}_k \mathbf{C}_{\mathbf{d}}^{-1/2} \mathbf{R}_k^{-1} \mathbf{C}_{\mathbf{d}}^{-1/2} \mathbf{d}_k$

Solve forward problem and Compute misfit from model \mathbf{m}_{k+1}

Phase I: Compare misfit from different \(\lambda\)s to seek for minimum misfit

Phase II: Compare norm from different λs to seek minimum norm $% \left(1\right) =\left(1\right) +\left(1\right) +\left$

End

Exit when misfit less than desired level with minimum norm

End DASOCC outer loop iteration

รูปที่ 1 - Pseudo-code สำหรับ WSINV3DMT และ DASOCC

Data Space Conjugate Gradient (DCG) method

อย่างไรก็ตาม ถ้าแบบจำลอง m และ ข้อมูล d มีขนาดใหญ่ขึ้น data space method ก็เป็นไปไม่ได้ เพราะว่าต้องใช้หน่วยความจำมากขึ้น โดยเฉพาะในการเก็บ sensitivity matrix ที่มีขนาด N x M จาก กรณีตัวอย่าง หน่วยความจำที่ต้องใช้ในการเก็บ representer matrix ใน data space คือ 8 MByte แต่ ว่าต้องใช้อีก 121 MByte ในการเก็บ sensitivity matrix และถ้าในกรณีที่เป็นข้อมูลจริงซึ่ง N และ M มีขนาดใหญ่มากก็ยิ่งเป็นไปไม่ได้ หรือต้องทำงานบนเครื่องคอมพิวเตอร์สมรรถนะสูงเท่านั้น

ดังนั้นแทนที่เราจะแก้สมการที่ (8) ด้วยวิธีโดยตรงซึ่งใน WSINV3DMT ใช้คือ Cholesky Decomposition เราเปลี่ยนวิธีการแก้สมการโดยหันมาใช้วิธี conjugate gradient (CG) ซึ่งเป็นวิธี ทางอ้อม วิธีนี้จะทำให้เราไม่ต้องเก็บ sensitivity matrix ไว้ในหน่วยความจำ เพราะวิธีนี้ต้องการแค่ผล คูณของ sensitivity matrix กับ vector ใดๆ ซึ่งสามารถทำได้โดยการแก้สมการไปข้างหน้าเพียงหนึ่งครั้ง เท่านั้น

CG method เป็น relaxation method ที่ใช้สำหรับแก้ระบบสมการ $\mathbf{A}\mathbf{x} = \mathbf{b}$ ที่มีความสมมาตร โดยทำการ iteratively minimizing the quadratic form $\mathbf{Q}(\mathbf{x}) = \frac{1}{2} \mathbf{x}^\mathsf{T} \mathbf{A} \mathbf{x} - \mathbf{x}^\mathsf{T} \mathbf{b}$ ซึ่ง algorithm นี้สามารถ หาดูได้จากสิ่งตีพิมพ์อื่นๆ (e.g., Press et al., 1992; Barret et al., 1994) จากสมการที่ (8) เขียนใหม่ จะได้เป็น

$$\boldsymbol{\beta}_{k+1} = \left[\lambda \mathbf{C}_{d} + \mathbf{J}_{k} \mathbf{C}_{m} \mathbf{J}_{k}^{\mathsf{T}}\right]^{-1} \underline{\mathbf{d}}_{k} \tag{9}$$

จากสมการนี้จะเห็นได้ว่า $\mathbf{A} = [\lambda \mathbf{C_d} + \mathbf{J_k} \mathbf{C_m} \mathbf{J_k}^\mathsf{T}]$ และ \mathbf{x} คือ $\boldsymbol{\beta}_{k+1}$ ส่วน \mathbf{b} คือ $\underline{\mathbf{d}}_k$ การแก้สมการที่ (9) ต้องการเพียง $\mathbf{J_k} \mathbf{x}$ หรือ $\mathbf{J_k}^\mathsf{T} \mathbf{x}$ ซึ่งสามารถทำได้โดยการแก้สมการไปข้างหน้า (forward problem) หนึ่ง ครั้ง (Mackie and Madden, 1993) ซึ่งในสมการที่ (9) ต้องทำทั้งหมดสองครั้ง รายละเอียดดูเพิ่มเติมได้ ใน Siripunvaraporn and Egbert (2007) Pseudo code สำหรับ DCG3DMT (หรือ DCG2DMT สำหรับ

 \mathbf{d} = observed data, $\mathbf{C}_{\mathbf{d}}$ = data error, $\mathbf{m}_{\mathbf{0}}$ = initial model, $\mathbf{C}_{\mathbf{m}}$ = model covariance

2-D) แสดงในรูปที่ 2

Solve forward problem and compute misfit from model m_{θ} Select λ

Start DCG outer loop iteration *k*:

Solve forward problem and Compute $\mathbf{d}_k = \mathbf{d} - \mathbf{F}[\mathbf{m}_k] + \mathbf{J}_k(\mathbf{m}_k - \mathbf{m}_0)$

Start CG iteration icg

Solve forward problem twice to find \mathbf{m}_{k+1} - $\mathbf{m}_0 = \mathbf{C}_{m} \mathbf{J}_{k} \mathbf{C}_{d}^{-1/2} \mathbf{R}_{k}^{-1} \mathbf{C}_{d}^{-1/2} \mathbf{d}_{k}$,

where $\mathbf{R}_{k} = [\lambda \mathbf{I} + \mathbf{C}_{d}^{1/2} \mathbf{J}_{k} \mathbf{C}_{m} \mathbf{J}_{k}^{\mathrm{T}} \mathbf{C}_{d}^{1/2}]$

Stop CG iteration if r_{stop} less than desired level

End icg

Solve forward problem and Compute misfit from model $\boldsymbol{m}_{k^{+}1}$

Exit when misfit less than desired level

End DCG outer loop iteration

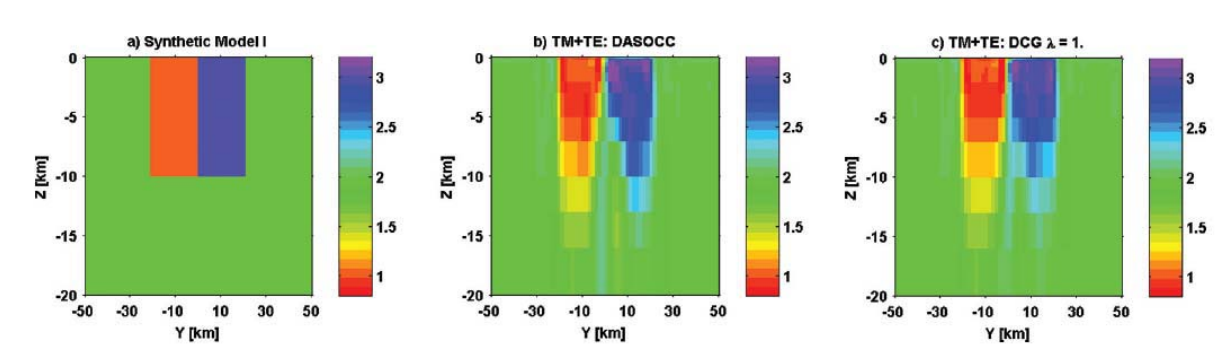
รูปที่ 2 - Pseudo-code สำหรับ DCG3DMT และ DCG2DMT

การประเมินผลโปรแกรมและผลการทดสอบ

ในการประเมิน เราจะเปรียบเทียบการทำงานของสองโปรแกรมคือ WSINV3DMT กับ DCG3DMT สำหรับข้อมูลในสามมิติ และ DASOCC กับ DCG2DMT สำหรับข้อมูลสองมิติ ซึ่งผลการทดสอบจากทั้ง สองมิติและสามมิตินั้นคล้ายคลึงกัน ดังนั้นในที่นี้เราจะนำเสนอผลเฉพาะจากสองมิติเท่านั้น

วิธีการเปรียบเทียบการทำงาน คือ เรานับจำนวนการแก้ปัญหาไปข้างหน้า (forward problem) เพราะการแก้ปัญหาไปข้างหน้าในแต่ละครั้งนั้นใช้เวลานาน โปรแกรมไหนใช้จำนวนการแก้ปัญหาไปข้างหน้ามาก ก็แสดงว่าใช้เวลาในการคำนวณมากเช่นกัน นอกจากนี้ เรายังเปรียบเทียบจำนวนหน่วยความจำที่แต่ละวิธีใช้ โดยเราจะนำเสนอการทดสอบกับข้อมูลจำลองที่เราสร้างขึ้นมา

ข้อมูลจำลองนี้เป็นข้อมูลจำลองที่สร้างมาจากแบบจำลองดังแสดงในรูปที่ 3(a) เมื่อนำข้อมูลที่ ได้มาไปผ่านกระบวนการ inversion จากโปรแกรม DASOCC จะได้ผลดังแสดงในรูปที่ 3(b) และเมื่อ ผ่านโปรแกรม DCG2DMT จะได้ผลดังแสดงในรูปที่ 3(c) ผลการทดสอบแสดงให้เห็นว่าโปรแกรมทั้งสอง ทำงานได้ใกล้เคียงกัน สามารถ recover ทั้งก้อน resistance และ ก้อน conductance จากแบบจำลองได้ อย่างถูกต้อง



ร**ูปที่ 3** – (a) แบบจำลองที่ใช้ในการสร้างข้อมูลจำลองที่ 1 (b) แบบจำลองที่ได้จากการนำข้อมูลจำลองที่ ได้ไปผ่านโปรแกรม DASOCC (c) แบบจำลองที่ได้จากการนำข้อมูลจำลองที่ได้ไปผ่านโปรแกรม DCG2DMT

แบบจำลองที่ได้จากโปรแกรมทั้งสองนั้นมีความถูกต้องสูง แสดงว่าประสิทธิภาพในการทำ inversion ของทั้งสองโปรแกรมใกล้เคียงกัน เพื่อดูเวลาที่ใช้ในการคำนวณ เราทำการเปรียบเทียบ จำนวนการแก้ปัญหาไปข้างหน้าของทั้งสองโปรแกรม ตารางที่ 1 แสดงจำนวนการแก้ปัญหาไปข้างหน้าของโปรแกรม DASOCC ส่วนตารางที่ 2 แสดงจำนวนการแก้ปัญหาไปข้างหน้าของโปรแกรม DCG2DMT

Table 1. Number of iteration for DASOCC inversion to reach desired level of misfit for TM, TE and joint TM + TE inversions for synthetic test case I.

Outer loop DASOCC Iter no.	TM			TE	TM + TE	
	RMS	# of FWD to form \mathbf{J}_k	RMS	# of FWD to form J_k	RMS	# of FWD to form J_k
0	12.49	_	8.60	_	10.73	_
1	3.24	324	2.89	324	3.82	648
2	0.97	324	1.29	324	1.36	648
3			0.99	324	1.00	648
Total FWD		648		972		1944

Note: The number of forward modelling calls (FWD) required for each iteration, and the total over all iterations are also given.

Table 2. Number of iterations for the DCG inversion with different r_{stop} levels for TM (a), TE (b) and TM + TE (c) inversions for test case I.

Outer loop DCG Iter. no.	Relative error (r_{stop}) for stopping CG iterative process ($\lambda = 1.0$)								
	$r_{\text{stop}} = 1.\text{E-06}$		$r_{\text{stop}} = 1.\text{E-04}$		$r_{\text{stop}} = 1.\text{E-}02$		$r_{\text{stop}} = 1.\text{E-}01$		
	RMS	No. of CG Iter	RMS	No. of CG Iter	RMS	No. of CG Iter	RMS	No. of CG Iter	
(a) TM: Initial RMS = 12.4	19								
1	3.24	58	3.24	39	3.22	23	3.70	11	
2	1.44	45	1.44	32	1.44	16	1.57	7	
3	1.01	43	1.01	29	1.01	14	1.37	6	
4							1.37	6	
5							1.33	6	
6							1.33	6	
Total CG Iter.		146		100		53		_	
Total FWD		2628		1800		954		-	
(b) TE: Initial RMS = 8.60									
1	2.89	46	2.89	31	2.89	17	2.96	10	
2	1.94	37	1.94	26	1.94	15	2.04	8	
3	1.19	34	1.19	24	1.20	13	1.30	7	
4	1.04	34	1.04	24	1.04	12	1.25	6	
5							1.21	6	
6							1.21	6	
Total CG Iter.		151		105		57		_	
Total FWD		2718		1890		1026		-	
(c) TM + TE: Initial RMS:	= 10.73								
1	4.38	77	4.38	49	4.38	28	4.38	16	
2	2.60	61	2.60	41	2.61	22	2.98	12	
3	1.17	50	1.17	36	1.19	20	1.75	10	
4	0.95	50	0.95	36	0.96	19	1.18	9	
5							1.08	7	
6							1.08	7	
Total CG Iter.		238		162		89		_	
Total FWD		8568		5832		3204		_	

Note: For $r_{\text{stop}} = 1.\text{E-}01$, the inversion cannot reach the desired level of misfit. Essentially the same RMS misfit is attained for all values of $r_{\text{stop}} = 1.\text{E-}02$ or less. Note that for each CG iteration 2 forward model solutions are required for each period.

การทดสอบนี้แสดงให้เห็นว่า จำนวนการแก้ปัญหาไปข้างหน้าของโปรแกรม DCG นั้นส่วนใหญ่ แล้วจะมากกว่าของโปรแกรม DASOCC ซึ่งแสดงว่าเวลาที่ใช้ในการคำนวณนั้นจะมากกว่า นอกจาก ข้อมูลจำลองชุดนี้แล้ว เรายังได้ทดสอบกับข้อมูลจำลองชุดอื่นๆ ซึ่งให้ผลที่สอดคล้องกัน แม้ว่าเวลาที่ใช้ ในการคำนวณของ DCG2DMT จะมากกว่า แต่เป็นที่แน่นอนที่ปริมาณหน่วยความจำที่ใช้มีค่าน้อยกว่า มากๆ เพราะ DCG2DMT ไม่ต้องทำการเก็บ sensitivity matrix ไว้ในหน่วยความจำ ทำให้ประหยัด หน่วยความจำไปได้มากทีเดียว แต่การประหยัดหน่วยความจำนี้กลับทำให้เวลาการคำนวณมีค่าสูงมาก ขึ้น

สรุปผล

เราได้พัฒนา ทั้ง 2-D และ 3-D inversion programs สำหรับข้อมูล MT โดยเทคนิคที่ใช้เป็นการพัฒนา มาจากวิธีใน data space เพียงแต่ว่าวิธีการแก้ระบบของสมการนั้นเราใช้เทคนิคที่เรียกว่า conjugate gradient มาใช้แทนที่การแก้สมการแบบโดยตรง โปรแกรมที่พัฒนาขึ้นมาใหม่มีศักยภาพที่สูงเทียบเท่า กับโปรแกรมที่เคยพัฒนามาแล้วเช่น WSINV3DMT และ DASOCC แต่ใช้หน่วยความจำที่น้อยกว่า มากๆ ซึ่งในขณะเดียวกันก็ใช้เวลาในการคำนวณที่สูงกว่า ดังนั้นการจะเลือกใช้โปรแกรมใดก็ขึ้นกับผู้ใช้ และข้อมูลที่จะนำไปไปใช้

หนังสืออ้างอิง

- Constable, C. S., Parker, R. L., and Constable, C.G., 1987, Occam's inversion: A practical algorithm for generating smooth models from electromagnetic sounding data: *Geophysics*, 52, 289-300.
- Jones, A. G., 1992, Electrical conductivity of the continental lower crust, in Fountain, D. M., Arculus, R. J., and Kay, R. W.,
 Eds., Continental Lower Crust: Elsevier Science Publ. Co., Inc., 81-143.
- Mackie, R. L., and Madden, T. R., 1993, Three-dimensional magnetotelluric inversion using conjugate gradients: *Geophys. J. Internat.*, 115, 215-229.
- Orange, A. S., 1989, Magnetotelluric Exploration for Hydrocarbons: Proc. IEEE, 77, 287-317.
- Parker, R. L., 1994, Geophysical Inverse Theory: Princeton Univ. Press.
- Siripunvaraporn, W., Egbert, G. D., Eisel, M., and Unsworth, M., 1998, A High Resolution EM Survey of the San Andreas Fault (SAF): Local Conductivity Structure in a Regional Context: Eos, Trans. Am. Geophys. Union, 79, 45, Fall Meet. Suppl., F227.
- Siripunvaraporn W. and Egbert, G. D., 2000, An Efficient Data-Subspace Inversion for Two-Dimensional Magnetotelluric Data, Geophysics, 65, 791-803.
- Siripunvaraporn, W., G. Egbert, Y. Lenbury and M. Uyeshima, 2005a, Three-Dimensional Magnetotelluric Inversion: Data Space Method, *Phys. Earth and Planet. Interior.*, 150, 3-14.
- Siripunvaraporn, W., G. Egbert and M. Uyeshima, 2005b, Interpretation of two-dimensional magnetotelluric profile data with three-dimensional inversion: synthetic examples, *Geophys. J. Int.*, **160**, 804-814.
- Siripunvaraporn W. and G. Egbert, 2007, Data Space Conjugate Gradient Inversion for 2-D Magnetotelluric Data, Geophysical Journal International, 170, 986-994.
- Tuncer V., M. Unsworth, W. Siripunvaraporn, J. Craven, 2006, Audio-magnetotelluric exploration for unconformity type uranium deposits at the McArthur River Mine, northern Saskatchewan (Canada), *Geophysics*, 71, B201-209.
- Unsworth M., P. Bedrosian, M. Eisel, G. Egbert and W. Siripunvaraporn, 2000, Along strike variations in the electrical structure of the San Andreas Fault at Parkfield, California, Geop. Res. Lett., 27, 3021-3024.
- Vozoff, K., 1972, The Magnetotelluric Method in the Exploration of Sedimentary Basins: Geophysics, 37, 98-141.

Output ที่ได้จากโครงการ

ผลงานตีพิมพ์ในวารสารวิชาการนานาชาติ

- Siripunvaraporn W. and G. Egbert, 2007, Data Space Conjugate Gradient Inversion for 2-D Magnetotelluric Data, Geophysical Journal International, 170, 986-994.
- Tuncer V., M. Unsworth, **W. Siripunvaraporn**, J. Craven, 2006, Audio-magnetotelluric exploration for unconformity type uranium deposits at the McArthur River Mine, northern Saskatchewan (Canada), *Geophysics*, **71**, B201-209.
- Siripunvaraporn W., G. Egbert and M. Uyeshima, 2005, Interpretation of 2-D Magnetotelluric Profile Data with 3-D Inversion: Synthetic Examples, *Geophys. Jour. Inter.*, 160, 804-814

Software

- Siripunvaraporn W., 2006, WSINV3DMT & WSFWD3DMT; Three-Dimensional inversion and forward modeling programs for MT data. The code is written in Fortran 77 with more than 10,000 lines. The programs have been released to public (only for academic purpose) since February 2006 which have been requested from more than 20 countries worldwide. See more detail at http://mucc.mahidol.ac.th/~scwsp/wsinv3dmt/index.htm
- Siripunvaraporn W., 2007, WSDCG2DMT, The code is not released to public. Two-Dimensional inversion program based on the data space conjugate gradient technique. The code is written with Fortran 95.
- Siripunvaraporn W. and G. Ebgert, 2007, WSDCG3DMT, The code is not released to public. Three-Dimensional inversion program based on the data space conjugate gradient technique. The code is written with Fortran 95. The code is part of the modular system designed with Prof. Gary Egbert. From Oregon State University.

การเสนอผลงานในที่ประชุมวิชาการนานาชาติบางส่วน

- Volkan Tuncer, Martyn J. Unsworth, Weerachai Siripunvaraporn, James A. Craven, 2006, Audio-magnetotelluric exploration for unconformity uranium deposits in the Athabasca Basin, Saskatchewan, Canada, SEG International Exposition and Seventy-Sixth Annual Meeting, New Orleans, Louisiana, USA, October 1-6.
- Volkan Tuncer, Martyn J. Unsworth, Weerachai Siripunvaraporn, James A. Craven, 2006,
 Uranium exploration with audio-magnetotelluric (AMT) data at the McArthur River Mine,
 Saskatchewan (Canada), Induction Workshop #18, El Vendrell, Spain, September 17-23.
- M. Uyeshima, T. Ogawa, S. Koyama, S. Yamaguchi, H. Toh, H. Murakami, R. Yoshimura, N. Oshiman, T. Kasaya, T. Tanbo and W. Siripunvaraporn, 2006, Network-MT survey in Central Japan and its first results, Induction Workshop #18, El Vendrell, Spain, September 17-23.
- G. D. Egbert, and W. Siripunvaraporn, 2006, Modular System, Induction Workshop #18, El Vendrell, Spain, September 17-23.
- G. D. Egbert, and W. Siripunvaraporn, 2006, Efficient Inversion of Multi-Frequency EM
 Data: A Hybrid Conjugate Gradients/ Occam Algorithm, Induction Workshop #18, El
 Vendrell, Spain, September 17-23.
- Siripunvaraporn W. and G. Egbert, 2005, Data space conjugate gradient inversion for 2-D
 Magnetotelluric data, IAGA 2005 Scientific Assembly, Toulouse, France, July 18-29.
- Uyeshima M., W. Siripunvaraporn and H. Utada, 2005, Deep conductivity structure beneath the Hokkaido Island, IAGA 2005 Scientific Assembly, Toulouse, France, July 18-29.
- Uyeshima M., Y. Ogawa, S. Koyama, N. Ujihara, Y. Honkura, W. Siripunvaraporn, T. Mogi, S. Yamaguchi, I. Shiozaki and T. Noguchi, 2005, Resistivity imaging across the source region of the 2004 Mid-Niigata Prefecture Earthquake (M6.8), central Japan, IAGA 2005 Scientific Assembly, Toulouse, France, July 18-29.

ภาคผนวก

ภาคผนวก ก. Reprint

Siripunvaraporn W. and G. Egbert, 2007, Data Space Conjugate Gradient Inversion for
 2-D Magnetotelluric Data, Geophysical Journal International, 170, 986-994.

ภาคผนวก ข. Reprint

Tuncer V., M. Unsworth, W. Siripunvaraporn, J. Craven, 2006, Audio-magnetotelluric exploration for unconformity type uranium deposits at the McArthur River Mine, northern Saskatchewan (Canada), *Geophysics*, 71, B201-209.

ภาคผนวก ค. Reprint

 Siripunvaraporn W., G. Egbert and M. Uyeshima, 2005, Interpretation of 2-D Magnetotelluric Profile Data with 3-D Inversion: Synthetic Examples, *Geophys. Jour.* Inter., 160, 804-814

ภาคผนวก ง. USER MANUAL ของ WSINV3DMT program และ รายชื่อผู้ใช้โปรแกรม WSINV3DMT

• Siripunvaraporn W., 2006, User Manaul for WSINV3DMT.

ภาคผนวก จ. ข่าวที่เกี่ยวข้องกับงานวิจัย

Data space conjugate gradient inversion for 2-D magnetotelluric data

Weerachai Siripunvaraporn¹ and Gary Egbert²

¹Department of Physics, Faculty of Science, Mahidol University, Rama VI Rd., Rachatawee, Bangkok 10400, Thailand. E-mail: scwsp@mahidol.ac.th ²College of Oceanic and Atmospheric Sciences, Oregon State University, Corvallis, OR 97331, USA

Accepted 2007 April 25. Received 2007 April 25; in original form 2006 December 18

SUMMARY

A data space approach to magnetotelluric (MT) inversion reduces the size of the system of equations that must be solved from $M \times M$, as required for a model space approach, to only $N \times N$, where M is the number of model parameter and N is the number of data. This reduction makes 3-D MT inversion on a personal computer possible for modest values of M and N. However, the need to store the $N \times M$ sensitivity matrix \mathbf{J} remains a serious limitation. Here, we consider application of conjugate gradient (CG) methods to solve the system of data space Gauss–Newton equations. With this approach \mathbf{J} is not explicitly formed and stored, but instead the product of \mathbf{J} with an arbitrary vector is computed by solving one forward problem. As a test of this data space conjugate gradient (DCG) algorithm, we consider the 2-D MT inverse problem. Computational efficiency is assessed and compared to the data space Occam's (DASOCC) inversion by counting the number of forward modelling calls. Experiments with synthetic data show that although DCG requires significantly less memory, it generally requires more forward problem solutions than a scheme such as DASOCC, which is based on a full computation of \mathbf{J} .

Key words: data space method, inversion, magnetotellurics.

INTRODUCTION

Three-dimensional (3-D) magnetotelluric (MT) inversion can reveal the 3-D resistivity structure beneath the Earth's surface, and can be applied to 3-D data sets (e.g. Tuncer *et al.* 2006), as well as to 2-D profile data (Siripunvaraporn *et al.* 2005b). In recent years a number of 3-D MT inversion algorithms have been developed (e.g. Mackie & Madden 1993; Mackie, personal communication 2002; Newman & Alumbaugh 2000; Zhdanov *et al.* 2000; Sasaki 2001; Siripunvaraporn *et al.* 2004, 2005a). There are many similarities in the formulation of the inverse problem used by all of these authors—in all cases a data misfit/model roughness penalty functional is minimized—but a number of different computational approaches have been pursued. All approaches have pros and cons, as discussed in Siripunvaraporn *et al.* (2005a).

Newman & Alumbaugh (2000) and Mackie (personal communication 2002) used the non-linear conjugate gradient method to minimize a data misfit/model roughness penalty functional. Sasaki (2001) and Mackie & Madden (1993) both used a Gauss–Newton (GN) method, however in the latter case the system of normal equations was solved by the conjugate gradient method. Siripunvaraporn *et al.* (2004, 2005a) developed a 3-D inversion algorithm based on the Occam inversion of Constable *et al.* (1987), another variant of the GN method. In this work, the data space approach previously used for 2-D MT (Siripunvaraporn & Egbert 2000) was extended to the 3-D case. This transformation to the data space significantly reduced memory requirements, and making it possible to run 3-D MT

inverse problems of modest size on a desktop PC. However, memory required to store the sensitivity matrix is still quite substantial, and this limits the size of both data sets and model parametrization. Here, we consider another possible approach, the 'data space conjugate gradient' (DCG) inversion. This is again a GN variant, formulated in the data space as in Siripunvaraporn & Egbert (2000), but without forming and storing the sensitivity matrix as in Mackie & Madden (1993).

We begin the paper by reviewing the Occam inversion, comparing model and data space approaches. We then introduce the DCG method, and test this using synthetic 2-D MT data set. In these tests we compare computational efficiency of DCG and previously described, proven MT inverse methods (Siripunvaraporn & Egbert 2000).

REVIEW OF OCCAM'S INVERSION

The data space Occam's (DASOCC) inversion has been successfully applied to 2-D (Siripunvaraporn & Egbert 2000) and 3-D (Siripunvaraporn *et al.* 2004, 2005a) magnetotelluric (MT) inversion. DASOCC follows the general Occam approach of Constable *et al.* (1987) to seek the 'minimum structure' model subject to an appropriate fit to the data. Mathematically, an unconstrained functional $U(\mathbf{m}, \lambda)$ is varied:

$$U(\mathbf{m}, \lambda) = (\mathbf{m} - \mathbf{m}_0)^{\mathrm{T}} \mathbf{C}_{\mathbf{m}}^{-1} (\mathbf{m} - \mathbf{m}_0)$$

$$+ \lambda^{-1} \{ (\mathbf{d} - \mathbf{F}[\mathbf{m}])^{\mathrm{T}} \mathbf{C}_{\mathbf{d}}^{-1} (\mathbf{d} - \mathbf{F}[\mathbf{m}]) - X^{*2} \},$$
(1)

to minimize the model norm subject to the condition that the normalized squared total misfit is equal to X^{*2} . Here \mathbf{m} is the resistivity model of dimension M, $\mathbf{m_0}$ the prior model, $\mathbf{C_m}$ the model covariance matrix which defines the model norm, \mathbf{d} the observed data with dimension N, $\mathbf{F[m]}$ the forward model response, $\mathbf{C_d}$ the data covariance matrix, X^* the target misfit, and λ^{-1} a Lagrange multiplier.

The Occam scheme of Constable *et al.* (1987) is based on linearizing the forward response to obtain the following iterative sequence of linear equations (see Constable 1987; Siripunvaraporn & Egbert 2000),

$$\mathbf{m}_{k+1} - \mathbf{m}_0 = \left[\lambda \mathbf{C}_{\mathbf{m}}^{-1} + \mathbf{J}_k^{\mathsf{T}} \mathbf{C}_{\mathbf{d}}^{-1} \mathbf{J}_k \right]^{-1} \mathbf{J}_k^{\mathsf{T}} \mathbf{C}_d^{-1} \mathbf{d}_k, \tag{2}$$

where the subscript k denotes iteration number, $\mathbf{J}_k = (\partial \mathbf{F}/\partial \mathbf{m})_k$ is the $N \times M$ sensitivity matrix calculated at \mathbf{m}_k , and $\mathbf{d}_k = \mathbf{d} - \mathbf{F}[\mathbf{m}_k] + \mathbf{J}_k(\mathbf{m}_k - \mathbf{m}_0)$. In (2) the dimension of the inverted matrix is $M \times M$, controlled by the size of the model space. For realistic 3-D problems M is usually very large, making application of this model space approach impractical.

To reach the ultimate goal of finding a stationary point of (1), in each iteration (2) is solved with a series of trial values of λ . In early iterations (Phase I), the Occam algorithm searches over λ for the model that minimizes misfit. The process continues until the target X^{*2} is attained. Once the misfit reaches the desired level, the next stage (Phase II) begins by keeping the misfit at the desired level, varying λ to seek the model of smallest norm achieving the target misfit. One advantage of Occam's inversion is that only a small number of iterations are required to converge to the solution.

Siripunvaraporn & Egbert (2000) transformed the Occam scheme for the 2-D MT problem from the model space to the data space, developing a variant of Occam in which the size of the inversion depends on the number of data N, instead of the number of model parameters M. See Parker (1994), Bennett $et\ al.$ (1996) and Egbert (1997) for data space approaches to other inversion problems. In the data space approach, the series of iterative approximate solutions is

obtained as

$$\mathbf{m}_{k+1} - \mathbf{m}_0 = \mathbf{C}_{\mathbf{m}} \mathbf{J}_k \left[\lambda \mathbf{C}_d + \mathbf{J}_k \mathbf{C}_{\mathbf{m}} \mathbf{J}_k^{\mathrm{T}} \right]^{-1} \mathbf{d}_k^{\mathrm{T}}, \tag{3}$$

see Siripunvaraporn & Egbert (2000) and Siripunvaraporn *et al.* (2005) for details. The system of equation as given in (3) shows that the system of equations that must be solved for the inversion is in the data space, and thus of size $N \times N$. As in the model space Occam scheme, (3) is solved for a series of trial values of λ to search for the minimal misfit (Phase I) and then to minimize the model norm while keeping the misfit constant (Phase II). We refer to this 'data space' variant on Occam as DASOCC. Provided N is much less than M, DASOCC will be considerably more efficient than the original model space Occam. In particular, DASOCC allows an Occam type scheme to be used for 3-D inversion of MT data on a personal computer or workstation, as shown in Siripunvaraporn *et al.* (2004; 2005a). Pseudo-code for the DASOCC algorithm is given in Fig. 1.

Though the size of the system of equations that must be solved in the inversion can be significantly reduced with a data space approach, very significant computer memory is still required to store the $N \times M$ sensitivity matrix \mathbf{J}_k for realistic values of N and M, particularly for 3-D MT problems. Furthermore, computation of the sensitivity matrix requires many forward model solutions. Here, we present an alternative approach that avoids storing the large matrix \mathbf{J}_k . Instead of forming and factoring the matrix ($\lambda \mathbf{C}_d + \mathbf{J}_k \mathbf{C}_m \mathbf{J}_k^T$) as in Siripunvaraporn & Egbert (2000) and Siripunvaraporn et al. (2004, 2005a), we apply a conjugate gradient (CG) technique to solve (3). With the CG method, there is no need to explicitly form the full $N \times M$ sensitivity matrix. Rather, only multiplication of the sensitivity matrix or its transpose with a given vector (p or q) to form $\mathbf{J}_k \mathbf{p}$ or $\mathbf{J}_k^{\mathrm{T}} \mathbf{q}$ is required. Each of these matrix vector products in turn requires one forward model solution per period. A very similar approach has been used before in the model space EM inversion algorithms developed by Mackie & Madden (1993), Newman & Alumbaugh (1996), Rodi & Mackie (2001) and Haber et al. (2000) among

d = observed data, C_d = data error, m_0 = initial model, C_m = model covariance

Solve forward problem and compute misfit from model m_0

Start DASOCC outer loop iteration *k*:

For i = 1 to $N_s * N_m * N_p$

Call forward solver to form sensitivity for data i

End

Compute $\mathbf{d}_k = \mathbf{d} - \mathbf{F}[\mathbf{m}_k] + \mathbf{J}_k(\mathbf{m}_k - \mathbf{m}_0)$

Compute $\Gamma_k = \mathbf{C}_d^{-1/2} \mathbf{J}_k \mathbf{C}_m \mathbf{J}_k^T \mathbf{C}_d^{-1/2}$

For various values of λs

Use J_k to compute representer matrix $\mathbf{R}_k = [\lambda \ \mathbf{I} + \Gamma_k]$

Use Cholesky decomposition to solve \mathbf{m}_{k+1} - $\mathbf{m}_0 = \mathbf{C}_{\mathbf{m}} \mathbf{J}_k \mathbf{C}_{\mathbf{d}}^{-1/2} \mathbf{R}_k^{-1} \mathbf{C}_{\mathbf{d}}^{-1/2} \mathbf{d}_k$

Solve forward problem and Compute misfit from model \mathbf{m}_{k+1}

Phase I : Compare misfit from different $\,\lambda s$ to seek for minimum misfit

Phase II: Compare norm from different λs to seek minimum norm

End

Exit when misfit less than desired level with minimum norm

End DASOCC outer loop iteration

Figure 1. Pseudo-code for DASOCC.

others. Here, we describe and test DCG, a data space variant on this algorithm. Although the primary rationale for developing this limited memory scheme is to increase practicality of 3-D inversion, we report here initial tests and comparisons on synthetic 2-D MT. A key goal here is to compare computational efficiency of DCG and DASOCC, and these simpler tests are already instructive.

Note that an alternative approach to improving computational efficiency is the Reduced Basis Occam (REBOCC) approach of Siripunvaraporn & Egbert (2000). REBOCC is based on the observation that the updated inverse solution \mathbf{m}_{k+1} of (3) is a linear combination of the N columns of $C_m J_k$. In REBOCC sensitivites for a subset of K data are calculated (e.g. skipping every other frequency or every other site in a profile) and an approximate solution is sought as a linear combination of the corresponding K columns of $C_{\mathbf{m}} \mathbf{J}_k$. The full data set is still fit, using this reduced set of basis functions. This scheme is more efficient than DASSOCC, particularly for MT data sets that are highly redundant, either in spatial or frequency sampling, To simplify our comparisons here we only consider the DASOCC and DCG schemes, and we restrict our comparisons to test data sets which are not heavily oversampled, for which only modest gains in efficiency would be achieved with REBOCC. Indeed, it is not obvious how, or even if, REBOCC might be usefully extended to make use of a subset of sites for general 3-D problems. Furthermore, as we shall see, DASOCC is generally already more efficient in terms of computational time than DCG, so there is little point to direct comparison of efficiency of DCG and REBOCC.

DATA SPACE CONJUGATE GRADIENT (DCG) METHOD

With the DASOCC approach, eq. (3) is solved for a series of values of λ using Cholesky decomposition. In the data space, each such solution is very fast, compared to the time required for forming the Jacobian. Such an Occam approach is not so well suited to using CG as the solver, since in the latter case $\bf J$ is not explicitly calculated and stored. To literally apply the Occam approach, the CG method would have to be applied to solve (3) for each λ , requiring a very large number of forward solutions.

We therefore, take a more traditional regularized optimization approach, taking λ as a fixed damping parameter. Thus, instead of solving the constrained optimization problem implied by (1), we minimize the penalty functional $W_{\lambda}(\mathbf{m})$,

$$W_{\lambda}(\mathbf{m}) = (\mathbf{m} - \mathbf{m}_0)^{\mathrm{T}} \mathbf{C}_{\mathrm{m}}^{-1} (\mathbf{m} - \mathbf{m}_0)$$

+ $\lambda^{-1} \{ (\mathbf{d} - \mathbf{F}[\mathbf{m}])^{\mathrm{T}} \mathbf{C}_{d}^{-1} (\mathbf{d} - \mathbf{F}[\mathbf{m}]) \},$ (4)

with λ fixed. Linearizing F[m], we obtain the same system of data space eq. (3). With the data normalized with diagonal matrix $\mathbf{C_b}^{-1/2}$, this can be written

$$\mathbf{m}_{k+1} - \mathbf{m}_0 = \mathbf{C}_{\mathrm{m}} \mathbf{J}_k \mathbf{C}_{\mathrm{d}}^{-1/2} \left[\lambda \mathbf{I} + \mathbf{C}_d^{-1/2} \mathbf{J}_k \mathbf{C}_{\mathrm{m}} \mathbf{J}_k^{\mathrm{T}} \mathbf{C}_d^{-1/2} \right]^{-1} \mathbf{C}_d^{-1/2} \mathbf{\tilde{d}}_k,$$
(5)

where I is the identity matrix. This simple transformation results in a better conditioned system, with the term λ I acting to stabilize the inversion. This simple transformation is analogous to the preconditioning of the model space equations by approximate solution of Poisson's equation, used by Haber & Ascher (2001) and Rodi & Mackie (2001).

CG is a relaxation method for solving the symmetric system of equations $\mathbf{R}\mathbf{x} = \mathbf{b}$ by iteratively minimizing the quadratic form $Q(\mathbf{x}) = \frac{1}{2}\mathbf{x}^T\mathbf{R}\mathbf{x} - \mathbf{x}^T\mathbf{b}$. The CG algorithm and its details can be found in various publications (e.g. Press et al. 1992; Barret et al. 1994). In our application \mathbf{R} is $[\lambda \mathbf{I} + \mathbf{C}_{\mathbf{d}}^{-1/2} \mathbf{J}_{\mathbf{k}} \mathbf{C}_{\mathbf{m}} \mathbf{J}_{\mathbf{k}}^{\mathrm{T}} \mathbf{C}_{\mathbf{d}}^{-1/2}]$, \mathbf{b} is $\mathbf{C}_{\mathbf{d}}^{-1/2} \mathbf{d}_{\mathbf{k}}$ and **x** is the unknown, which must be multiplied with $C_{\mathbf{d}}^{-1/2}$ to obtain the model \mathbf{m}_{k+1} as given in eq. (5). Implementation of CG requires only code to form the matrix-vector product Rp for arbitrary data space vectors p, rather than actually forming the matrix **R**. Thus we can also avoid forming and storing J_k , provided we have routines for multiplication of model space vectors by \mathbf{J}_{k} and data space vectors by $\mathbf{J}_k^{\mathrm{T}}$. Both of these matrix-vector products can be computed by solving one forward problem, as shown in Mackie & Madden (1993). Pseudo-code for the DCG algorithm is given in Fig. 2. Since J_k is never explicitly computed, one clear advantage of this approach is that storage of the large dense matrix J_k is not needed, as it is with DASOCC.

To compare the computational efficiency of DASOCC and DCG, we consider the total number of forward modelling steps required.

 $\begin{aligned} \textbf{d} &= \text{observed data, } \textbf{C}_d = \text{data error, } \textbf{m}_0 = \text{initial model, } \textbf{C}_m = \text{model covariance} \\ &\text{Solve forward problem and compute misfit from model } \textbf{m}_0 \\ &\text{Select } \lambda \\ &\text{Start DCG outer loop iteration } \textbf{k} : \\ &\text{Solve forward problem and Compute } \textbf{d}_k = \textbf{d} - \textbf{F}[\textbf{m}_k] + \textbf{J}_k(\textbf{m}_k - \textbf{m}_0) \\ &\text{Start CG iteration } \textit{icg} \\ &\text{Solve forward problem twice to find } \textbf{m}_{k+1} - \textbf{m}_0 = \textbf{C}_m \textbf{J}_k \textbf{C}_d^{-1/2} \textbf{R}_k^{-1} \textbf{C}_d^{-1/2} \textbf{d}_k, \\ &\text{where } \textbf{R}_k = [\lambda \textbf{I} + \textbf{C}_d^{-1/2} \textbf{J}_k \textbf{C}_m \textbf{J}_k^T \textbf{C}_d^{-1/2}] \\ &\text{Stop CG iteration if } \textbf{r}_{stop} \text{ less than desired level} \\ &\text{End } \textit{icg} \\ &\text{Solve forward problem and Compute misfit from model } \textbf{m}_{k+1} \\ &\text{Exit when misfit less than desired level} \\ &\text{End DCG outer loop iteration} \end{aligned}$

Figure 2. Pseudo-code for DCG.

In DASOCC, where the full sensitivity is formed, the number of forward solver calls required to form all of ${\bf J}$ is $N_{\rm m}N_{\rm s}N_{\rm p}$ using the reciprocity technique (Rodi 1976), where $N_{\rm m}$ is the number of modes (1 or 2 for MT), $N_{\rm s}$ is the number of sites and $N_{\rm p}$ is the number of periods. Then for each iteration, a further $N_{\rm p}$ forward solutions per mode are required for each λ in order to compute the actual data misfit. Thus the total number of forward solutions required per outer loop DASOCC iteration is about $N_{\rm m}N_{\rm s}N_{\rm p}+N_{\lambda}N_{\rm p}N_{\rm m}$ where N_{λ} is the typical number of values of λ tried in each iteration. Since N_{λ} is typically 4–5, $N_{\lambda}N_{\rm p}N_{\rm m}$ is negligible compared to $N_{\rm m}N_{\rm s}N_{\rm p}$, and will thus be ignored in the following comparisons.

With the DCG approach, the number of forward problems to be solved depends on the number of CG iterations in each step in the outer loop. For each (inner loop) CG iteration the number of forward solver calls required is $2N_{\rm p}N_{\rm m}$: one for computing ${\bf J_kp}$ and a second for computing ${\bf J_kT_q}$, for each mode and for each period. At the end of one outer loop iteration of DCG, $N_{\rm m}N_{\rm p}$ forward modelling calls are required to form the background solution required for the next iteration, and to determine the misfit. Thus, the number of forward solver calls per outer loop DCG iteration is $2N_{\rm p}N_{\rm m}N_{\rm cg}+N_{\rm m}N_{\rm p}$, where $N_{\rm cg}$ is number of CG iterations. Similar to the DASOCC case, we ignore $N_{\rm m}N_{\rm p}$ here because it is a small fraction of $2N_{\rm p}N_{\rm m}N_{\rm cg}$. Thus, we can see that the DCG method will be more efficient than DASOCC only if the total number of CG iterations remains the same

NUMERICAL EXAMPLES

Two 2-D synthetic data examples are used to test the relative efficiency of DCG and DASOCC. For this comparison we consider only the numbers of forward modelling calls used in each method, ignoring other computational overhead, such as solving the system of data space eq. (5) with Cholesky decomposition, as these represent only a small part of the total computational burden.

Synthetic Example I

First, we test DCG on the simple synthetic example illustrated in Fig. 3(a). The model is discritized into 100×31 blocks. The impedance Z_{xy} (TM mode) and Z_{yx} (TE mode) are generated from this model with 36 stations distributed uniformly from -40 to 40 km with a site spacing of 2.5 km. At each site, nine periods distributed uniformly in logarithmic period in the range from 0.01 to 100 s were computed. Random errors with a relative magnitude of 5 per cent were added to the real and imaginary part of the impedance data before inversion. The initial model for all inversion tests is a 50 Ohm-m half-space.

Data space Occam's inversion (DASOCC)

Convergence statistics from using DASOCC to invert TM mode, TE mode and TM + TE mode data are summarized in Table 1. For these three cases the inversion required 2, 3 and 3 outer loop iterations, respectively, to reach the desired target misfit of 1. This corresponds to Phase I of the Occam algorithm. For comparison with DCG we omit the additional 1-2 Phase II iterations, which fine tune the regularization parameter, and generally modify the solution only slightly. The result from joint inversion of the TM and TE data, fitting to an RMS misfit of one, is shown in Fig. 3(b). For DASOCC, the number of forward solver calls is fixed $(=N_s N_p N_m)$, since the sensitivity matrix J_k is explicitly formed. Thus, in each iteration of DASOCC, the number of forward solutions required for this example is $324 (36 \times 9)$ for TM and TE single mode inversions, and 648 (36 \times 9 \times 2) for the joint TM + TE inversion. The total number of forward solutions required to reach the target misfit is thus 648 (324 \times 2) for TM, 972 (324 \times 3) for TE and 1944 (648 \times 3) for TM + TE. These numbers provide a standard for evaluating the computational efficiency of the DCG algorithm.

Data space conjugate gradient method (DCG)

When solving (5) with CG, some stopping criteria must be defined. Rodi & Mackie (2001) terminate the CG process at three iterations per GN step in their MM method. Here, instead of fixing the number of iterations, we terminate when the relative error in the system of equations $||\mathbf{A}\mathbf{x} - \mathbf{b}||/||\mathbf{b}||$ reaches a specified tolerance r_{stop} . Initially we fix $\lambda = 1$, and compare the overall computational efficiency of the DCG scheme with different values of r_{stop} , such as 10^{-6} , 10^{-4} , 10^{-2} and 10^{-1} . The outer loop is terminated when the inversion reaches (or drops below) the desired RMS misfit of 1. Results for the TM mode are given in Table 2(a).

When r_{stop} is small, the number of iterations required is high, but when the actual data misfit is computed, the RMS is not reduced relative to the case $r_{\rm stop}=10^{-2}$. Clearly it is not necessary (or useful) to use a very stringent stopping criterion for inner loop DCG iterations. When r_{stop} is reduced further to 10^{-1} , the number of inner loop iterations is reduced, but the outer loop does not converge to the desired misfit in this case. Furthermore, even when the outer loop does converge, the number of outer loop iterations may be greater, resulting in a larger total number of forward modelling calls with this reduced value of r_{stop} . This example suggests that terminating the CG solver at a fixed small number of iterations, as in Rodi & Mackie (2001), will not always allow convergence to the target level. Indeed, in their tests examples Rodi & Mackie (2001) found that the CG scheme stalled in the later iterations, unable to achieve reduction in the objective function to levels achieved by GN, and non-linear CG (NLCG) approaches. At the same time it is worth

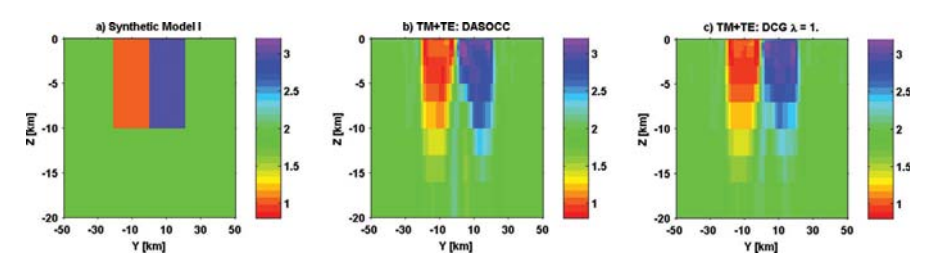


Figure 3. (a) Model I used to generate synthetic data, \mathbf{Z}_{xy} and \mathbf{Z}_{yx} for TM and TE modes. (b) Inverse model recovered from joint inversion of TM and TE modes using DASOCC inversion. (c) Same as (b) but using DCG with $\lambda = 1$. The 36 stations are distributed uniformly from -40 to 40 km.

Table 1. Number of iteration for DASOCC inversion to reach desired level of misfit for TM, TE and joint TM + TE inversions for synthetic test case I.

Outer loop DASOCC Iter no.	TM			TE	TM + TE	
	RMS	# of FWD to form J_k	RMS	# of FWD to form J_k	RMS	# of FWD to form J_k
0	12.49	_	8.60	_	10.73	_
1	3.24	324	2.89	324	3.82	648
2	0.97	324	1.29	324	1.36	648
3			0.99	324	1.00	648
Total FWD		648		972		1944

Note: The number of forward modelling calls (FWD) required for each iteration, and the total over all iterations are also given.

Table 2. Number of iterations for the DCG inversion with different r_{stop} levels for TM (a), TE (b) and TM + TE (c) inversions for test case I.

Outer loop DCG Iter. no.	Relative error (r_{stop}) for stopping CG iterative process ($\lambda = 1.0$)								
	$r_{\text{stop}} = 1.\text{E-06}$		$r_{\text{stop}} = 1.\text{E-04}$		$r_{\text{stop}} = 1.\text{E-02}$		$r_{\text{stop}} = 1.\text{E-01}$		
	RMS	No. of CG Iter	RMS	No. of CG Iter	RMS	No. of CG Iter	RMS	No. of CG Iter	
(a) TM: Initial RMS = 12.4	19								
1	3.24	58	3.24	39	3.22	23	3.70	11	
2	1.44	45	1.44	32	1.44	16	1.57	7	
3	1.01	43	1.01	29	1.01	14	1.37	6	
4							1.37	6	
5							1.33	6	
6							1.33	6	
Total CG Iter.		146		100		53		_	
Total FWD		2628		1800		954		-	
(b) TE: Initial RMS = 8.60									
1	2.89	46	2.89	31	2.89	17	2.96	10	
2	1.94	37	1.94	26	1.94	15	2.04	8	
3	1.19	34	1.19	24	1.20	13	1.30	7	
4	1.04	34	1.04	24	1.04	12	1.25	6	
5							1.21	6	
6							1.21	6	
Total CG Iter.		151		105		57		_	
Total FWD		2718		1890		1026		-	
(c) TM + TE: Initial RMS	= 10.73								
1	4.38	77	4.38	49	4.38	28	4.38	16	
2	2.60	61	2.60	41	2.61	22	2.98	12	
3	1.17	50	1.17	36	1.19	20	1.75	10	
4	0.95	50	0.95	36	0.96	19	1.18	9	
5							1.08	7	
6							1.08	7	
Total CG Iter.		238		162		89		_	
Total FWD		8568		5832		3204		_	

Note: For $r_{\text{stop}} = 1.\text{E-}01$, the inversion cannot reach the desired level of misfit. Essentially the same RMS misfit is attained for all values of $r_{\text{stop}} = 1.\text{E-}02$ or less. Note that for each CG iteration 2 forward model solutions are required for each period.

noting that in the early outer loop steps similar misfit values are achieved with many fewer iterations when a larger value of $r_{\rm stop}$ is used. A more complex stopping criteria, with $r_{\rm stop}$ becoming smaller as the inversion converges may be worth considering.

Similar results are obtained for the TE and joint TM + TE inversions, as shown in Table 2(b) and (c), respectively. The inverse model obtained from the TM + TE inversion is shown in Fig. 3(c). Another general observation from these tables is that as the outer loop converges the number of CG iterations is reduced, even though it becomes necessary to use a more stringent stopping criteria to continue to make progress.

Next, we apply DCG using various values of λ , but with r_{stop} now fixed at 10^{-2} . Results for these experiments are given in

Table 3(a) for TM, Table 3(b) for TE and Table 3(c) for joint TM + TE inversions. From these tables, we conclude that with smaller values of λ a larger number of CG iterations is required. This is because the system of equations becomes much stiffer. Higher values of λ on the other hand result in a well-conditioned system which converges in a smaller number of iterations. However, in this case, it may be impossible to reach the target misfit.

In all three inversion tests (TE, TM and TE + TM), optimal convergence occurs when $\lambda=1$, and $r_{\rm stop}$ is 10^{-2} . For each of the outer loop iterations, the number of CG steps is roughly half the number of stations. However, the total number of outer loop iterations is slightly greater than what is required by DASOCC, that is, three for TM, four for TE and four for TM + TE inversions. The

Table 3. Number of iterations for the DCG inversion with different values of λ for TM (a), TE (b) and TM + TE (c) inversions of synthetic test case I.

Outer loop DCG Iter. no.		Different values of λ ($r_{\text{stop}} = 1.0\text{E-}02$)							
		$\lambda = 0.1$		$\lambda = 1$	$\lambda = 10$				
	RMS	No. of CG Iter	RMS	No. of CG Iter	RMS	No. of CG Ite			
(a) TM: Initial RMS = 12.49									
1	4.98	48	3.22	23	4.83	11			
2	3.03	44	1.44	16	3.64	7			
3	1.81	45	1.01	14	3.54	6			
4	0.76	37			3.47	6			
5					3.46	6			
Total CG Iter.		174		53		_			
Total FWD		3132		954		_			
(b) TE: Initial RMS = 8.60									
1	3.33	40	2.89	17	3.80	8			
2	3.65	40	1.94	15	3.33	6			
3	4.36	35	1.20	13	3.23	6			
4	4.14	38	1.04	12	3.22	6			
5	2.95	38			3.21	6			
6	4.23	38			3.21	6			
Total CG Iter.				57		_			
Total FWD		_		1026		_			
(c) TM + TE: Initial RMS =	10.73								
1	5.48	69	4.38	28	4.06	13			
2	4.49	64	2.61	22	2.69	8			
3	3.40	60	1.19	20	2.50	7			
4	2.00	50	0.96	19	2.45	7			
5	1.43	50			2.44	7			
6	0.64	45			2.43	7			
Total CG Iter.		338		89		_			
Total FWD		12 168		3204		_			

Note: For $\lambda = 10$, the inversion cannot reach the desired level of misfit, and for λ less than 0.1, the inversion diverges. For this test case $\lambda = 1$ is at least approximately optimal.

total number of CG steps required to reach the target misfit are thus 53, 57 and 89 for TM, TE and joint TM + TE inversions, respectively (Table 3). Each CG step requires two forward solutions for TM and TE, and four forward solutions for joint TM + TE inversions, per period. Thus, the total number of forward solver calls required are 954 (53 \times 2 \times 9), 1026 (57 \times 2 \times 9) and 3204 (89 \times 4 \times 9) for TM, TE and TM + TE inversions, respectively.

These numbers are higher than were required by the DASOCC method, by factors of roughly 1–1.6 times: 954 to 648 for TM, 1026 to 972 for TE and 3204–1944 for TM + TE inversions. Thus, for this example the computational efficiency of the DCG method is not superior to DASOCC in terms of CPU time. Numerous experiments with other synthetic examples support the general validity of this conclusion. Another issue for DCG is that we may need to try several different values of λ , particularly for real data sets. Values of λ that

are too large may result in failure of the inversion to converge, while values that are too small will require a high number of CG iterations to converge, or may not result in convergence. However, DCG does have a very significant advantage with regard to memory, since storage of the sensitivity matrix is not required. Thus, there is a trade-off between computational efficiency and memory.

Synthetic Example: Case II

We next compare DCG and DASOCC on the more complicated structure shown in Fig. 4(a). This synthetic model may not look geologically realistic, but it provides a more challenging test of the inversions, and demonstrates that the relative performance of DCG and DASOCC will depend on the data set. As in the first example impedances Z_{xy} (TM mode) and Z_{yx} (TE mode) are generated for

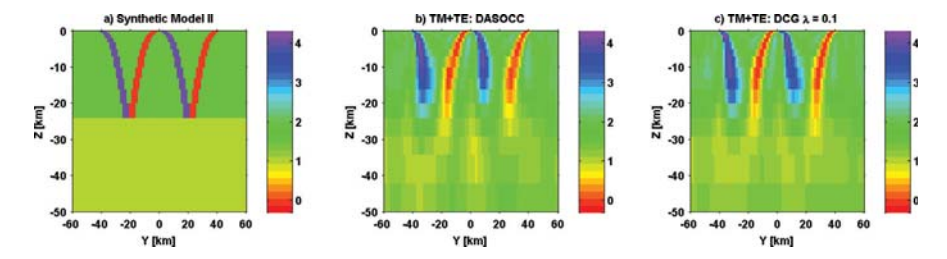


Figure 4. (a) Model II used to generate synthetic data, \mathbf{Z}_{xy} and \mathbf{Z}_{yx} for TM and TE modes. (b) Inverse model recovered from joint inversion of TM and TE modes using DASOCC inversion. (c) Same as (b) but using DCG with $\lambda = 0.1$. The 36 stations are distributed uniformly from -40 to 40 km.

TM TE TM + TEOuter RMS RMS RMS # of # of # of loop DASOCC FWD to FWD to FWD to Iter no. form J_k form J_k form J_k 0 23.19 26.34 24.82 8.38 324 6.71 324 9.27 648 1 2 3.96 324 2.82 324 3.76 648 3 3.93 324 1.54 324 2.13 648 4 4.35 324 324 1.35 648 1.11 0.97 5 3.62 324 324 1.24 648 1.53 324 1.00 648 0.97 324 Total FWD 2268 1620 3888

Table 4. Number of iteration for DASOCC inversion to reach desired level of misfit for TM, TE and joint TM + TE inversions for synthetic test case II.

Note: The number of forward modelling calls (FWD) required for each iteration, and the total over all iterations are also given.

36 stations and nine periods from 0.01 to 100 s with 5 per cent random errors. The model discretization is again 100×31 blocks, and the initial model for all inversion tests is a 50 Ohm-m half-space.

Data space occam's inversion (DASOCC)

Convergence of the DASOCC inversion for the TM, TE and TM + TE modes are shown in Table 4. The result from the joint TM + TE inversion at RMS misfit one is shown in Fig. 4(b) along with results from the comparable DCG inversion. Because the model is more complicated than the first case, the number of main loop iterations is higher: seven, five and six iterations are required to reach the desired target misfit of 1.0 for TM, TE and joint TM + TE inversion, respectively. This results in 2268 (324 \times 7), 1620 (324 \times 5) and 3888 (648 \times 6) forward solutions for the three cases, as listed in Table 4.

Data space conjugate gradient method (DCG)

Next, we apply the DCG method to the same synthetic data sets. Results are summarized in Tables 5(a)–(c). Here, in all case r_{stop} was set at 10^{-2} . For the TE mode, with $\lambda = 0.1$, the inversion converges to below the target misfit in three iterations. Although this is less than what was required by DASOCC, the number of CG steps per outer loop iteration is about 1.5 times the number of stations, and the total number of CG iterations is 119. Thus the total number of forward solutions (2142 = 119 \times 2 \times 9) still exceeds that required by DASOCC (1620). The joint inversion requires 14 outer loop iterations, for a total of 806 CG steps, or 29 016 $(806 \times 4 \times 9)$ forward solver calls. These numbers are huge compared to those required for DASOCC (Table 4). Tests with other values for λ did not yield better results; for λ lower than 0.1 there was generally no convergence. For the TM mode case no value of λ resulted in convergence of the DCG inversion. This example thus illustrates two potential shortcomings of the DCG approach. First, convergence can sometimes be very slow, and DCG may even fail to converge, even in cases where a DASOCC scheme works perfectly well. Second, DCG can be sensitive to the choice of regularization parameter λ , and the optimal choice is seldom known a priori. In the first synthetic example $\lambda = 1$ was optimal, but in the second example DCG worked considerably better with $\lambda = 0.1$. With real

data sets one should plan on running the inversion for a range of values of this damping parameter.

DISCUSSION AND CONCLUSION

We have developed and tested a data space variant on the CG scheme (DCG) for 2-D MT data. The proposed scheme is essentially a GN scheme reformulated in the data space. Solution of the data space equivalent of the standard GN equations is then accomplished with CG, instead of computing the sensitivity matrix, forming the dense data space cross-product matrix, and solving the normal equations using Cholesky decomposition.

A widely perceived advantage of such CG approaches is that because they avoid explicit calculation of the sensitivity matrix, they are faster and computationally more efficient. However, in our numerical tests for 2-D MT data we find that a CG approach generally requires as many or more forward solver calls than an algorithm (DASOCC) which computes the full sensitivity. This is similar to results reported by Rodi & Mackie (2001). In their computational experiments, the numbers of forward solutions used in both their CG based MM and preconditioned NLCG methods were greater than those required for a more conventional GN method. However, they used a model space formulation, and the additional computational time required to form and solve the very large $M \times M$ system of normal eqs (2), made the GN approach slow, especially for large problems. This additional computational time is very significantly reduced when the problem is formulated in the data space, as with the DASOCC approach used here.

One disadvantage of a data space formulation is that there is no analogue of NLCG, which Rodi & Mackie (2001) found to be somewhat more efficient than CG in the late stages of convergence. However, these authors did not find substantial overall performance differences (in terms of forward solver calls required) between NLCG and the model space CG scheme they tested. Thus, it is far from clear that NLCG would require fewer forward calls than a GN approach such as DASOCC. It is possible that as the number of sites N_s is increases DCG may achieve convergence in many fewer than $N_s/2$ iterations, and hence be faster than DASSOC, although this remains to be demonstrated. Furthermore, as the number of sites increases a reduced basis approach such as REBOCC (Siripunvaraporn & Egbert 2000) will also become more favourable.

One advantage of Occam in general, and DASOCC in particular, is that once J_{k} is computed and stored, this system of equations can

Table 5. Number of iterations for the DCG inversion with different values of λ for TM (a), TE (b) and TM + TE (c) inversions, synthetic test case II.

-	Different values of λ ($r_{\text{stop}} = 1.0\text{E-}02$)									
		$\lambda = 0.1$		$\lambda = 1$	$\lambda = 10$					
Outer loop DCG Iter. No.	RMS	No. of CG Iter	RMS	No. of CG Iter	RMS	No. of CG Iter				
(a) TM: Initial RMS = 26.34										
1	8.39	80	8.96	35	9.47	13				
2	4.40	55	3.88	20	5.74	9				
3	3.02	52	2.88	17	5.34	7				
4	3.51	46	2.53	17	5.38	7				
5	2.84	49	2.30	17	5.34	7				
6	3.69	48	2.24	17	5.35	7				
7	2.81	50	2.32	17	5.34	7				
8	3.70	45	2.96	17	5.34	7				
9	2.92	48	3.59	18	5.34	7				
10	3.59	45	5.65	20	5.34	7				
Total CG Iter.		_		_		_				
Total FWD		_		_		_				
(b) TE: Initial RMS = 23.19										
(b) 1E. Illidai KWIS = 25.19	6.92	48	7.12	22	7.84	11				
2	2.50	39	2.53	23 15	4.08	7				
3	0.99	39	1.50	13	3.77	6				
	0.99	32	1.30							
4				13	3.75	6				
5			1.42	13	3.73	6				
6 T + 1 CC I		110	1.42	13	3.73	6				
Total CG Iter.		119		_		_				
Total FWD		2142		_		_				
(c) $TM + TE$: Initial $RMS = 2$										
1	9.53	99	9.32	39	9.31	16				
2	4.08	70	3.88	25	4.86	10				
3	2.55	59	2.56	20	4.23	8				
4	2.10	58	2.23	20	4.21	8				
5	2.13	54	2.05	20	4.19	8				
6	2.83	53	1.97	20	4.19	8				
7	2.18	57	1.94	20	4.19	8				
8	1.83	53	1.94	20	4.19	8				
9	1.47	52	1.94	21	4.19	8				
10	1.42	52	1.94	21	4.19	8				
11	1.19	52	1.94	21	4.19	8				
12	1.18	49	1.94	21	4.19	8				
13	1.08	49	1.94	21	4.19	8				
14	1.01	49	1.94	21	4.19	8				
Total CG Iter.		806		_		_				
Total FWD		29 016		_		_				

Note : For TM, none of the values of λ tested allow the target level of misfit to be reached.

be solved repeatedly for different values of λ . Thus, the Lagrange multiplier λ^{-1} can be used both for damping and for step length control (Parker 1994). This guarantees, at least in theory, convergence to a local minimum of the model norm, subject to the data misfit achieved (Parker 1994). This property cannot be guaranteed for more standard GN-CG or NLCG methods, where λ is independently chosen and left fixed during penalty functional optimization. Because J_k is not explicitly formed and stored in the DCG scheme, we also cannot directly use an Occam style approach. The optimal prior choice of λ is not obvious, and, as shown in our numerical tests, performance of the CG inversion can be greatly influenced by this parameter. Possible approaches to picking λ are given, for example, in Haber et al. (2000). Another idea, which deserves further exploration but is beyond the scope of this paper, would be to use Lanczos tridiagonalization (the basis for CG; Gloub & Van Loan 1989). At the cost of increased memory (required to store all search

directions) the system (3) could then be efficiently solved for a range of values of λ .

For realistic 3-D problems, both model and data sizes become significantly larger. Therefore, DASOCC for 3-D MT inversion (Siripunvaraporn *et al.* 2004; 2005a) requires huge amounts of RAM. For example, in the EXTECH data set (Tuncer *et al.* 2006), $N=16\times131\times4=8,384$ and $M=56\times56\times33=103$ 488, requiring about $8NM\approx7$ Gbyte to store just the sensitivity matrix. This data set thus requires running the 3-D inversion on a workstation or even a supercomputer. Applying DCG to 3-D MT inversion is straightforward, and would allow running large problems such as this on a common desktop PC. However, our 2-D numerical tests suggest that the number of forward modelling calls are actually likely to be larger for DCG, resulting in even longer run times. Clearly there is a trade-off between memory used and CPU run time, and the choice between DASOCC and DCG will depend on the application.

ACKNOWLEDGMENTS

This research has been supported by a grant from the Thailand Research Fund (RSA4780021) to WS, and by DOE-FG0302ER15318 to GE. The authors would like to thank Oliver Ritter (Editor) and two anonymous reviewer for their comments to help improving the manuscript.

REFERENCES

- Barret, R. et al., 1994. Templates for the Solution of Linear Systems: Building Blocks for Iterative Methods, Soc. Ind. Appl. Math., Philadelphia, PA.
- Bennett, A.F., Chua, B.S. & Leslie, L.M., 1996. Generalized inversion of a global numerical weather prediction model, *Meteorol. Atmos. Phys.*, 60, 165–178.
- Constable, C.S., Parker, R.L. & Constable, C.G., 1987. Occam's inversion: a practical algorithm for generating smooth models from electromagnetic sounding data, *Geophysics*, 52, 289–300.
- Egbert, G.D., 1997. Tidal data inversion: interpolation and inference, *Prog. Oceanog.*, 40, 53–80.
- Golub, G. & Van Loan, C., 1989. Matrix Computations, 2nd ed., The Johns Hopkins University Press.
- Haber, E., Ascher, U.M., Aruliah, D.A. & Oldenburg, D., 2000. On optimization techniques for solving nonlinear inverse problems, *Inverse Problems*, 16, 1263–1280.
- Haber, E. & Ascher, U., 2001. Preconditioned all-at-once methods for large, sparse parameter estimation problems, *Inverse Problems*, 17, 1847–1864.
- Mackie, R.L. & Madden, T.R., 1993. Three-dimensional magnetotelluric inversion using conjugate gradients, *Geophys. J. Int.*, 115, 215–229.
- Newman, G.A. & Alumbaugh, D.L., 1996. Three-dimensional massively parallel electromagnetic inversion-I. Theory, *Geophys. J. Int.*, 128, 340– 354.

- Newman, G.A. & Alumbaugh, D.L., 2000. Three-dimensional magnetotelluric inversion using non-linear conjugate gradients, *Geophys. J. Int.*, 140, 410–424.
- Parker, R.L.,1994. Geophysical Inverse Theory, Princeton University Press, Princeton, NJ.
- Press, W.H., Teukolsky, S.A., Vetterling, W.T. & Flannery, B.P., 1992. *Numerical Recipes in FORTRAN: The Art of Scientific Computing*, 2nd ed., Cambridge Univ. Press, Cambridge, UK.
- Rodi, W.L., 1976. A technique for improving the accuracy of finite element solutions for Magnetotelluric data, *Geophys. J. Roy. Astr. Soc.*, 44, 483– 506.
- Rodi, W.L. & Mackie, R.L., 2001. Nonlinear conjugate gradients algorithm for 2-D magnetotelluric inversion, *Geophys.*, **66**, 174–187.
- Sasaki, Y., 2001. Full 3D inversion of electromagnetic data on PC., J. Appl. Geophys., 46, 45–54.
- Siripunvaraporn, W. & Egbert, G., 2000. An efficient data-subspace inversion method for 2-D magnetotelluric data, *Geophysics*, 65, 791–803.
- Siripunvaraporn, W., Uyeshima, M. & Egbert, G., 2004. Three-dimensional inversion for Network-Magnetotelluric data, *Earth Planets Space*, 56, 893–902.
- Siripunvaraporn, W., Egbert, G., Lenbury, Y. & Uyeshima, M., 2005a. Threedimensional magnetotelluric inversion: data space method, *Phys. Earth Planet. Interior.*, 150, 3–14.
- Siripunvaraporn, W., Egbert, G. & Uyeshima, M., 2005b. Interpretation of two-dimensional magnetotelluric profile data with three-dimensional inversion: synthetic examples, *Geophys. J. Int.*, 160, 804–814.
- Zhdanov, M.S., Fang, S., Hursan, G., 2000. Electromagnetic inversion using quasi-linear approximation, *Geophysics*, 65, 1501–1513.
- Tuncer, V., Unsworth, M.J., Siripunvaraporn, W. & Craven, J.A., 2006, Exploration for unconformity-type uranium deposits with audiomagnetotelluric data: a case study from the McArthur River mine, Saskatchewan, Canada, *Geophysics*, 71, B201–B209.

Exploration for unconformity-type uranium deposits with audiomagnetotelluric data: A case study from the McArthur River mine, Saskatchewan, Canada

Volkan Tuncer¹, Martyn J. Unsworth¹, Weerachai Siripunvaraporn², and James A. Craven³

ABSTRACT

Unconformity-type deposits supply a significant amount of the world's uranium and consist of uranium that is generally codeposited with graphite in a fault zone. The low resistivity of the graphite produces a significant contrast in electrical resistivity, which can be located with electromagnetic (EM) methods. The Athabasca Basin in Western Canada hosts significant uranium deposits, and exploration in deeper parts of the basin has required the application of new EM methods. This paper presents an evaluation of the audiomagnetotelluric (AMT) exploration method at the McArthur River mine in the Athabasca Basin. AMT data were collected at 132 stations on a grid, and two-dimensional (2D) and three-dimensional (3D) inversions were used to generate resistivity models. These models showed two major results: (1) a significant conductor coincident with a major basement fault (P2) and the uranium deposits (this conductor begins at the unconformity at a depth of 550 m and extends to a depth of at least three km) and (2) a resistive halo which might be caused by the silicification associated with mineralization. However, synthetic inversions showed that this halo could be an artifact of smoothing function in the inversion scheme. The 2D inversions were validated by synthetic inversions, comparison with the 3D inversion models, and correlation with well-log information. 3D AMT forward modeling showed that strong 3D effects are not present in the AMT impedance data. Induction vectors showed more evidence of complexity, but the inclusion of these data in the inversion improved subsurface resolution.

INTRODUCTION

Unconformity-type deposits are a major source of uranium. The Athabasca Basin, located in northwest Saskatchewan and northeast Alberta, produces one-third of the Western world's uranium (Jefferson et al., 2003). As exploration has proceeded, many of the shallowest deposits have been mined out, and exploration has moved into deeper parts of the basin. This is challenging existing exploration methods, and government and industrial partners initiated the EXTECH-IV (EXploration science and TECHnology initiative) project to develop new techniques for locating unconformity-type uranium deposits. The EXTECH-IV project has included a range of geophysical and geological studies (Jefferson et al., 2003). Most of the geophysical studies took place at the McArthur River mine, which hosts the largest known high-grade uranium deposit in the world

Electrical and electromagnetic (EM) methods are widely used in mineral exploration and have played an important role in uranium exploration in the Athabasca Basin (McMullan et al., 1987; Crone, 1991). The uranium deposits are found where basement faults intersect the unconformity (Figure 1). Because graphite is commonly found in the faults, the resulting low electrical resistivity often allows detection with EM methods. However, not all unconformitytype uranium deposits occur above or within graphitic faults. As part of the EXTECH-IV project, alternative EM methods were evaluated to determine if they could map basement conductors at depth in the Athabasca Basin. One such method is the audiomagnetotelluric (AMT) method, which uses natural EM signals to image the upper 1-2 km of the subsurface. In contrast to loop-loop EM methods and the controlled-source audiomagnetotelluric (CSAMT) method, AMT is logistically simple because no transmitter is required. In this paper, a pilot AMT survey over a known uranium deposit is described.

Manuscript received by the Editor May 4, 2005; revised manuscript received March 7, 2006; published online October 3, 2006.

¹University of Alberta, Department of Physics, Edmonton, Alberta, Canada. E-mail: vtuncer@phys.ualberta.ca; unsworth@phys.ualberta.ca.

²Mahidol University, Department of Physics, Faculty of Science, Bangkok, Thailand. E-mail: scwsp@mahidol.ac.th.

³Geological Survey of Canada, 601 Booth Street, Ottawa, Ontario, Canada. E-mail craven@NRCan.gc.ca.

© 2006 Society of Exploration Geophysicists. All rights reserved.

B202 Tuncer et al.

GEOLOGIC SETTING AND MINERALIZATION

At the McArthur River mine, the near-surface structure is characterized by overburden that is up to 100 m thick. The underlying Athabasca Group rocks (Figure 1) are sandstones and conglomerates of late paleo- to Meso-Proterozoic age (Ruzicka, 1996). Beneath the unconformity, the crystalline (gneissic) basement comprises the 2.5-2.6-Ga (billion years ago) Wollaston Group (McMullan et al., 1987). Uranium deposits in the Athabasca Basin are structurally controlled by the Paleo-Proterozoic (sub-Athabasca) unconformity and faults that exhibit a northeastern or eastern strike (Ruzicka, 1996). The uranium orebodies range in shape from massive subhorizontal lenses at the unconformity to veins and veinlets in the fault zones (Ruzicka, 1996). The deposits formed where oxidizing basinal fluids carried uranium from the sandstone and reducing fluids carried other minerals (such as silica) from the basement rocks to the unconformity through the fault (Figure 1). This deposited uranium at the top of the fault near the unconformity; silicification occurs above the unconformity because of the fluid flow. Prior to uranium ore deposition, intense silicification developed where ascending fluids flooded the sandstone with quartz. Significant silicification surrounds the ore deposit at the McArthur River, although most other Athabasca Basin deposits are surrounded by extensive zones of quartz dissolution (Ruzicka, 1996). In addition, a thin alteration halo of quartz dissolution and illite clay alteration was formed around the uranium deposit (Ruzicka, 1996). Mwenifumbo et al. (2004) suggested that at McArthur River, silicification is localized between the unconformity and a depth of 375 m. Limited alteration has occurred in the basement gneisses (Ruzicka, 1996), and hydrothermal clay alteration is spatially limited at McArthur River (Mwenifumbo et al., 2004).

Polymetallic deposits (U-Ni-Co-As) occur more often within the unconformity, although monometallic deposits occur either below or rarely above the unconformity. The monometallic-type McArthur River P2 North deposit is the only known exception from this rule

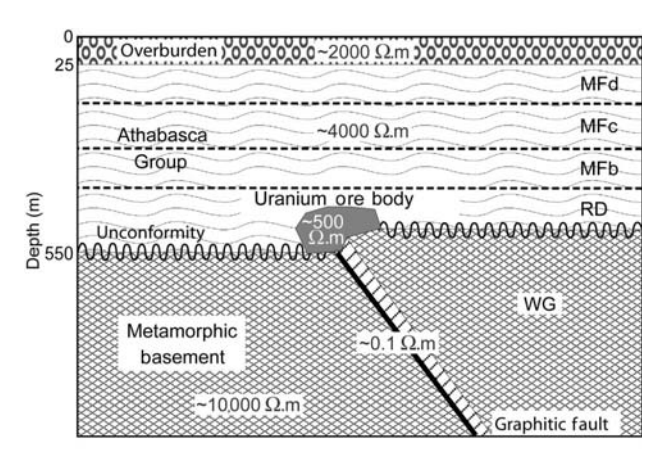


Figure 1. Generic model of an unconformity-type uranium deposit in the Athabasca Basin (after McMullan et al., 1987; Mwenifumbo et al., 2004). The Athabasca Group consists of four major units from bottom to top. The Read Formation (RD, formerly MFa) comprises discontinuous basal conglomerate, intercalated coarse sandstone, conglomerate and red mudstone. The Manitou Falls Formation comprises MFb: interbedded conglomerate and pebbly sandstone; MFc: granule sandstone; and MFd: medium-fine sandstone with mudstone intraclasts. WG is the Wollaston Group.

(Ruzicka, 1996). Pods of the McArthur River P2 North deposit extend 60 m downdip along the P2 fault zone from immediately beneath the unconformity in the footwall and just above the P2 reverse fault in the nose of the uplifted hanging wall basement wedge. This southeast-dipping reverse fault offsets the basement by 60–80 m. The approximate size of the orebody is 100 m long, 10 m wide, and 60 m high, and is located between depths of 500 and 600 m (Ruzicka, 1996).

PREVIOUS GEOPHYSICAL STUDIES

A significant amount of geophysical data has been acquired at the McArthur River deposit, both before and during the EXTECH-IV project. Gravity studies were used to map the depth of the unconformity and to locate zones of alteration (Wood and Thomas, 2002). However, nonuniqueness restricts the ability of gravity data to distinguish between silicified and desilicified zones that might be associated with underlying ore deposits. Seismic reflection data were able to image the unconformity and faults that offset it but did not detect the uranium orebody or graphite directly (Hajnal et al., 2002; White et al., 2002; White et al., 2003). The faults that underlie the uranium deposits are often graphitic. Electrical and EM methods have been used to locate them in the Athabasca Basin. In shallow parts of the basin, basement conductors have been located with direct current (dc) resistivity, transient electromagnetic methods, horizontal-loop EM method (HLEM), and very-low-frequency (VLF) data (Craven et al., 2003). These methods are convenient for shallow exploration but less effective where the target depth exceeds 500 m.

To explore deeper parts of the Athabasca Basin, other EM methods must be used. The pulse EM method (DEEPEM) was used over the Cigar Lake deposit and defined a conductor at a depth of 450 m, but exploration was complicated by the low-resistivity regolith (Crone, 1991). Controlled-source EM exploration at greater depth requires larger loops to be used and thus increases the logistical effort and cost. As exploration expands into the deeper part of the Athabasca Basin, alternative EM methods are needed for effective and economical exploration. The audiomagnetotelluric (AMT) method uses natural EM signals to image near-surface structures. With improved magnetic sensors, it is no longer necessary to use a controlled source, and this has reduced the cost and increased the use of this technique in recent years. Recent applications of AMT in mineral exploration include studies by Livelybrooks et al. (1996), Chouteau et al. (1997), and Jones and Garcia (2003). The EXTECH-IV study described in this paper evaluated the role that AMT could play in uranium exploration in the Athabasca Basin. It was anticipated that AMT could locate basement conductors and determine their depth.

AMT DATA ACQUISITON

AMT data were recorded in 2002 by Geosystem SRL at 132 stations on 11 profiles that crossed the P2 fault (Figure 2). Data collection used Metronix AMT systems, and the magnetic fields were measured with BF-6 and BF-10 induction coils produced by Electro-Magnetic Instruments. The distance between profiles was approximately 800 m, and the station spacing was approximately 300 m. Electric-field dipoles were 50 m in length, and time series were recorded with sampling rates of 40,960, 4096, and 256 Hz. Usable AMT data were obtained over the frequency range 10,200–3 Hz. Coherent time-series segments from each sampling rate were select-

ed automatically for robust analysis to reduce the effects of bias because of noise. An iterative reweighting scheme was used to provide a robust estimate of the apparent resistivities and phases (Larsen et al., 1996).

AMT DATA ANALYSIS

The dimensionality of the AMT data was investigated using tensor decomposition (McNeice and Jones, 2001). In the frequency range of 1000-1 Hz, the geoelectric strike direction is well defined as 45° and parallel to the P2 fault direction (Figure 3). Figure 3 shows the spatial distribution of the rms misfit obtained by the decomposition, and the relatively low values (less than one) suggest that a 2D interpretation was valid. All data then were rotated to a coordinate system with the x-axis in the N45°E direction. Apparent resistivities can be computed from the along-strike electric currents (TE mode) and also from the across-strike electric currents (TM mode). Over a 2D earth, these two modes give different apparent resistivity values and are sensitive to different aspects of the subsurface structure. The TE mode is the most sensitive to along-strike conductors, whereas the TM mode is the most sensitive to resistors and shallow structure (Berdichevsky et al., 1998). AMT data for these two modes are illustrated in pseudosections for line 224 in Figure 4, which shows limited site-to-site variation in apparent resistivity in TE mode because the electric field is parallel to the geoelectric strike. The TM-mode pseudosection shows more site-to-site variation because near-surface bodies strongly affect the apparent resistivity. In the TE-mode pseudosection, the location of the conductor is indicated by generally lower apparent resistivities in the center of the profile. Sample data curves of apparent resistivity and phase from different locations are shown in Figure 5. Note that the TM-

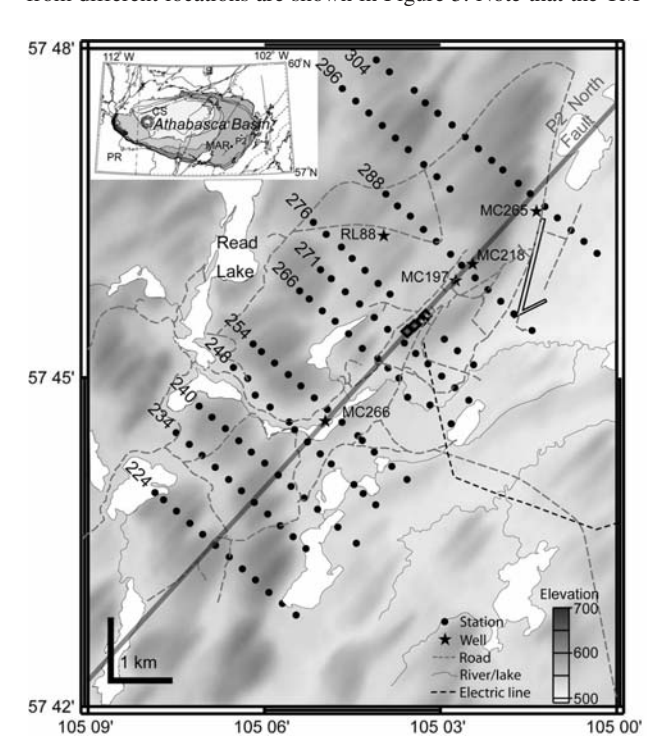


Figure 2. AMT station locations used in the McArthur River AMT survey. Black diamonds on the P2 North Faultline between lines 271 and 276 show the uranium ore pods. (MAR: McArthur River CS: Carswell structure; PR: Phanerozoic rocks, P2: P2 North fault).

mode data are less sensitive to the presence of the basement conductors than the TE-mode data. The TE-mode electric currents generate a vertical magnetic field (H_z) , that is related to the horizontal magnetic fields by

$$H_z = T_{zx}H_x + T_{zy}H_y, \tag{1}$$

where T_{zx} and T_{zy} are components of the magnetic field transfer function (tipper). This real transfer function changes sign above a conductor, as observed in Figure 4, with positive values on the left of the conductor and negative signs on the right. This sign reversal at 1.5 km indicates the horizontal location of the conductor. These transfer functions can also be displayed as induction vectors at a given frequency. In the convention of Parkinson (1959), the real part of the induction arrow points toward a conductor. Figure 6 shows the real induction vectors at a frequency of 100 Hz, which sample the subsurface to a depth of approximately 2 km. The direction of the vectors on most profiles shows a reversal, marking the location of a basement conductor. Induction vectors parallel to the profile are an indication of a 2D resistivity structure and are observed on lines 224-248. The situation is more complex to the north, and the induction vectors are at a significant angle to the strike direction. Note that induction vectors show more evidence of 3D behavior than the tensor decomposition. This can be explained because AMT impedances are primarily sensitive to structure below the station, whereas vertical magnetic fields are most sensitive to structures located to one side.

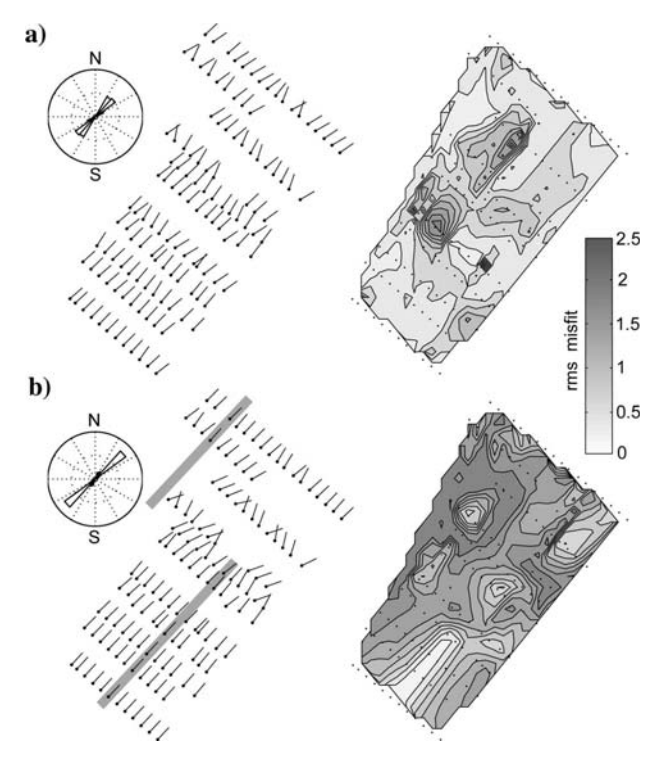


Figure 3. Results of tensor decomposition for real data and synthetic 3D model over frequency range 1000–1 Hz. (a) Shows best-fitting strike direction in map format and the misfit obtained by the tensor decomposition. Low misfit values indicate the 2D assumption is well satisfied. (b) Same quantities for synthetic data generated for a 3D resistivity model. Gray rectangular bars show the locations of conductors in the 3D synthetic models.

B204 Tuncer et al.

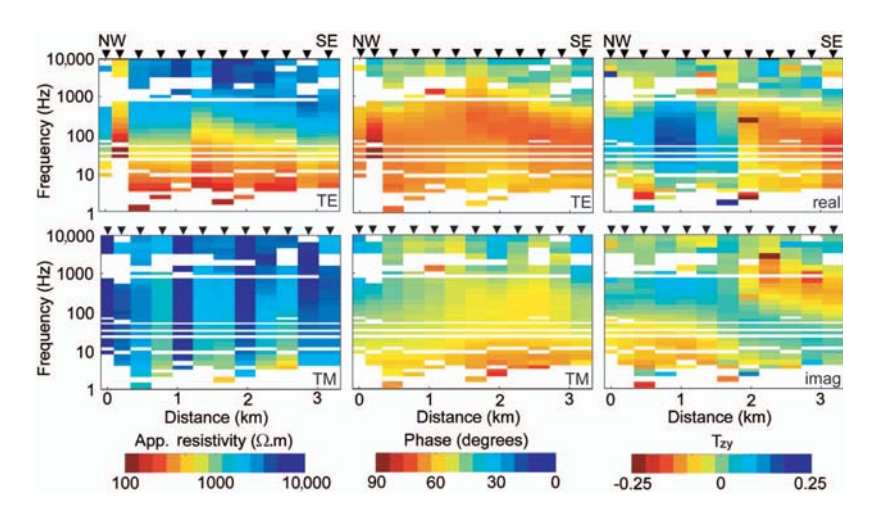


Figure 4. Pseudosections for TE, TM, and magnetic field transfer function data from line 224.

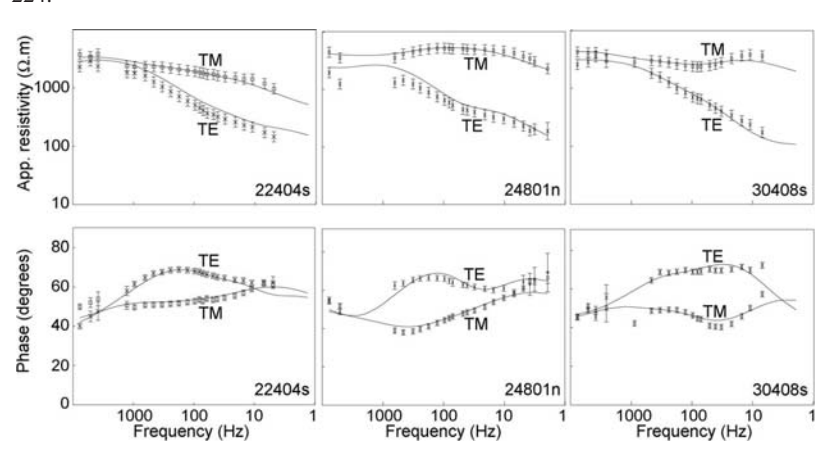


Figure 5. Sample data curves of TE and TM-mode for stations on lines 224, 248, and 304. Continuous lines show the response of the inversion models in Figure 9.

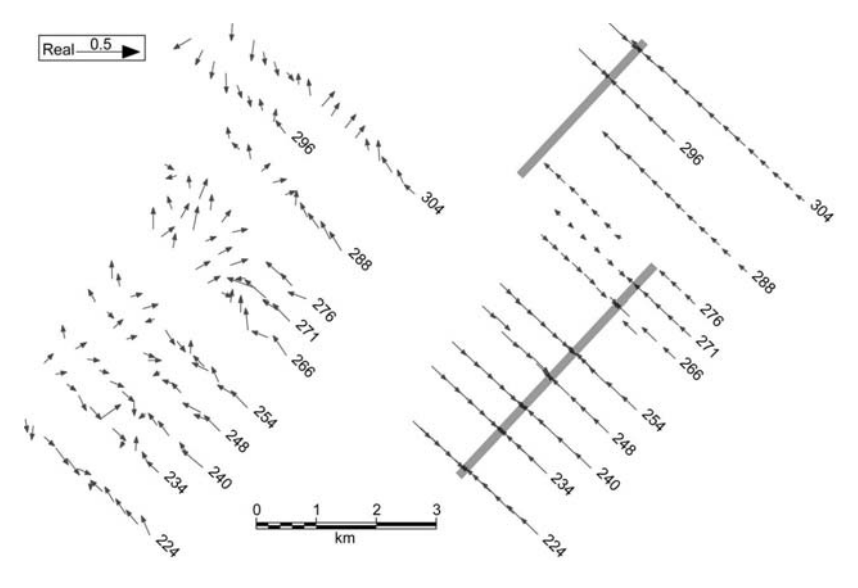


Figure 6. (a) Induction vectors at 100 Hz frequency. Note the real induction vectors point at a conductor. (b) Synthetic induction vectors for a simple 3D model. Gray-shaded rectangular bars show the locations of basement conductors.

INVERSION OF AMT DATA

Two-dimensional inversion

The dimensionality analysis and the similarity of the pseudosections for adjacent profiles suggest that a 2D analysis is valid for these AMT data. For each profile, AMT data were inverted using the nonlinear conjugate gradients (NLCG) algorithm of Rodi and Mackie (2001). This inversion seeks a resistivity model that fits the observed AMT data and which also satisfies a specified regularization function. This generally requires a spatially smooth model but can also include other requirements. AMT data for each profile were inverted with the NLCG6 algorithm. Separate inversions of the TE mode, TM mode, and T_{zy} were used to check the internal consistency of the AMT data (Figure 7). The TE mode is most sensitive to along-strike conductors and clearly images a conductor in the center of profile 224, although the TM mode does not image the conductor at all. The T_{zy} data locate the horizontal position of the conductor but do not determine its depth. To obtain a reliable image of subsurface resistivity, joint inversion of all data is required and gives a sharper image of the basement conductor (Figure 7). The fit of the model response to the measured data is shown at selected stations in Figure 5, and the fit at other stations is of similar quality. Static shifts encountered in the data were small, and it was not necessary to correct for them explicitly. The error floors used in these inversions for apparent resistivity, phase, and tipper are 20%, 5%, and 0.025, respectively. Lower error floors were also applied to the apparent resistivity, but models were rougher with low error floors (e.g., 10%). Simultaneous inversion of all data gave very similar models to those obtained by a sequential approach (TE or TE-TM first, then TE-TM- T_{zv}). Resistivity models and misfits for all profiles are shown in Figures 8 and 9. Around the mine area, the rms misfit values are higher but still acceptable. The TE-TM and TE-TM- T_{zy} inversions appear to be similar except for line 276 (Figure 9). The TE-TM inversion gives a better fit to the data (Figure 8), but the model differs from the other TE-TM models. This might be because of the gap on line 276 or because the mine is located on this profile and cultural noise may have degraded the quality of the AMT data. However, this is not seen on the chosen time series data around the mine.

As noted earlier, the induction vectors for the northern profiles (lines 266-304) suggest a departure from a simple 2D geometry. Thus, tipper data from the northern profiles must be used with caution. Although the TE-TM- T_{zy} results give low rms misfits for profiles 224–254, the TE-TM inversion is more reliable for the other profiles. The rms misfits shown in Figure 8 also support this

idea because the TE-TM- T_{zy} inversions have smaller rms misfits for line 224, possibly because of the two-dimensionality indicated by the profile parallel induction vectors. The rms misfits are higher for the TE-TM- T_{zy} inversions where the induction vectors are not parallel to the profile, perhaps indicating 3D or anisotropic effects in the data.

To examine the robustness of the inversion models, a range of inversions was performed with different control parameters α and τ . The smoothing parameter τ controls the trade-off between fitting the AMT data and producing a spatially smooth model. The parameter α controls the ratio of horizontal and vertical smoothness. The resistivity models in Figure 9 were obtained with default parameters ($\tau=10$ and $\alpha=1$) that gave results typical of a range of α and τ values.

The conductor imaged in the inversions is located in the basement with the top at a depth of 500 m and extending to a depth of at least

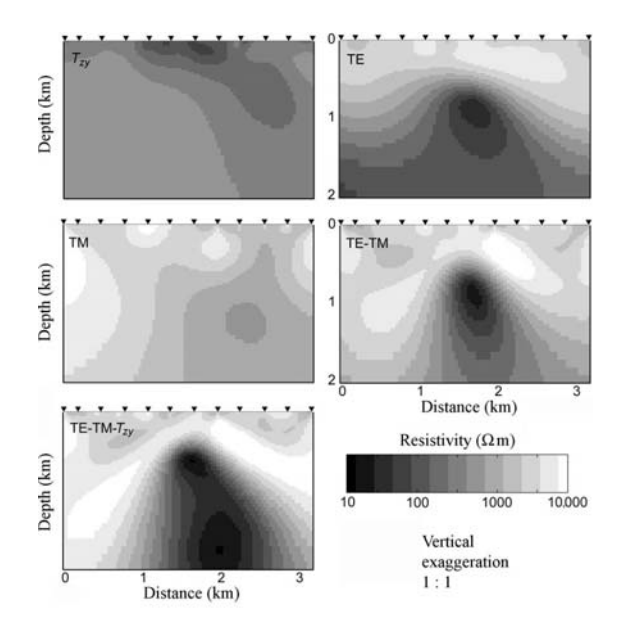


Figure 7. Resistivity models derived for profile 224 with 2D AMT inversions. The inversions for line 224 give the following root mean square (rms) misfits: T_{zy} only 1.125, TE only 2.152, TM only 0.833, TE-TM 1.703, and TE-TM- T_{zy} 1.687. An ideal misfit would be in the range of 1.0–1.5, but these values are certainly acceptable.

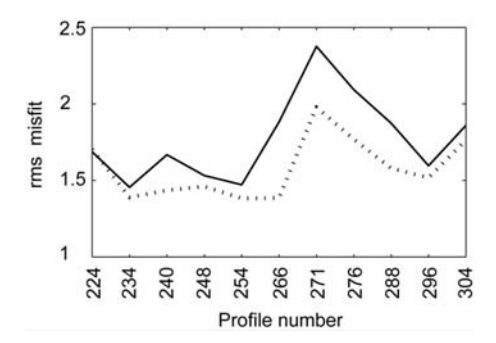


Figure 8. Root-mean-square (rms) misfit values for the TE-TM (dashed) and TE-TM- T_{zy} (solid) inversions for each profile.

2 km. In the southwestern part of the survey area, the conductor appears to dip to the southeast. Around the mine, the conductor is weaker, but the AMT data from these profiles are lower in quality than data from other profiles. In the northeastern part of the survey area, two basement conductors are imaged. The second stronger conductor could be another graphitic fault northwest of the main conductor (P2 reverse fault). The inversion results suggest that this second conductor may extend to the southwest, because the same feature can be seen just beyond the NW end of the models for profiles 224-248 (this part of the models is not shown in Figure 9). The induction vectors (Figure 6) also indicate the presence of these conductors. This is clear at 100 Hz, where induction vectors at the NW

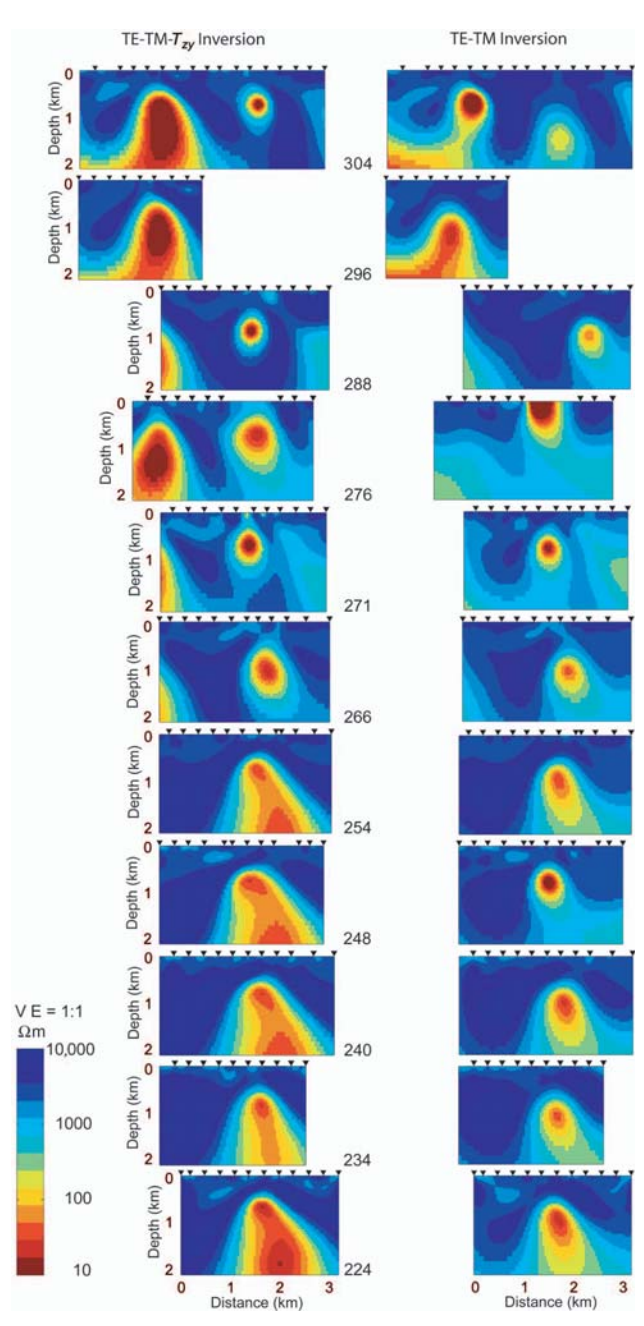


Figure 9. Resistivity models for all profiles derived with 2D inversion.

B206 Tuncer et al.

end of lines 240, 248, 254, 266, and 271 may indicate another conductor

The other feature that is obvious in Figure 9 is a resistive halo (5000–10,000 Ω .m) that appears above and on the sides of the basement conductor. This feature is clearest on lines 224-254. This feature could be caused by the silicification or alteration associated with uranium ore formation. However, it could be an artifact of the regularization used in the inversion, because of the high resistivity contrast between the graphite conductor and the host rock.

3D inversion

The validity of the 2D inversions was investigated by performing a 3D inversion of the whole AMT data set using the algorithm of Siripunvaraporn et al. (2005a). The off-diagonal components of the impedance tensor at 16 frequencies and 131 sites were inverted using an impedance error floor of 5%. The inversion started from a 1000 Ω .m half-space and the vertical-to-horizontal smoothing ratio was set to unity. The initial and final rms misfits of the 3D inversion were 5.56 and 1.38, respectively. Figure 10 shows a comparison of the 2D and 3D inversion models with borehole log data. Note that the

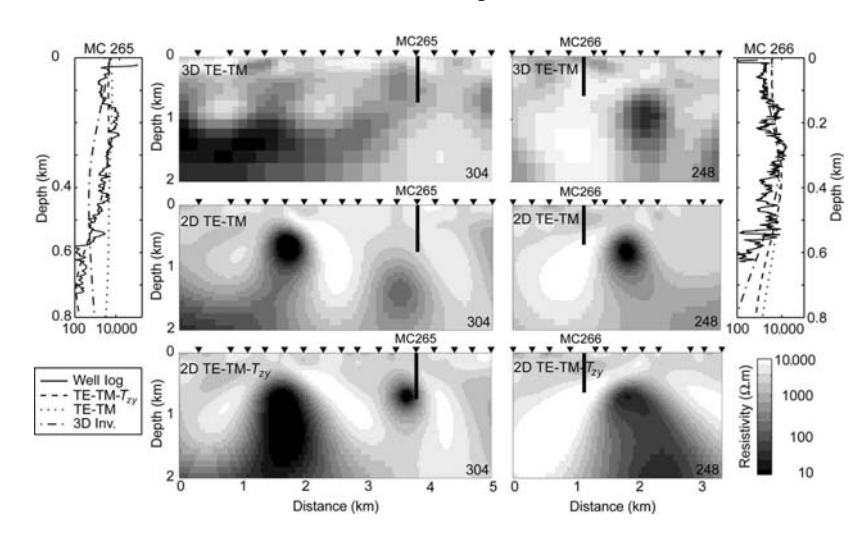


Figure 10. Comparison of 2D and 3D inversion results for lines 248 and 304. Comparison with resistivity in adjacent borehole logs is also shown.

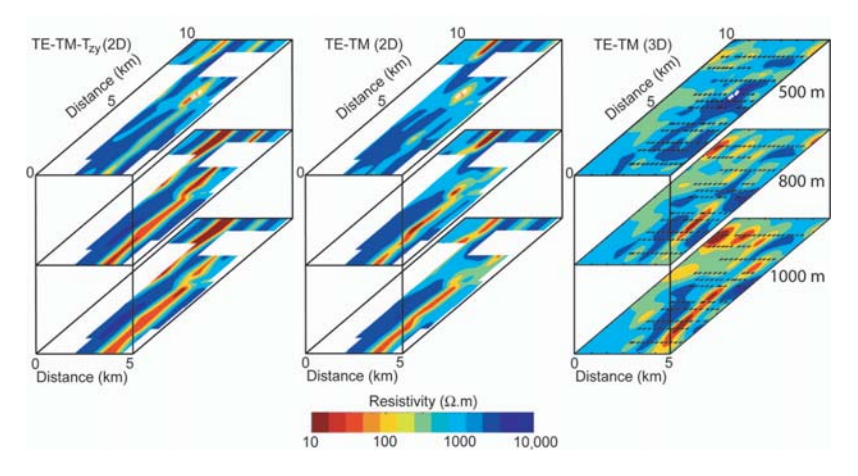


Figure 11. Comparison of the horizontal slices of the 2D and 3D inversion models. The white rectangles show the locations of the uranium pods.

3D inversion did not include the T_{zy} data. Resistivity values in the 2D and 3D models agree well in the center of the array (line 248), where both the 2D and 3D models are compatible with borehole log results. Significant differences are observed between the 2D and 3D models for line 304. These differences may be a consequence of profile 304 being on the edge of the grid of AMT data.

The 3D and 2D inversion models can also be compared as horizontal slices for different depths (Figure 11). Both inversions show that the basement conductor, the surrounding resistive halo, and all other significant model features are similar below 500 m. The conductor appears stronger in the TE-TM- $T_{\rm zy}$ inversion than in the other two results, probably because the $T_{\rm zy}$ data are primarily sensitive to the basement conductor.

VALIDATION OF INVERSION MODELS

Comparison of resistivity model with borehole logs

Extensive borehole data were acquired at the McArthur River Mine (Mwenifumbo et al., 2004). Five resistivity logs are compared

with the 2D and 3D AMT inversion models in Figure 12. A 7-point moving average filter was applied to the borehole log data to allow a more objective comparison of the two measures of subsurface resistivity. The agreement between well logs and the 2D and 3D resistivity models is acceptable in the shallow wells (MC197, MC218, and RL088). However, at depths below 300 m, there are significant differences between the 2D and 3D models that may be a consequence of how deeper structure is smoothed into shallower structure. MC265 and MC266 extend deeper and terminate in a zone of lower resistivity (100 Ω .m) that is well resolved in the 2D inversion model. The 3D model agrees with the well log and 2D inversion at MC266, but agreement is poorer at MC265, perhaps because of the location of this well at the edge of the survey grid. Overall, acceptable agreement is observed between well logs and 2D inversion models. However, the basement conductor is not sampled by the well logs, and this feature dominates the spatial smoothness of the whole resistivity model. As a consequence, the different regularization used in the 2D and 3D inversion is likely the result of the differences between the 2D and 3D models.

Synthetic 2D AMT inversions

The sensitivity of the inversion models to the measured AMT data was investigated through synthetic inversions. This procedure can reveal whether features in the resistivity models are required by the AMT data or are artifacts of the inversion. Generic resistivity models were created that contain the basic resistivity features of the ore deposit. Forward modeling was then used to compute the predicted AMT data, and 5%–10% Gaussian noise was added. Then, the synthetic AMT data were inverted, using the same parameters as in the inversions of field AMT data. Many

models were considered; two representative models are shown in Figure 13. The first synthetic model represents a basement conductor, with a modest resistivity contrast across the unconformity. Figure 13 show the results of different values of α , the factor that controls the ratio of horizontal and vertical smoothness. Larger α values generate horizontal structures, and smaller values of α yield vertical structures. Because the target body in this study is a vertical, or steeply dipping, conductor, α less than one is clearly appropriate. Increasing α gives higher rms misfit values because a horizontally smooth model is incompatible with the original model. Note that the AMT inversion does not recover the correct width of the conductor. The smoothing reflects the diffusive physics of AMT exploration, and small features cannot be recovered properly. The parameter τ controls the trade-off between fitting the data and producing a spatially smooth model. Increasing τ results in a smoother model (Figure 1) and the producing a spatially smooth model. Increasing τ results in a smoother model (Figure 2) and the producing a spatially smooth model. Increasing τ results in a smoother model (Figure 2) and the producing a spatially smooth model. Increasing τ results in a smoother model (Figure 2) and the producing a spatially smooth model is a smoother model (Figure 2).

ure 13), and very small τ values produce a rough model with a second conductor above the basement conductor. This second conductor is clearly an artifact.

The synthetic inversion studies suggest that the values $\alpha=1$ and $\tau=10$ are most suitable for inversion of the field AMT data. They also show that the measured AMT data can image structures up to a depth of 2 km. Other synthetic inversions showed that the AMT data are relatively insensitive to the dip of the basement conductor. Synthetic inversions were also used to study whether the AMT data could image the structure of the alteration chimney suggested by McMullan et al. (1987). The synthetic inversion study shows that a chimney could be resolved by the AMT data. The absence of such a feature in Figure 9 suggests a low-resistivity chimney is absent at McArthur River.

Finally, synthetic inversions were used to determine if a halo of silicification could be imaged with AMT data. The model in Figure 13b includes a simple basement conductor. The synthetic inversion produces a high-resistivity halo around the basement conductor. As previously described, this is a consequence of the regularization imposed on the model during inversion. Observing a resistive halo in an inversion model does not imply that one is present in the subsurface. However, AMT data are sensitive to a resistive zone above the unconformity (Craven et al., 2003).

3D forward modeling

Three-dimensional forward modeling was used to determine if the 2D inversion results are valid in a 3D geoelectric environment. The algorithm of Mackie et al. (1994) was used and the parameterization tested by comparison with 2D modeling. The basic question to be addressed is the 3D effect of the end of the conductors on 2D inversions. A suite of models similar to that shown in Figure 14 was generated; it represents the geoelectric structure typical of the McArthur River area. An overburden layer (2000 Ωm)

overlies sandstones (4000 Ω m) with 10,000 Ω m basement below the unconformity. Graphitic conductors (0.1 Ω m) are present in the basement and denoted with gray shading.

Figure 14 shows the apparent resistivity and phase curves at selected locations. The end effect is very strong on the TE mode at the north end of the conductor at site A and weaker at site B on line 224. Note that because electric charges develop on the end of the conductor in the 3D model, the TE apparent resistivity is increased at low frequency, even exceeding the TM-mode apparent resistivity. Thus, TE-mode data must be used with caution in a 3D environment (Wannamaker et al., 1984; Siripunvaraporn et al., 2005b). However, the TE mode must be used in this example because the conductor is essentially invisible to the TM-mode AMT data. However, the measured AMT data do not show the effect described above, and the TE-mode apparent resistivity is always less than the TM mode at all sta-

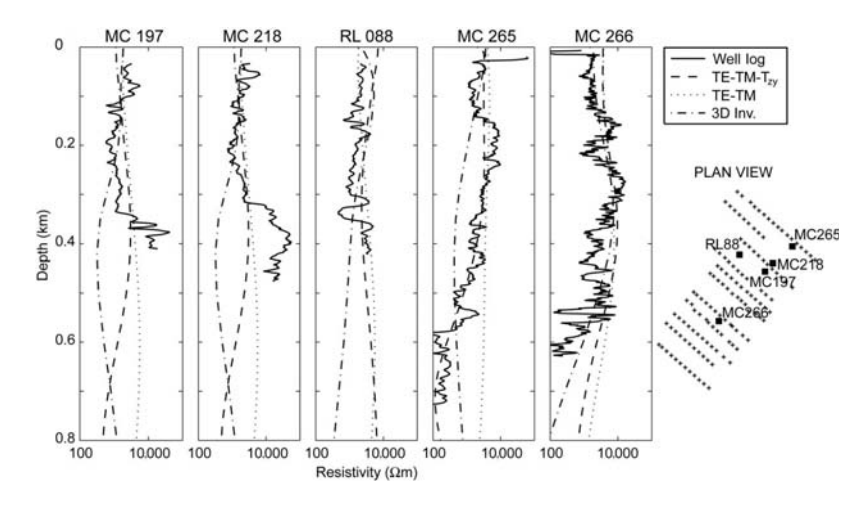


Figure 12. Comparison of borehole-log resistivity data (from Mwenifumbo et al., 2004) and inversion of 2D and 3D models.

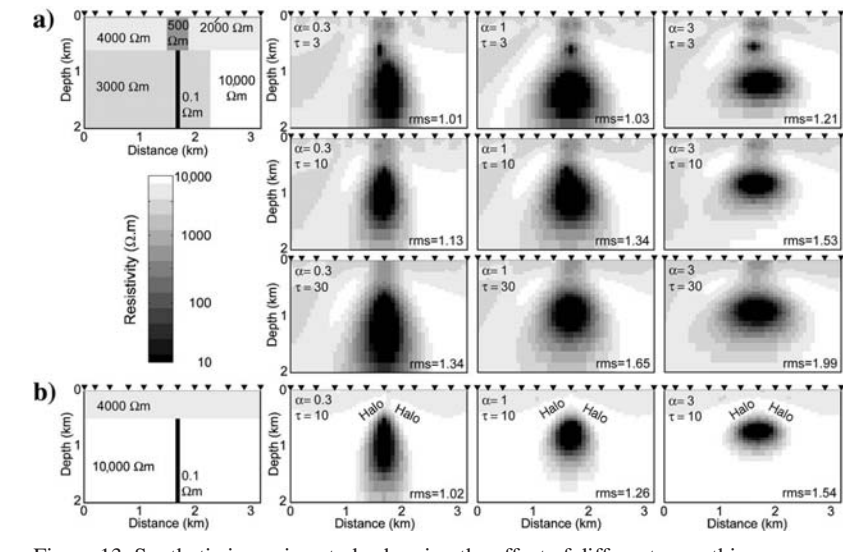


Figure 13. Synthetic inversion study showing the effect of different smoothing parameters. (a) The first model represents the alteration chimney (500 Ω m) beneath the 25-m-thick 2000- Ω m resistive overburden and shows resistivity contrast across the fault with different smoothing parameters. (b) The second model on the bottom row shows a basic two-layer model with a graphitic conductor that has an artificial resistive halo around the conductor.

B208 Tuncer et al.

tions (Figure 5). This strongly suggests that major 3D effects are not present in the field data and the McArthur River AMT data are largely two dimensional. Thus, if the basement conductor terminates close to a profile, a two dimensional inversion is not valid because the difference between the 2D and 3D forward responses is significant (Figure 14). This suggests that the resulting inversion model (Figure 15), with a graphitic conductor which terminates at the unconformity and dips to the east, is valid.

Tensor decomposition is widely used to determine if a 2D interpretation of an AMT data set is valid. Figure 3 shows the results of tensor decomposition for the synthetic data generated for the model in Figure 14. As expected, a strike direction parallel to the basement conductors is determined far from the ends, although a more complex pattern is observed close to the ends. Note that the degree of scatter in the synthetic strike directions is quite similar to that observed in the real AMT data (Figure 3). Figure 3 also shows the rms misfits, and they are significantly higher than values obtained for the field data. The rms misfit may represent a more reliable test than the

10

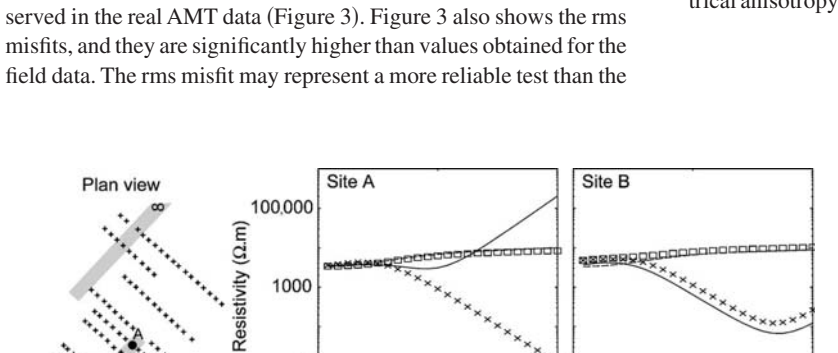
60

30

0 10,000

Phase (degrees)

2D TE



Frequency (Hz)

Figure 14. A 3D forward modeling study to investigate if 3D effects are present in the AMT data. Gray rectangular bars represent graphitic conductors; dark gray circles show station locations for this exercise. The apparent resistivity and phase data are shown at stations A and B for 2D and 3D resistivity models.

100

100

1 10.000

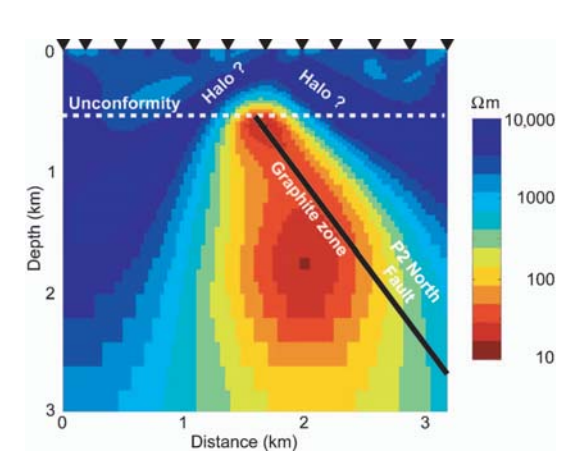


Figure 15. Interpretation of the resistivity model derived from a 2D inversion of the TE-TM- T_{zy} data for profile 224.

strike diagrams to determine if field AMT data can be considered two dimensional.

Induction vectors were also used to assess the dimensionality of the real and synthetic AMT data. In a 2D scenario, induction vectors are orthogonal to the geoelectric strike (i.e., parallel to the profiles). Figure 6 shows that 3D effects are only observed in the induction vectors close to the ends of the conductors. The scatter of induction vectors is much less in the synthetic AMT data than in the measured AMT data. A range of other models with different geometries of basement conductors were also analyzed, and none could reproduce the observed pattern with some vectors parallel to the basement conductors. The non-2D pattern in the measured induction vectors is likely because of surficial resistivity structures outside the survey area or another conductor northeast of the survey area. Alternatively, the pattern of orthogonal induction vectors might be caused by electrical anisotropy in the basement rocks (Heise and Pous, 2001).

CONCLUSIONS

This study has shown that AMT exploration is an effective tool for mapping basement conductors to a depth of 2-3 km in a setting such as the Athabasca Basin. The P2 basement conductor imaged with AMT in this study terminates at the unconformity and may dip to the east. The resistivity model is also consistent with a zone of silicification above the orebody, but it is possible that this feature may be an artifact of the inversion algorithm. The uranium orebodies are not imaged directly because of their small size and the lowresistivity contrast between the uranium ore and graphite in the fault zone. In the type of geometry encountered in this region, the 2D inversion appears to recover subsurface resistivity with confidence, and a full 3D inversion may not always be needed. In locations where the induction vectors indicate a 2D structure, the vertical magnetic field data add useful information to the inversion and enhance its resolution. However, the vertical magnetic field data must be used with caution. Severe 3D effects can be expected in the AMT apparent-resistivity and phase data at the ends of basement conductors.

ACKNOWLEDGMENTS

AMT data collection was funded by Cameco Corporation, AREVA subsidiary COGEMA Resources Inc., the Geological Survey of Canada, and Geosystem Canada. Data analysis at the University of Alberta was supported by research grants to Martyn Unsworth from NSERC and the Alberta Ingenuity Fund. Alan Jones and Gary McNeice are thanked for the use of their tensor decomposition software. We also thank Wen Xiao, Erşan Türkoğlu, and Wolfgang Soyer for their contributions and helpful discussions. The 3D inversion at Mahidol University was supported by a research grant from the Thailand Research Fund (RSA4780021) to Weerachai Siripunvaraporn. This manuscript benefited greatly from comments by Dan Brisbin, Charlie Jefferson, and Brian Powell. Reviews by editors George Jiracek and Randy Mackie improved the paper.

REFERENCES

- Berdichevsky, M. N., V. I. Dmitriev, and E. E. Pozdnjakova, 1998, On twodimensional interpretation of magnetotelluric soundings: Geophysical Journal International, 133, 585-606
- Chouteau, M., P. Zhang, D. J. Dion, B. Giroux, R. Morin, and S. Krivochieva, 1997. Delineating mineralization and imaging the regional structure with magnetotellurics in the region of Chibougamau (Canada): Geophysics, 62,
- Craven, J. A., G. McNiece, B. Powell, R. Koch, I. R. Annesley, G. Wood, and C. J. Mwenifumbo, 2003, First look at data from a three-dimensional audiomagnetotelluric survey at the McArthur River mining camp, northern Saskatchewan: Geological Survey of Canada Current Research, C25, accessed August 2006 (http://dsp-psd.communication.gc.ca/Collection/ GSC-CGC/M44-2003/Articles/c25.pdf). Crone, J. D., 1991, PEM case histories, Cigar and Winston Lakes, Canada, in
- M. N. Nabighian ed., Electromagnetic methods in applied geophysics, vol. 2: SEG, 49Õ–494.
- Hajnal, Z., E. Takacs, D. White, B. Reilkoff, B. Powell, and R. Koch, 2002, Regional seismic images beneath the McArthur River ore bodies, Saskatchewan, *in* Summary of investigations 2002, vol. 2: Saskatchewan Geological Survey, Saskatchewan Industry Resources, Miscellaneous Report 2002–4.2, Paper D-4, accessed August 2006 (http://www.ir.gov.sk. ca/adx/asp/adxGetMedia.asp?DocID=4367,3574,3442,3440,3385,2936, Documents&MediaID=8694&Filename=hajnal.pdf).
- Heise, W., and J. Pous, 2001, Effects of anisotropy on the two-dimensional
- inversion procedure: Geophysical Journal International, 147, 610–621. Jefferson, C. W., G. Delaney, and R. A. Olson, 2003, EXTECH IV: Athabasca uranium multidisciplinary study of northern Saskatchewan and Alberta, Part 1, Overview and impact: Geological Survey of Canada Current Research, C18, accessed August 2006 (http://dsp-psd. communication. gc. ca/Collection/GSC-CGC/M44–2003/Articles/c18.pdf).

 Jones, A. G., and X. Garcia, 2003, Case history. Okak Bay AMT data-set case
- study: Lessons in dimensionality and scale: Geophysics, **68**, 70–91. Larsen, J., R. L. Mackie, A. Manzella, A. Fiordelisi, and S. Rieven, 1996, Ro-
- bust smooth magnetotelluric transfer functions: Geophysical Journal International, 124, 801-819.
- Livelybrooks, D., M. Mareschal, E. Blais, and J. T. Smith, 1996, Magnetotelluric delineation of the Trillabelle massive sulfide body in Sudbury, Ontario: Geophysics, **61**, 971–986.

 Mackie, R. L., J. T. Smith, and T. R. Madden, 1994. Three-dimensional elec-
- tromagnetic modeling using finite difference equations: The magnetotelluric example: Radio Science, 29, 923-935.
- McMullan, S. R., R. B. Matthews, and P. Robertshaw, 1987, Exploration geophysics for Athabasca uranium deposits: Proceedings of the Ontario

- Geological Survey, Exploration '87, 547–566. McNeice, G. M., and A. G. Jones, 2001, Multisite, multifrequency tensor decomposition of magnetotelluric data: Geophysics, 66, 158–173.
- Mwenifumbo, C. J., B. E. Elliott, C. W. Jefferson, G. R. Bernius, and K. A. Pflug, 2004, Physical rock properties from the Athabasca Group: Designing geophysical exploration models for unconformity uranium deposits: Journal of Applied Geophysics, 55, 117–135.
- Parkinson, W. D., 1959, Directions of rapid geomagnetic variations: Geo-physical Journal of the Royal Astronomical Society, 2, 1–14.
- Rodi, W., and R. Mackie, 2001, Nonlinear conjugate gradients algorithm for 2D magnetotelluric inversion: Geophysics, **66**, 174–187.
- Ruzicka, V., 1996, Unconformity associated uranium: Geology of Canada, 8,
- Siripunvaraporn, W., G. Egbert, Y. Lenbury, and M. Uyeshima, 2005a, Three-dimensional magnetotelluric inversion: Data-space method: Physics of the Earth and Planetary Interiors, 150, 3-14.
- Siripunvaraporn, W., G. Egbert, and M. Uyeshima, 2005b, Interpretation of two-dimensional magnetotelluric profile data with three-dimensional inversion: Synthetic examples: Geophysical Journal International, 160, 804-814
- Wannamaker, P. E., G. W. Hohmann, and S. H. Ward, 1984, Magnetotelluric responses of three-dimensional bodies in layered earths: Geophysics, 49, 1517-1533.
- White, D. J., Z. Hajnal, I. Gyorfi, E. Takacs, B. Roberts, C. Mueller, B. Reilkoff, R. Koch, B. Powell, I. R. Annesley, S. Bernier, and C. W. Jefferson, 2003, Interim results of the EXTECH-IV seismic-reflection program in the Athabasca Basin, northern Saskatchewan: Geological Survey of Canada Current Research, C8, accessed August 2006 (http://dsp-psd.com-munication.gc.ca/Collection/GSC-CGC/M44-2003/Articles/c08.pdf).
- White, D. J., B. Roberts, C. Mueller, Z. Hajnal, I. Gyorfi, B. Reilkoff, R. Koch, and B. Powell, 2002, Seismic reflection profiling: An effective exploration tool in the Athabasca Basin? An interim assessment, *in* Summary of investigations 2002, Vol. 2, Saskatchewan Geological Survey, Saskatchewan Industry Resources, Miscellaneous Report 2002–4.2, Paper D-2, accessed August 2006 (http://www.ir.gov.sk.ca/adx/asp/adxGetMedia.asp?DocID=4367,3574,3442,3440,3385,2936,Documents&MediaID=8692&Filename=white.pdf).
- Wood, G., and M. D. Thomas, 2002, Modeling of high-resolution gravity data near the McArthur River uranium deposit, Athabasca Basin: Summary of Investigations 2002, Vol. 2, Saskatchewan Geological Survey, Saskatchewan Industry Resources, Miscellaneous Report 2002-42, PaperD-16, accessed August 2006 (http://www.ir.gov.sk.ca/adx/asp/adxGetMedia.asp?DocID=4367,3574,3442,3440,3385,2936,Documents& MediaID=8706&Filename=wood.pdf>.

Interpretation of two-dimensional magnetotelluric profile data with three-dimensional inversion: synthetic examples

Weerachai Siripunvaraporn, ¹ Gary Egbert² and Makoto Uyeshima³

- Department of Physics, Faculty of Science, Mahidol University, Rama VI Rd, Rachatawee, Bangkok, 10400, Thailand. E-mail: scwsp@mahidol.ac.th
- ²College of Oceanic and Atmospheric Science, Oregon State University, Corvallis, OR 97331, USA. E-mail: egbert@coas.oregonstate.edu

Accepted 2004 November 15. Received 2004 November 11; in original form 2004 July 20

SUMMARY

Traditional methods for interpretation of magnetotelluric (MT) profile data are based on 2-D inversion, under the assumption that 3-D complications in the data can be treated as 'geological noise'. We show with synthetic models that fitting 3-D data with a 2-D inversion can result in spurious features, especially if transverse electric (TE) data are used. Inversion of a single profile of MT data with a 3-D algorithm results in significantly more realistic images of structure beneath the data profile, and also allows some resolution of nearby off-profile structure. We also consider the importance of including the on-diagonal impedance tensor terms, Z_{xx} and Z_{yy} , in the inversion. In synthetic test cases, fitting these diagonals improves the accuracy of images of off-profile structure, particularly near the edge of a conductive feature.

Key words: 3-D effects, 3-D inversion, electromagnetic induction, magnetotellurics.

1 INTRODUCTION

In most cases, magnetotelluric (MT) data are still collected on 2-D profiles across an assumed geoelectrical strike. The strike is typically chosen prior to data acquisition, based on the trend of a coastline, known faults (e.g. Unsworth et al. 2000) or other regional structures (e.g. Sakkas et al. 2002; Wu et al. 2002; Brasse et al. 2002). After data collection and processing, various techniques such as the Groom-Bailey (Groom & Bailey 1989) or other tensor decomposition (e.g. Chave & Smith 1994; Caldwell et al. 2004), induction arrow plots (Parkinson 1959,) and skews (Swift 1967; Vozoff 1972) are used to check (and sometimes refine) assumptions about dimensionality or geoelectrical strike (e.g. Ogawa et al. 2001; Mitsuhata et al. 2001; Sakkas et al. 2002; Pous et al. 2002; Bai & Meju 2003; Bielinski et al. 2003). Once the geoelectrical strike has been determined, impedances are rotated into the strike direction, and the off-diagonal impedances (or transverse electric (TE) and transverse magnetic (TM) apparent resistivities and phases) are fitted with a 2-D inversion (e.g. deGroot-Hedlin & Constable 1990; Smith & Booker 1991; Ogawa & Uchida 1996; Siripunvaraporn & Egbert 2000; Rodi & Mackie 2001) to generate cross-sections of electrical resistivity.

In reality, the assumption that the data are purely, or even almost, 2-D seldom holds over the full range of periods used. Off-profile (i.e. 3-D) structures affect most data sets to at least some degree (e.g. Brasse *et al.* 2002). In trying to fit such data with a 2-D inversion, there is a significant danger of introducing spurious structure or unrealistic resistivity values beneath the profile, especially as data misfits are reduced. Most researchers are well aware of these potential pitfalls to 2-D interpretation,

and are careful to state their conclusions with due caution. But deciding how well to fit a given data set with a 2-D model, and which of the features in the resulting conductivity images are robust, remains a serious challenge in the interpretation of MT data.

Many previous publications (e.g. Wanamaker et al. 1984; Berdichevsky et al. 1998; Ledo et al. 2002) have considered some of the limitations of 2-D interpretation of 3-D MT data using the techniques outlined above. Although we touch on this issue briefly here, our primary goal in this paper is to demonstrate the value of applying a 3-D inversion algorithm to interpretation of individual MT profiles. Using synthetic data generated from a simple 3-D model, we show that inverting MT profile data with a 3-D inversion helps avoid contamination by off-plane structures. Cross-sections of resistivity beneath and near the profile reflect more closely the model used to generate the synthetic data than those obtained with 2-D inversions. In addition, we also consider the importance of including the diagonal impedance elements Z_{xx} and Z_{yy} in the 3-D inversion. These terms are strongly affected by off-profiles structures, so including these leads to a more reasonable model near the data transect, especially if there are significant off-profile structures nearby.

2 TEST MODEL AND SYNTHETIC DATA

The test model (Fig. 1) consists of a 1 Ω m conductive block of dimension 4 km \times 2 km \times 1 km inside a 100 Ω m host. Here we consider two cases, with the conductor buried from 800 m to 1.8 km depth (model BC; buried conductor) and with the conductor

804 © 2005 RAS

³Earthquake Research Institute, University of Tokyo, 1-1-1 Yayoi, Bunkyo-ku, Tokyo 113-0032, Japan. E-mail: Uyeshima@eri.u-tokyo.ac.jp

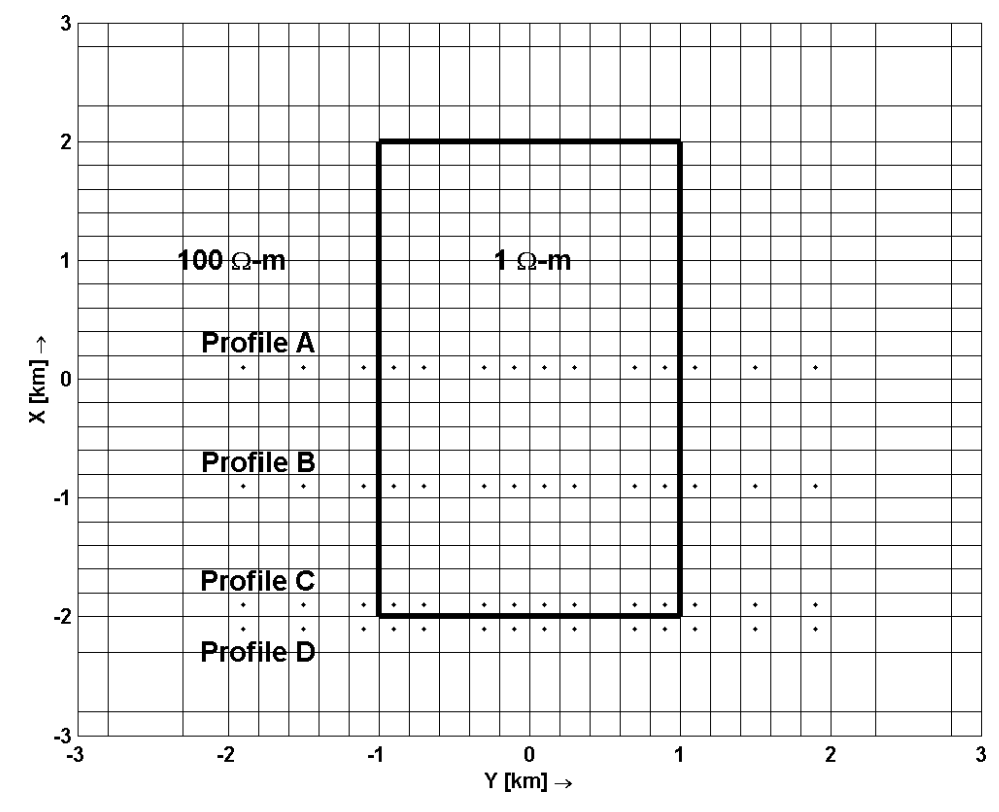


Figure 1. Plan view of the synthetic model used to generate MT data on four profiles, labelled A, B, C and D. The solid dots indicate the data sites. The dominant geoelectric strike is in the *x* direction. Two models are considered: one with a 1 km thick conductor exposed at the surface (model SC), and one with the conductor buried from 800 m to 1.8 km depth (model BC).

exposed at the surface (model SC; surface conductor). Both models are discretized on a 38 \times 36 \times 30-layer (+7 air layers) grid. Four profiles (A, B, C and D), shown as solid dots in Fig. 1, are considered. Profile A cuts nearly across the middle of the conductive block, while profile B is located midway between the centre and the southern edge of the conductive block. Profiles C and D are located 100 m on either side of the southern Edge of the block. Complex impedance tensors (Z_{xx} , Z_{xy} , Z_{yx} and Z_{yy}) were generated for all profiles at 18 sites and 12 periods (0.001, 0.003, 0.010, 0.031, 0.100, 0.316, 1.000, 3.160, 10.000, 31.600, 100.000 and 316.000 s) using a 3-D forward modelling code of Siripunvaraporn et al. (2002). Gaussian noise, with an amplitude of 5 per cent of $|Z_{xy}Z_{yx}|^{1/2}$ was added to the synthetic data. In addition, to simulate the 2-D case, we consider profile O computed for a conductive block of infinite north-south extent. Profile O will be used as a control data set for comparison with other profiles. For 2-D inversion tests the off-diagonal impedance components for all profiles were converted into apparent resistivities and phases in the usual way.

The noise-free apparent resistivities and phases are shown in Figs 2 and 3, and pseudo-sections of the diagonal impedance components, Z_{xx} and Z_{yy} , are shown in Figs 4 and 5. Edge effects due to truncation of the conductor can be clearly seen at most periods in the diagonal terms, Z_{xx} and Z_{yy} , especially for profiles B, C and D in both models (Figs 4 and 5). Even though profile A is located almost in the middle of the conductor, these edge effects can also be observed (Figs 4 and 5), but magnitudes are much lower than those of other profiles. The edge of the conductor is more clearly evident for case SC where the conductor extends to the surface than

for case BC where the conductor is buried. Thus, we may anticipate that edge effects will be less important for the case of a buried conductor.

Figs 2 and 3 show apparent resistivities and phases for the *yx* polarization (i.e. the TM mode for the 2-D case; third and fourth rows of Figs 2 and 3). These are quite similar for profiles O, A, B and even C at almost all periods. However, for the *xy* polarization (the TE mode for the 2-D case; first and second rows of Figs 2 and 3), results are similar only for shorter periods. This shows that truncation of the conductor in our simple models affects the *xy* polarization strongly, but has minimal effects on the *yx* polarization, consistent with the observations of Wanamaker *et al.* (1984) and many others since (but see Berdichevsky *et al.* 1998 for further discussion).

3 NUMERICAL INVERSION EXPERIMENTS AND DISCUSSIONS

Our goal in this paper is to demonstrate the application of a 3-D inversion algorithm to a single MT profile crossing an elongated structure of finite length. We do not consider issues of dimensionality or strike analysis, topics which have been discussed in numerous previous publications (e.g. Ledo *et al.* 2002; Brasse *et al.* 2002, among others). In this paper, we first apply a 2-D inversion to all profiles of both models BC and SC assuming that we know *a priori* that the geoelectric strike is north–south, so Z_{xy} and Z_{yx} are the nominal TE and TM mode impedances respectively. We then apply a 3-D inversion to all profiles of both models using all complex impedance tensor terms. Finally we consider

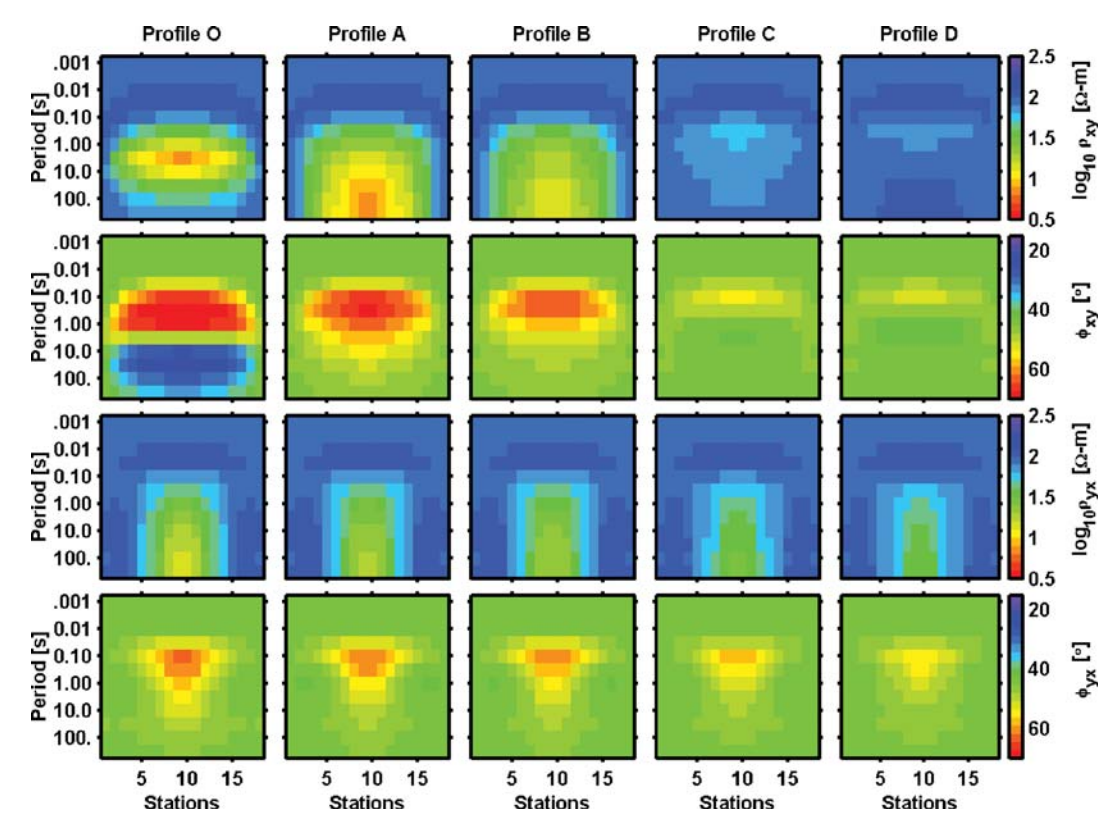


Figure 2. Apparent resistivities and phase pseudo-sections computed from Z_{xy} and Z_{yx} for each profile of model BC. From left to right data are plotted for profiles O, A, B, C and D, respectively. From top to bottom are $\log_{10} \rho_{xy}$, ϕ_{xy} , $\log_{10} \rho_{yx}$, ϕ_{yx} , respectively. The horizontal axis indicates the station number from west to east (y direction), and the vertical axis indicates period.

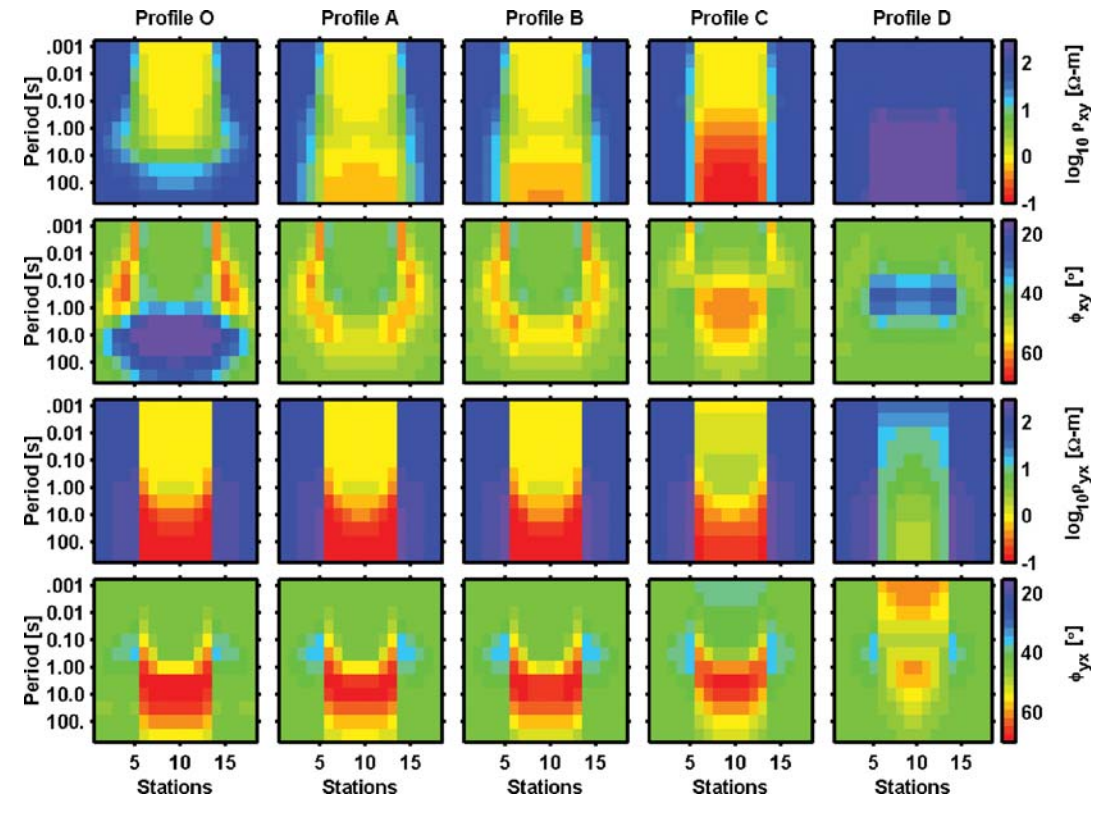


Figure 3. Apparent resistivities and phase pseudo-sections for each profile of model SC, with plotting conventions as in Fig. 2. Note that the colour scales for apparent resistivity differ from Fig. 2.

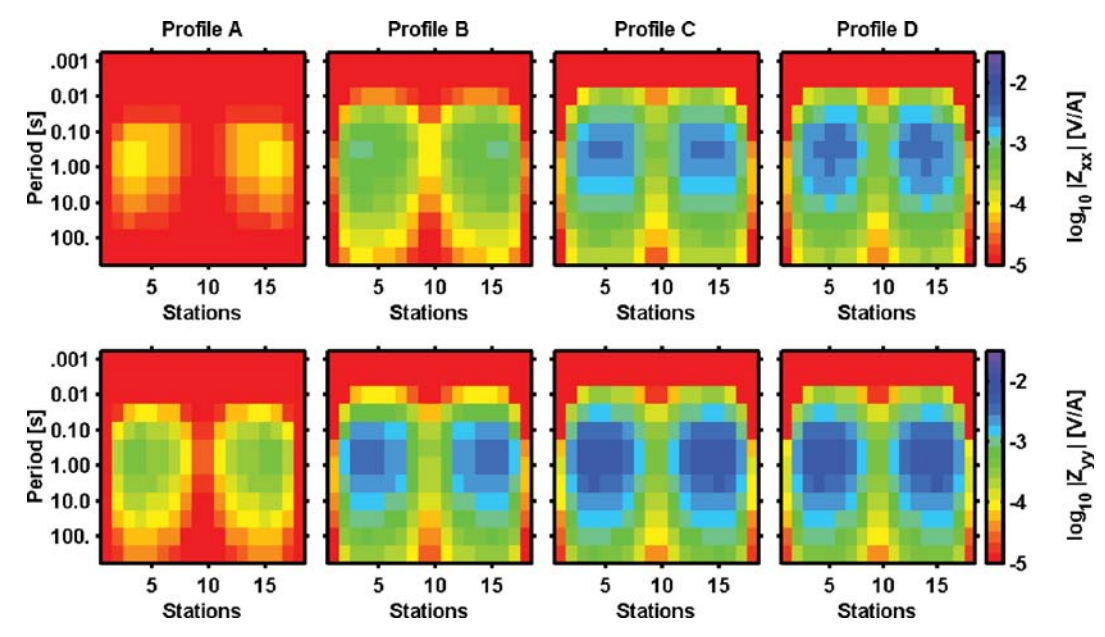


Figure 4. Diagonal impedance tensor terms, Z_{xx} and Z_{yy} , generated from model BC. Left to right are results for profiles A, B, C and D, respectively. The upper row is log10 $|Z_{xx}|$ and the lower row is log10 $|Z_{yy}|$. The horizontal axis indicates station number from west to east (y direction), and the vertical axis period.

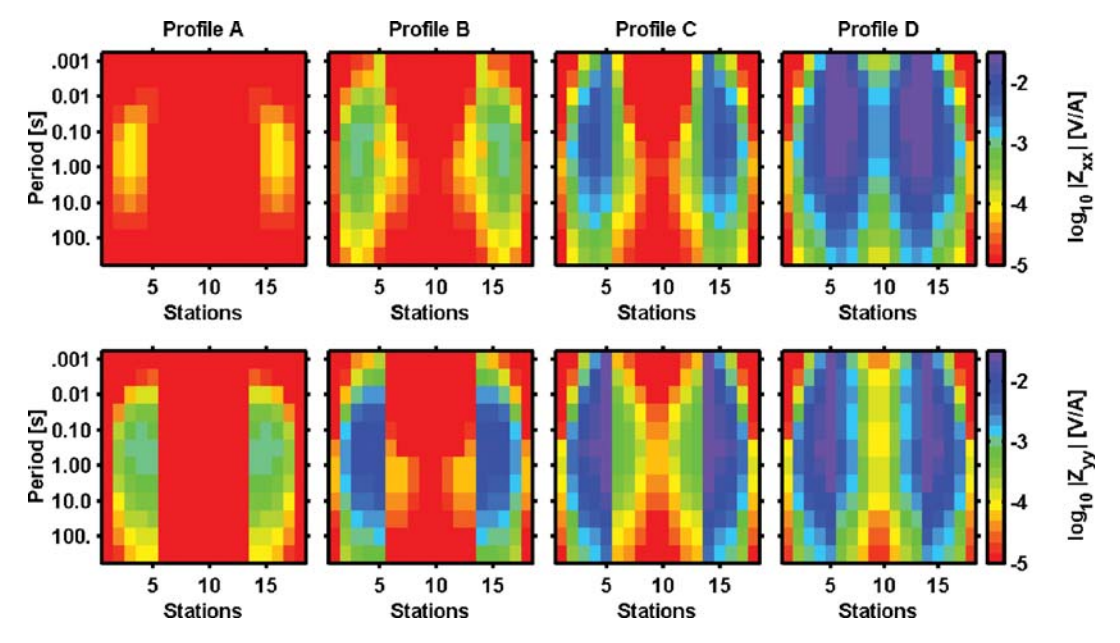


Figure 5. As in Fig. 4, but from model SC.

3-D inversion using only the off-diagonal terms used for the 2-D inversion.

3.1 2-D inversion results

For the 2-D inversion we used the REBOCC code described in Siripunvaraporn & Egbert (2000). This inversion is essentially a data space variant of the OCCAM scheme of Constable $et\ al.$ (1987) and deGroot-Hedlin & Constable (1990), which finds a minimum norm solution subject to fitting data to within a specified tolerance. All inversions were started from a 50 Ω m homogeneous half-space. Data errors are assumed to be 5 per cent, as used for generating the

synthetic data. Results of the 2-D inversions of models BC and SC are shown in Figs 6 and 7, respectively, for profiles O, A, B, C and D from top to bottom. Columns from left to right give results of inverting only the TE data (amplitude and phase), only the TM data, and jointly inverting both TM and TE data, respectively.

For the purely 2-D data set (profile O) the 2-D inversion scheme performs well for TE, TM and joint inversion for both models (first row of Figs 6 and 7). In all cases the inversion has no difficulty in retrieving the structure and fitting the data to within a normalized RMS of 1. For data generated from model BC, TM inversions can reduce the normalized RMS misfit to below 2 for profiles A and B, and to 1 for profiles C and D near the conductor's edge. For

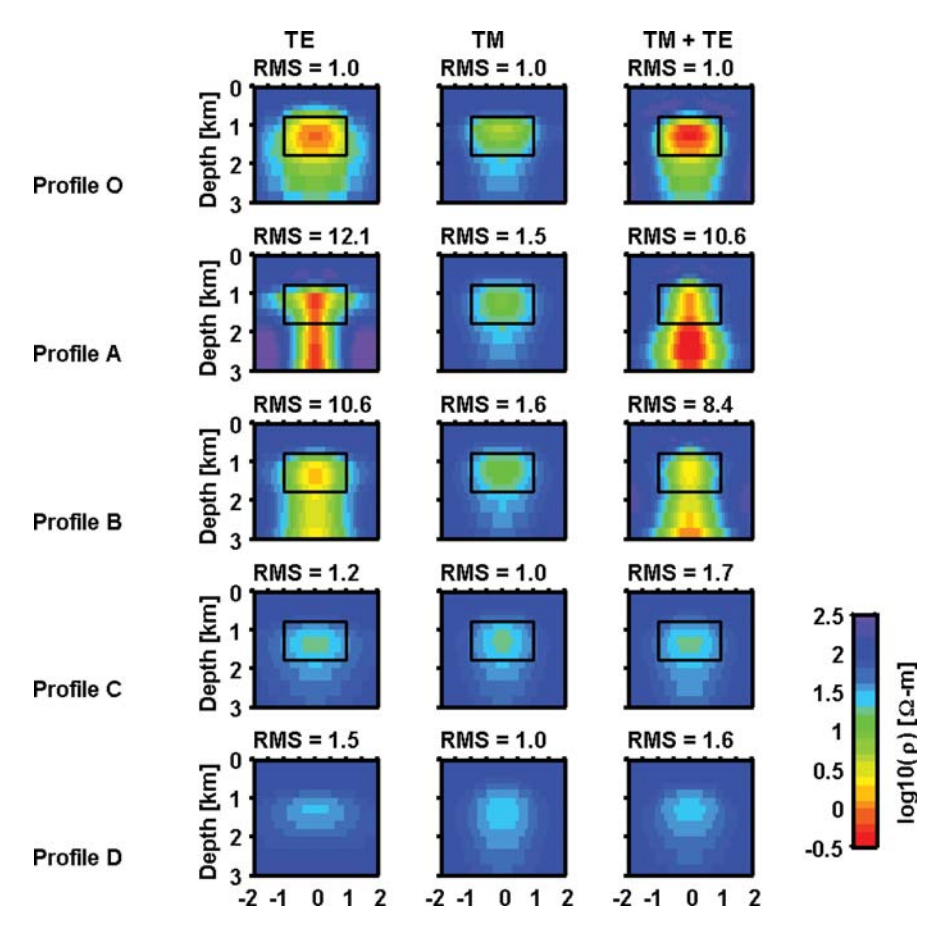


Figure 6. Resistivity cross-sections from 2-D inversion of data generated from model BC on profiles O, A, B, C and D, from top to bottom respectively. The first column gives results for inversion of only TE data, the middle column for only TM data and the last column for joint inversion of TM and TE data. The rectangle outlines the conductor in the synthetic model.

model SC where the conductor is exposed, an RMS misfit of 1 can be achieved for all profiles. Inverting only the TM mode generates a reasonable resistivity structure for most profiles (middle column of Fig. 7). This confirms results from a number of previous studies which have shown that TM mode data are least affected by 3-D effects (Wanamaker *et al.* 1984; Ledo *et al.* 2002). However, the true resistivity contrast is underestimated somewhat, especially for profiles near the edge. When the conductor is buried (model BC), models obtained by inverting only TM mode data show a conductor in the right area but with a resistivity about 10 times too high, approaching the host resistivity. This tendency to underestimate the resistivity contrast becomes more severe as the profile is moved closer to the end of the conductive feature.

The TE and joint TM + TE 2-D inversions do not perform well for either of the 3-D test cases (first and third columns of Figs 6 and 7). In no case is the desired normalized RMS misfit of 1 achieved. The inverse solutions from TE and joint TE and TM inversions of profiles A and B do contain conductive features in the general area of the conductor for both test cases. However, the size and shape of this structure is poorly resolved. For model BC the imaged conductive root extends to greater depth, and in model SC resistivities are unreasonably low (less than 0.1 Ω m). Similar extremely low resistivities are often encountered in 2-D inversion results with real data, and are clearly an artefact of over-fitting the data.

For profiles C and D of model BC, the effects from the conductor are weak, as seen in the similarity of TE responses from these two

profiles (Fig. 2). The solutions resulting from TE and joint TM + TE 2-D inversions are therefore almost the same (Fig. 6) and data fits are reasonable. In contrast, for model SC, where the responses for the two profiles differ significantly, the inverse solutions show conductive features in profile C and resistive features in profile D, as they should. However, spurious high- and low-resistivity regions can be seen in the inversion results for both profiles, and the data fits are now poor.

The biggest misfits in the TE and joint 2-D inversions are due to 3-D effects at longer periods. To fit the long-period data better, the inversion extends the conductive root deeper for model BC and reduces resistivities for model SC to an extremely low level. This failure is not specific to REBOCC, or any other 2-D inversion scheme. Almost certainly no 2-D model exists which can fit these 3-D data sets to a target RMS of 1. In this circumstance, deciding how well data should in fact be fitted in a 2-D inversion is problematic, especially since over-fitting the data even a little can result in spurious and poorly resolved structures in the inverse solutions. Most seriously these spurious features may appear to be at least physically sensible in some cases, and thus be erroneously interpreted as real geological structures.

3.2 3-D inversion results: all complex tensor terms

We will now show that by inverting single profile data with a 3-D inversion program, many of the problems encountered with a 2-D

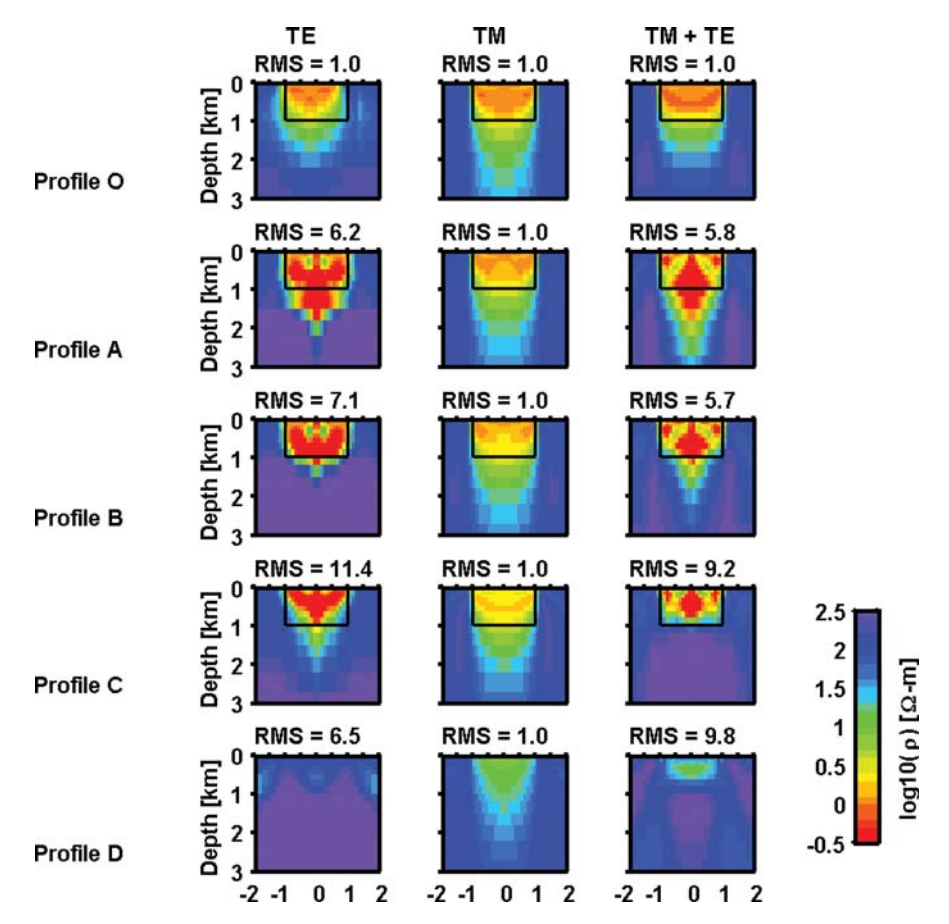


Figure 7. As in Fig. 6, but for model SC.

approach can be significantly reduced, and the data can be fitted with a reasonable model. We first invert the synthetic data from each profile with the 3-D inversion program of Siripunvaraporn et al. (2005), using all complex tensor terms, i.e. Z_{xx} , Z_{xy} , Z_{yx} and Z_{yy} . The 3-D inversion code is similar to the 2-D code in that it is a data space variant on the OCCAM minimum structure approach. Results of applying this inversion to the synthetic data discussed above are shown in Fig. 8 for model BC and Fig. 9 for model SC. Inverse solution cross-sections directly beneath each profile are shown in the middle (fourth) column, with solution cross-sections for profiles 1 km, 0.6 km and 0.2 km south, and 0.2 km, 0.6 km and 1 km north of the data transect shown in the first, second, third, fifth, sixth and seventh columns, respectively. In most cases data are readily fitted to a normalized RMS of 1. One exception is for profile C of model SC, where the inversion was only able to reduce the normalized RMS misfit to about 1.8.

For the 3-D inversions cross-sections directly beneath the data profile are always reasonably consistent with the true model used to generate the synthetic data, although the shape and resistivity are distorted to varying degrees. The most serious deficiency is in the inverse solutions for the buried conductor (model BC) where the conductivity contrast is systematically reduced. This bias almost certainly results primarily from the minimum norm formulation of the inverse problem, which trades off between minimizing conductivity variations and data misfit. When the effect of a structure on the data is weak, as for the buried conductor, conductivity contrasts that are systematically too small are favoured because these keep the model norm small, with little increase in data misfit. Improved data coverage (i.e. additional profiles) may improve accurate resolution

of the conductive anomaly (Siripunvaraporn *et al.* 2005). Different approaches to regularization of the inverse problem may possibly also improve results.

The bias toward low resistivity contrasts for buried structures is even more severe when only TM mode data are inverted with a 2-D approach (Fig. 6). Inclusion of data for both source polarizations in the 3-D inversion evidently improves accuracy of the estimated contrast. As we have seen, trying to include data from this second polarization in a 2-D inversion can lead to very poor results. These problems are not seen in the 3-D inversion results (Figs 8 and 9). The 2-D inversion inserts spurious structures such as deepened conductive roots (Fig. 6) or unrealistic resistivities (Fig. 7) beneath the profile in an effort to account for 3-D features in the long-period data. For the 3-D inversion these 3-D effects can be accounted for more reasonably with actual off-profile structure. In the simple case of model SC where the conductor is exposed to the surface, inverting only TM mode data generates a reasonable model, and one might argue that a 3-D inversion is unnecessary. However, real data sets are generally affected by both deep and shallow structures, and some of these are likely to be very poorly resolved using only TM mode data. As a consequence most interpretations of MT field surveys incorporate TE mode data to some degree. By reducing the weight given to fitting these data some of the spurious effects seen in our examples can probably be reduced, but one can never be certain that they have been completely eliminated

Using a 3-D inversion allows use of all of the data to image the structure beneath the data profile, with much less risk of introducing spurious structure, but how good are the images of off-profile

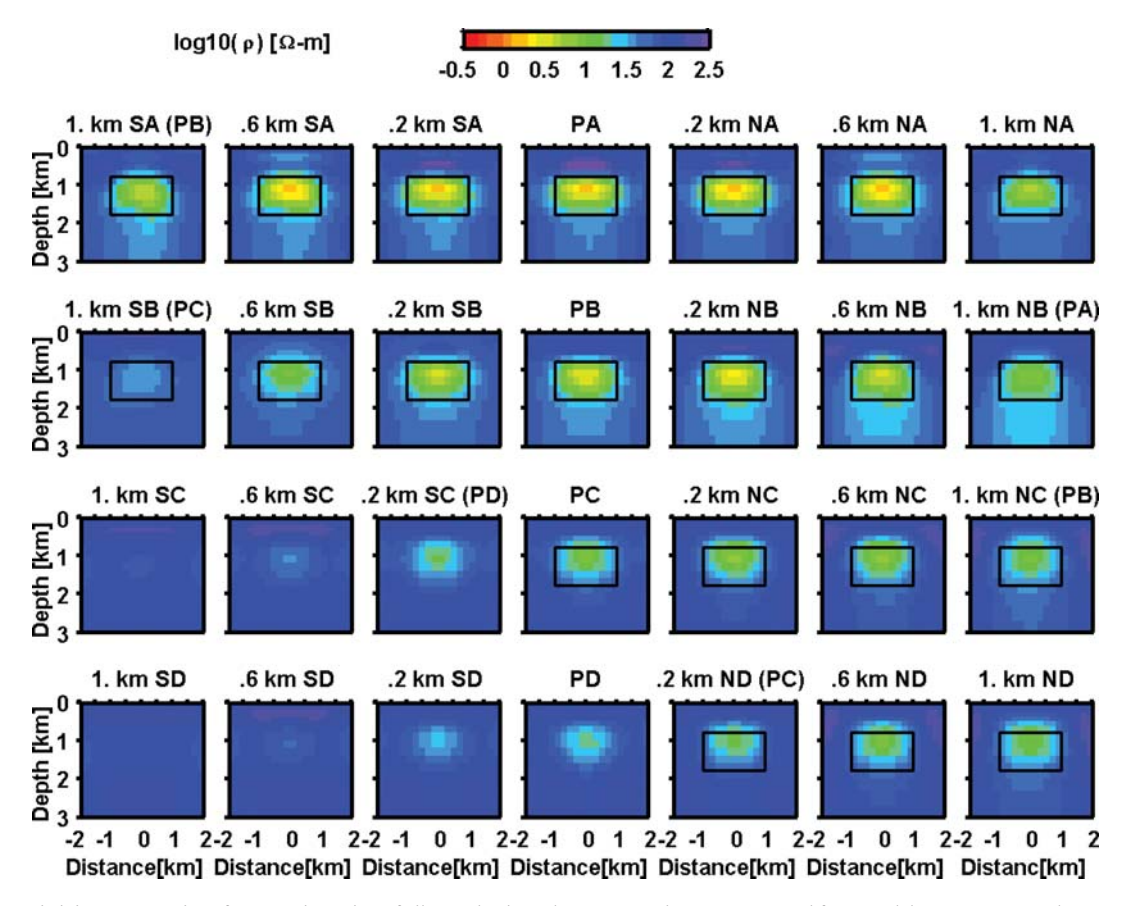


Figure 8. Resistivity cross-sections from 3-D inversion of all complex impedance tensor elements generated from model BC. From top to bottom are sections of the 3-D inverse solutions of data from profiles A, B, C and D, respectively. The centre column (fourth) shows the cross-section directly beneath each profile, PA, PB, PC and PD. The left (first, second, third) and right (fifth, sixth, seventh) columns show the models from 1 km, 600 m and 200 m south (SA, SB, SC and SD) and 200 m, 600 m and 1 km north (NA, NB, NC and ND) of the profile. The rectangle outlines the conductor.

structure? For 3-D inversion of data from profile A (first row of Figs 8 and 9), the imaged conductor continues for almost 1 km to the north and south. For the profile B inversion the conductor extends a similar distance to the north, and somewhat less to the south. In all cases for profiles A and B, the imaged conductor is shorter than the true structure. This again can be explained in terms of biases in a minimum norm solution. Structures more than about 1 km from the profile have limited effect on, and are thus not required by, the data.

For profiles C and D which are closer to the edge of the conductor the value of 3-D inversion of profile data is demonstrated even more clearly. For profile C, which is 100 m inside the southern edge of the conductor, the 3-D inversion shows a conductor beneath, and to the north of, the profile, but conductivity diminishes rapidly to the south for both models (third row of Figs 8 and 9). For profile D, which is located 100 m outside the southern edge of the conductor, the 3-D inversion shows little increase in conductivity beneath, and south of, the profile. However, the conductor is clearly displayed north of the profile, in roughly the correct location (fourth row of Figs 8 and 9). Thus, the edge of the conductor is reasonably recovered using profile data from either side, especially for the case of near-surface structure (Fig. 9, last two rows).

As discussed above, for the buried conductor responses on profiles C and D are quite similar. Not surprisingly, results of 3-D inversion for these profiles are also similar (third and fourth rows of Fig. 8), and the edge of the conductor is less clearly seen. Also, because the data on these edge profiles are only weakly affected by the conductor, resistivity contrasts resulting from these inversions are especially weak. Nevertheless, the 3-D inversion using all complex tensor elements still produces a qualitatively correct picture of a buried conductor extending northward (but not southward) from near profiles C and D.

Obviously information about off-profile structure that can be recovered from a single profile of MT data is limited. The results of 3-D inversion should clearly be interpreted cautiously, particularly with regard to the along-strike extent of structures. However, reasonable images can be obtained for structures beneath, and near, a single MT profile, while even this type of information cannot be obtained reliably with 2-D inversion.

3.3 3-D inversion results: inverting only Z_{xy} and Z_{yx}

In the examples considered above we inverted all four impedance tensor components, Z_{xx} , Z_{xy} , Z_{yx} and Z_{yy} . Now we consider inversion of only the off-diagonal terms Z_{xy} and Z_{yx} , comparable to a joint TE + TM 2-D inversion. Results are shown in Figs 10 and 11 for models BC and SC, respectively. The first point to note is that even though fewer data are used the inversion algorithm more frequently fails to reach the desired RMS of 1, especially for model

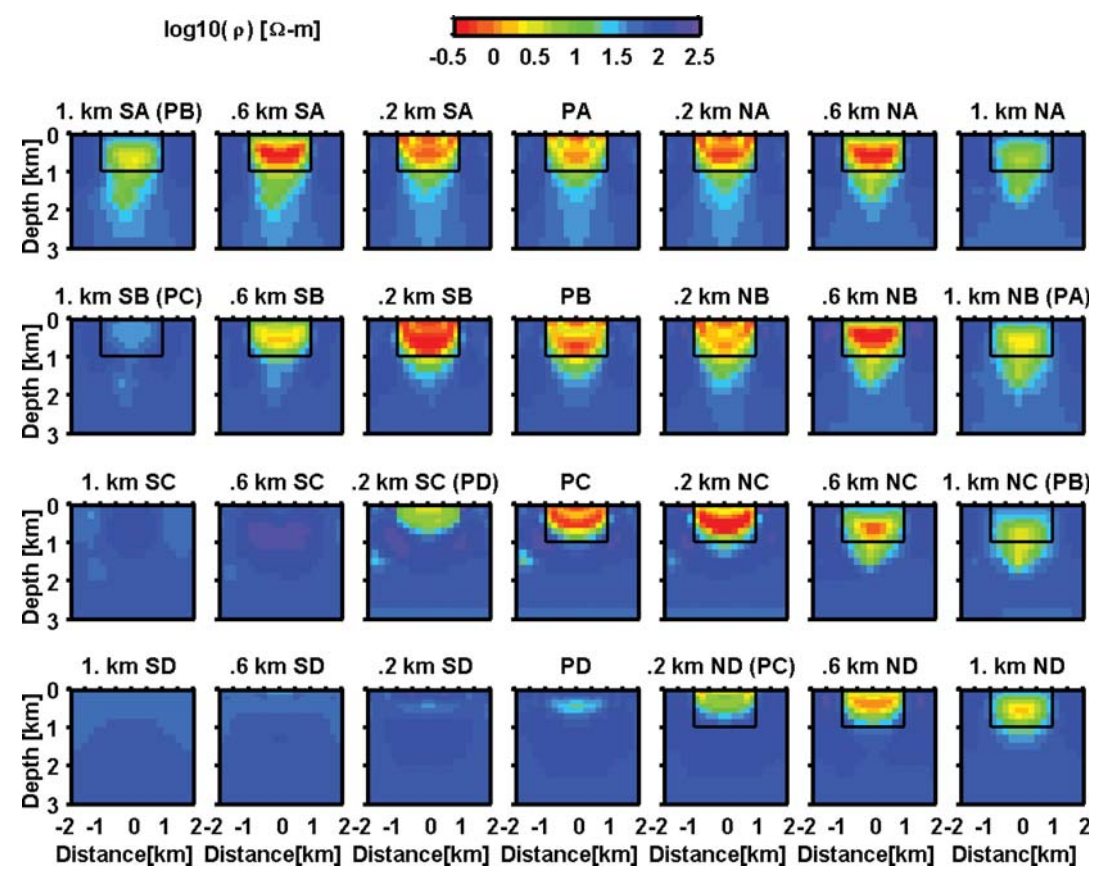


Figure 9. Resistivity cross-sections as in Fig. 8, but for data from model SC.

SC. The inverse solutions shown in Figs 10 and 11 achieved the minimum RMS misfit, which were for profiles A, B, C and D respectively, 1.25, 1.00, 1.00 and 1.00 for model BC, and 1.38, 1.10, 2.60 and 1.40, for model SC.

Similar to the inverse solutions in Figs 8 and 9, obtained using all tensor components, cross-sections directly beneath the MT profiles are in fair agreement with the true model, though the conductor's shape and size are slightly distorted (Figs 10 and 11). The extremely low resistivity values or deep conductor roots, seen when the same data were fitted with a 2-D inversion, are not seen here. This again clearly demonstrates the benefit of 3-D inversion of single-profile MT data. For profiles A and B, and for both models, the conductor in the inverse solutions continues to both north and south (first and second rows of Figs 10 and 11), as in the full impedance inversion results.

Greater differences between the full tensor and off-diagonal cases are seen for profiles C and D. Without Z_{xx} and Z_{yy} , the conductor is barely seen in model BC (third and fourth rows of Fig. 10), but appears continuously both north and south of the profiles in model SC (third and fourth rows of Fig. 11), though in this case the conductor is significantly reduced and shallower for profile D. The edge of the conductor is also lost in both models. This indicates that significant information about the conductor's edge is clearly present in the on-diagonal tensor elements, Z_{xx} and Z_{yy} . Without this information, the data do not distinguish between directions off profile.

Indeed, consider a profile the same distance to the north of the conductor as D is to the south. The off-diagonal tensor components,

 Z_{xy} and Z_{yx} would be the same as on D, but the diagonal tensor components Z_{xx} and Z_{yy} would have the opposite sign. Hence from off-diagonal components alone one could not determine on which side of the profile the conductive layer is; this information is only in the sign of the diagonal components.

Symmetry considerations also show that for any 3-D conductivity that is symmetric about the profile (in particular for the uniform conductivity Earth used as the starting model in our inversion) data sensitivities for the off-diagonal impedances will also be symmetric about the profile. This symmetry in sensitivities for the reduced data set may help explain why the inversion search algorithm fails to find a model which fits the data at the target misfit. Starting from a symmetric conductivity distribution, all data sensitivities (and for an Occam-style inversion approach, all model updates) should remain symmetric about the profile if only off-diagonal impedances are used. Models which fit the off-diagonal data adequately exist, but these are presumably all asymmetric, in contrast to the symmetric models that should result from a linearized search of the sort we use. It is interesting to note that this provides a simple example of a situation in which a linearized search may fail to converge to the global minimum of the penalty functional.

In fact, the models from inversion of only off-diagonal impedances from profiles C and D are nearly, but not exactly, symmetric (Figs 10 and 11). The symmetry in the sensitivity calculation is broken, both by numerical truncation error and due to some technical details in the approximate way in which we have implemented the model covariances (Siripunvaraporn & Egbert 2000). This breaking in symmetry could help the inversion find models that fit the data

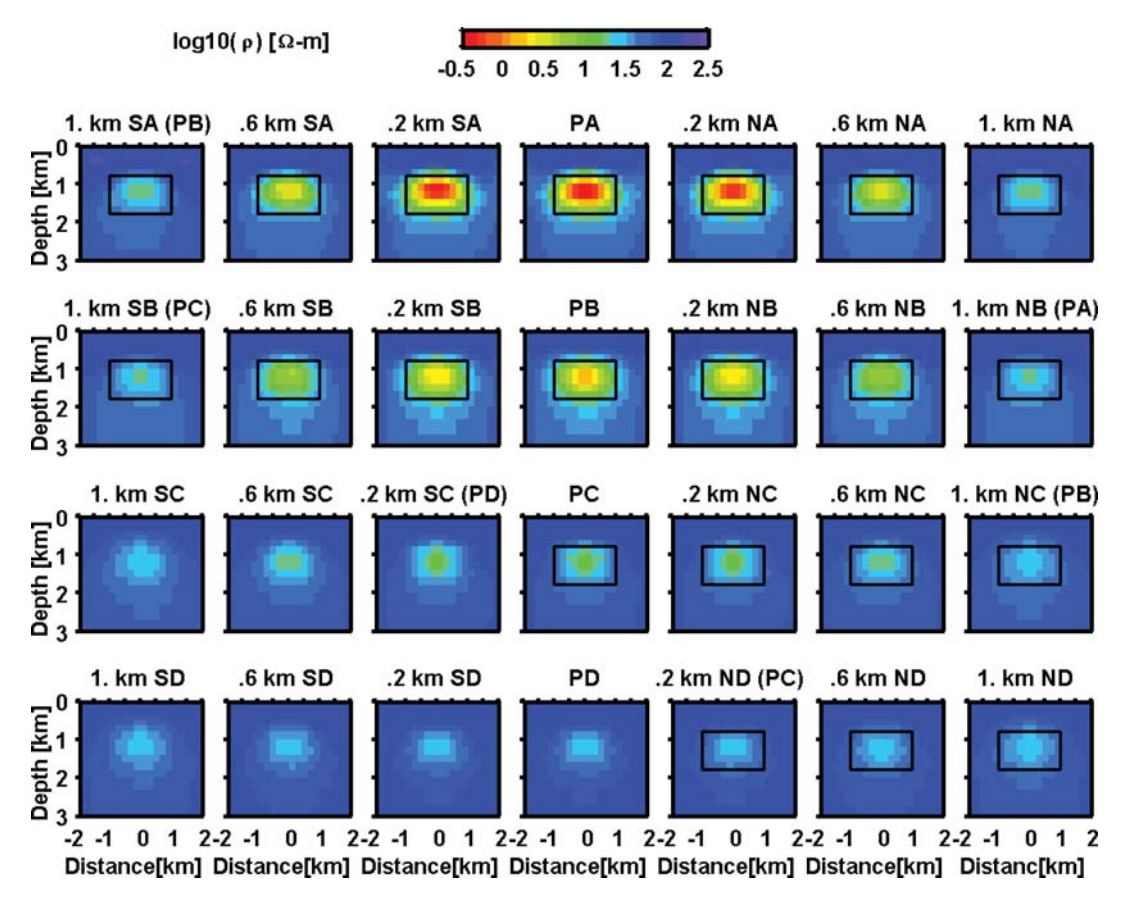


Figure 10. Resistivity cross-sections obtained by 3-D inversion of the off-diagonal tensor elements Z_{xy} and Z_{yx} generated for model BC. Plotting conventions are as in Fig. 8. Note that the model fit to the profile A data does not fit to the target level of 1 RMS.

better in some cases, as we have found it is possible to obtain a more reasonable (asymmetric) model similar to the full tensor inverse solutions for some starting models. But the off-diagonal terms by themselves cannot define the 'true' direction, so even if an asymmetric model fitting the data is found, off-profile structure will just as likely as not be imaged on the wrong side of the data profile. We conclude that interpretation of off-profile structure can be enhanced significantly by using all elements of the impedance tensor in the inversion.

4 CONCLUSIONS

Prior to 2-D inversion, it is necessary to identify a preferred geoelectrical strike. This is accomplished based on known local or regional geology or by performing some sort of dimensionality analysis on the data. Usually, the inferred geoelectrical strike varies over frequency, and over position on the profile. A compromise must usually be struck, and some data discarded or down-weighted so that 2-D inversion and interpretation can be justified. In some cases, e.g. for a single conductor exposed at the surface, inverting only TM mode data may yield a reasonable interpretation with minimal 3-D effects. However, not all structures are well resolved using only TM data, and in general the temptation is great to incorporate TE data in the interpretation. This data can easily be contaminated by 3-D effects, which are fitted by inserting spurious and misleading structure into the model.

By applying 3-D inversions to 2-D profile data, these potential problems can be minimized. In our examples the inversion produces reasonable results beneath the data. Although constraining the full 3-D structure would certainly require additional profiles, a single profile can provide at least a qualitatively reasonable picture of nearby off-profile structure. Much of the information about off-profile structure is contained in the diagonal elements Z_{xx} and Z_{yy} , so 3-D inversion should include all tensor components if possible.

In this paper we have considered explicitly the case of a conductor buried in a more resistive host. Additional tests with a resistive body buried in a more conductive host were also conducted, with similar results, though the periods used in the inversion must be adjusted to cope with the shorter diffusion length scales of the electromagnetic fields in the host. We have not yet done tests with significantly more complex 3-D models. It is possible that if the local response is strongly affected by complex regional scale 3-D structure (e.g. near a complicated coastline) 3-D inversion of a single profile may conceivably still be misleading. Further research on this question is warranted.

ACKNOWLEDGMENTS

This research has been supported by a grant from the Thailand Research Fund (RSA4780021) to WS, and by DOE-

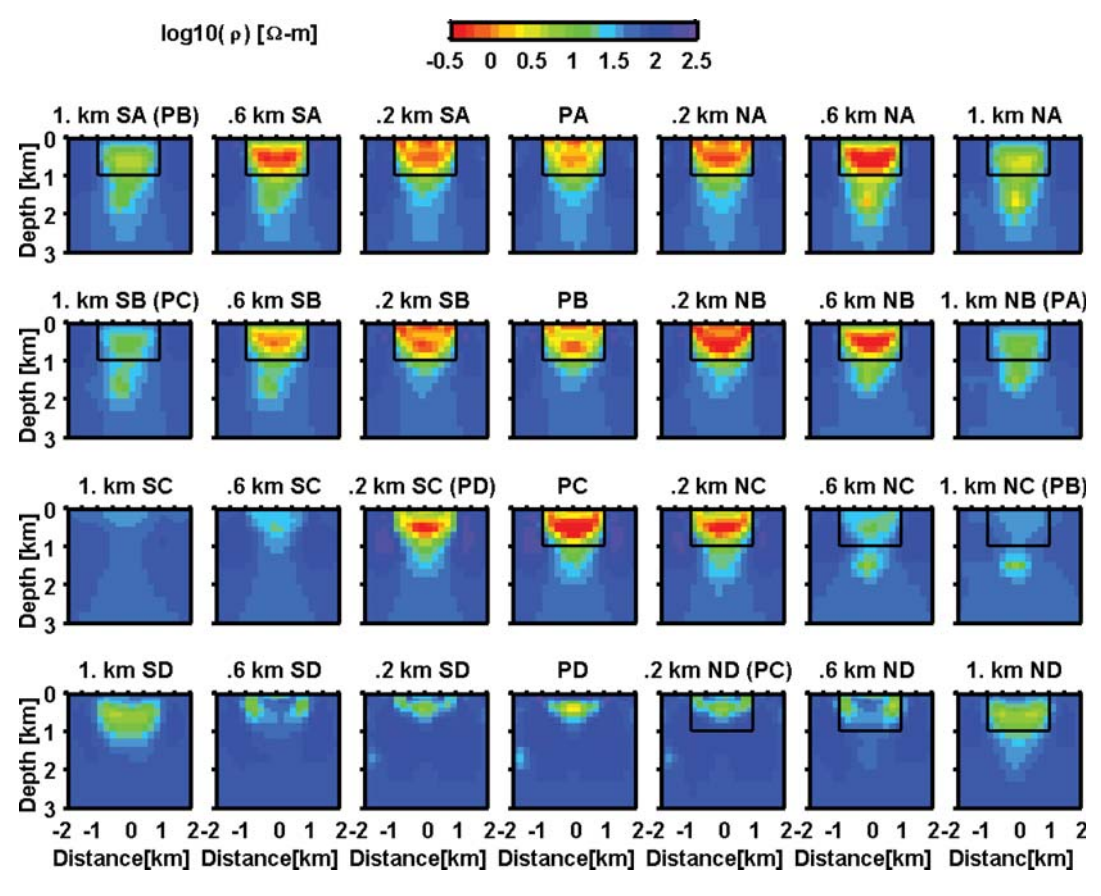


Figure 11. Resistivity cross-sections as in Fig. 10, obtained by inverting the off-diagonal tensor elements Z_{xy} and Z_{yx} , but for model SC. Note that none of these models fit the data to within the target level of 1 RMS.

FG0302ER15318 to GE, and partly by a JSPS postdoctoral fellowships (P02053) and a grant from MEXT, Japan (02053) to WS and MU. The authors would like to thank Wolfgang Soyer and Graham Heinson for their suggestions for improving this manuscript.

REFERENCES

Bai, D. & Meju, M.A., 2003. Deep structure of the Longling-Ruili fault underneath Rulili basin near the eastern Himalayan syntaxis: insights from magnetotelluric imaging, *Tectonophysics*, 364, 135–146.

Berdichevsky, M.N., Dmitriev, V.I. & Pozdnjakova, E.E., 1998. On twodimensional interpretation of magnetotelluric soundings, *Geophys. J. Int.*, 133, 585–606.

Bielinski, R.A., Park, S.K., Rybin, A., Batalev, V., Jun, S. & Sears, C., 2003. Lithospheric heterogeneity in the Kyrgyz Tien Shan imaged by magnetotelluric studies, *Geophys. Res. Lett.*, 30(15), 1806, doi:10.1029/2003GL017455.

Brasse, H., Lezaeta, P., Rath, V., Schwalenberg, K., Soyer, W. & Haak, V., 2002. The Bolivian Altiplano conductivity anomaly, *J. geophys. Res.*, 107(B5), 2096. doi:10.1029/2001JB000391.

Caldwell, T.G., Bibby, H. & Brown, C., 2004. The magnetotelluric phase tensor, *Geophys. J. Int.*, **158**, doi:10.1111/j.1365-246X.2004.02281.x.

Chave, A.D. & Smith, J.T., 1994. On electric and magnetic galvanic distortion tensor decompositions, J. geophys. Res., 99, 4669–4682.

Constable, C.S., Parker, R.L. & Constable, C.G., 1987. Occam's inversion: a practical algorithm for generating smooth models from electromagnetic sounding data, *Geophysics.*, 52, 289–300. deGroot-Hedlin, C. & Constable, S., 1990. Occam's inversion to generate smooth, two-dimensional models from magnetotelluric data, *Geophysics*, 55, 1613–1624.

Groom, R.W. & Bailey, R., 1989. Decomposition of magnetotelluric impedance tensors in the presence of local three-dimensional galvanic distortion, J. geophys. Res., 94, 1913–1925.

Ledo, J., Queralt, P., Marti, A. & Jones, A.G., 2002. Two-dimensional interpretation of three-dimensional magnetotelluric data: an example of limitations and resolution, *Geophys. J. Int.*, 150, 127–139.

Mitsuhata, Y., Ogawa, Y., Mishina, M., Kono, T., Yokokura, T. & Uchida, T., 2001. Electromagnetic heterogeneity of the seismogenic region of 1962 M6.5 Northern Miyagi Earthquake, northeastern Japan, *Geophys. Res. Lett.*, 28, 4371–4374.

Ogawa, Y. & Uchida, T., 1996. A two-dimensional magnetotelluric inversion assuming Gaussian static shift, *Geophys. J. Int.*, **126**, 69–76.

Ogawa, Y. et al., 2001. Magnetotelluric imaging of fluids in intraplate earth-quakes zones, NE Japan back arc, Geophys. Res. Lett., 28, 3741–3744.

Parkinson, W.D., 1959. Directions of rapid geomagnetic fluctuations, Geophys. J. R. astr. Soc., 2, 1–14.

Pous, J., Heise, W., Schnegg, P., Munoz, G., Marti, J. & Soriano, C., 2002. Magnetotelluric study of the Las Canadas caldera (Tenerife, Canary Islands): structural and hydrogeological implications, *Earth planet. Sci. Lett.*, 204, 249–263.

Rodi, W.L. & Mackie, R.L., 2001. Nonlinear conjugate gradients algorithm for 2-D magnetotelluric inversion, *Geophysics*, 66, 174–187.

Sakkas, V., Meju, M.A., Khan, M.A., Haak, V. & Simpson, F., 2002. Magnetotelluric images of the crustal structure of Chyulu Hills volcanic field, Kenya, *Tectonophysics*, 346, 169–185.

Siripunvaraporn, W. & Egbert, G., 2000. An efficient data-subspace inversion method for 2-D magnetotelluric data, *Geophysics*, 65, 791–803.

- Siripunvaraporn, W., Egbert, G. & Lenbury, Y., 2002. Numerical accuracy of magnetotelluric modeling: a comparison of finite difference approximations, Earth Planets Space, 54, 721-725.
- Siripunvaraporn, W., Egbert, G., Lenbury, Y. & Uyeshima, M., 2004. Threedimensional magnetotelluric inversion: data space method, Phys. Earth planet. Inter., doi:10.1016/j.pepi.2004.08.023
- Smith, J.T. & Booker, J.R., 1991. Rapid inversion of two- and threedimensional magnetotelluric data, J. geophys. Res., 96, 3905–3922.
- Swift, C.M., 1967. A magnetotelluric investigation of electrical conductivity anomaly in the southwestern United States, PhD thesis, MIT, Cambridge,
- Unsworth, M., Bedrosian, P., Eisel, M., Egbert, G. & Siripunvaraporn, W., 2000. Along strike variations in the electrical structure of the San Andreas Fault at Parkfield, California, Geophys. Res. Lett., 27, 3021–3024.
- Vozoff, K., 1972. The magnetotelluric method in the exploration of sedimentary basins, Geophysics, 37, 98-141.
- Wanamaker, P.E., Hohmann, G.W. & Ward, S.H., 1984. Magnetotelluric responses of three-dimensional bodies in layered earths, Geophysics, 49, 1517-1533.
- Wu, X., Ferguson, I.J. & Jones, A.G., 2002. Magnetotelluric response and geoelectric structure of the Great Slave Lake shear zone, Earth planet. Sci. Lett., 196, 35-50.

WSINV3DMT helps to reveal what beneath the Earth

ผศ. ดร. วีระชัย สิริพันธ์วราภรณ์ ภาควิชาฟิสิกส์ คณะวิทยาศาสตร์ มหาวิทยาลัยมหิดล ถ. พระราม 6 เขตราชเทวี กรุงเทพ 10400

scwsp@mahidol.ac.th; wsiripun@yahoo.com

ถ้าเราต้องการศึกษาโครงสร้างภายในร่างกายมนุษย์ โดยไม่ต้องทำการผ่าตัด เราสามารถทำได้ หลายๆ วิธี เช่น X-Ray, Ultrasound, CT scan หรือ MRI แต่ละวิธีก็ขึ้นกับการตอบสนองของ ร่างกายต่อสิ่งเร้าที่มนุษย์เราใส่เข้าไป เช่นต่อคลื่นเหนือเสียง เป็นต้น ผลที่ได้คือภาพตัดขวาง

หรือภาพเคลื่อนใหวของโครงสร้าง
ภายในร่างกายมนุษย์ ดังภาพที่ 1
ซึ่งเป็นประโยชน์อย่างมากต่อ
การแพทย์ เพราะทำให้ไม่ต้องทำการ
ผ่าตัดเจ็บตัวเปล่า

รูปที่ 1 ภาพแสดงทารกที่อยู่ใน ครรภ์มารดาโดยใช้คลื่นเหนือ เสียงในการตรวจสอบ

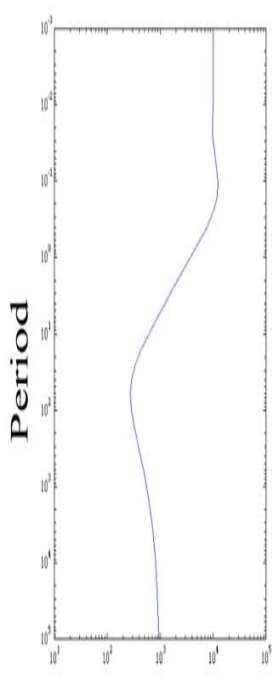


เช่นเดียวกัน ในการศึกษาโครงสร้างของโลก เราไม่สามารถขุดลึกลงไปใต้พื้นโลกได้ เพราะเทคโนโลยีที่ยังไม่เอื้ออำนวย รวมทั้งค่าใช้จ่ายที่สูงมาก วิธีการทางธรณีฟิสิกส์จึงถูก นำมาใช้เพื่อสำรวจโครงสร้างใต้พื้นโลก เช่นเดียวกับเทคนิคทางการแพทย์ วิธีการทางธรณี ฟิสิกส์ก็มีหลากหลายวิธี แต่ละวิธีตอบสนองต่อสิ่งเร้าที่ต่างกัน เช่นต่อคลื่นแผ่นดินไหว หรือต่อ การนำไฟฟ้า หรือต่อแรงโน้มถ่วงของโลก เป็นต้น

Magnetotelluric method เป็นวิธีหนึ่งที่ใช้กันแพร่หลายในทางธรณีฟิสิกส์เพื่อดู

โครงสร้างการนำไฟฟ้า (หรือต้านการนำไฟฟ้า) ในทั้งระดับตื้น และลึก วิธีการ คือ วัดสนามแม่เหล็กและสนามไฟฟ้าที่พื้นผิว ของโลกในลักษณะที่แนวยาว (profile) ผ่านโครงสร้างที่เรา ต้องการศึกษา ดังรูปที่ 2

รูปที่ 2 แสดงเครื่องมือวัด สนามแม่เหล็ก (ขวา) และ สนามไฟฟ้า (ซ้าย) ที่ พื้นผิวโลก

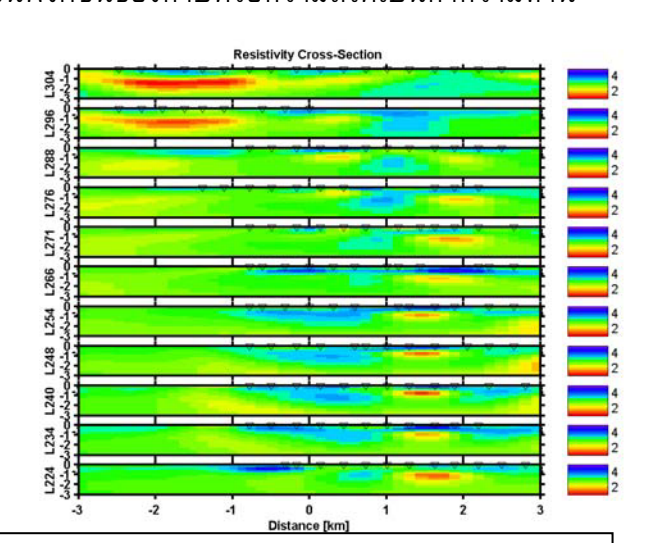


จากสนามแม่เหล็กและสนามไฟฟ้าที่วัดได้จะได้ความสัมพันธ์ เป็นค่าความต้านทางไฟฟ้าปรากฏเป็นฟังก์ชันของความถี่ (หรือคาบ) โดยความถี่สูง (คาบสั้น) แสดงถึงใต้พื้นโลกที่ระดับตื้น และความถี่ต่ำ (คาบยาว) แสดงถึงใต้พื้นโลกที่ระดับลึก ดังรูปที่ 3 ค่าความต้านทาน ไฟฟ้าปรากฏบอกเราได้อย่างคร่าวๆ ว่าโครงสร้างใต้พื้นโลกเป็น อย่างไร เนื่องจากไม่ใช่เป็นฟังก์ชันของความลึก เราจึงไม่สามารถ วิเคราะห์ได้ว่าโครงสร้างที่สนใจนั้นอยู่ที่ความลึกเท่าไร และมีขนาด เท่าไร การจะวิเคราะห์โดยตรงทำได้ยากและสลับซับซ้อน

ร**ูปที่ 3** แสดงความสัมพันธ์ของค่าความต้านทานไฟฟ้าปรากฏ (apparent resistivity) เป็นฟังก์ชันของคาบ (period)

WSINV3DMT ซึ่งได้รับการสนับสนุนจาก สกว. ด้วยทุน Apparent Resistivity PDF/37/2543 และ RSA4780021 เป็นโปรแกรมที่อาศัยสมการทาง คณิตศาสตร์และฟิสิกส์เพื่อช่วยให้เห็นว่าโครงสร้างที่สนใจนั้นอยู่ที่ความลึกเท่าไร โดยทำการ แปลงค่าความต้านทานไฟฟ้าปรากฏที่เป็นฟังก์ชันของคาบหรือความถี่ให้เป็นค่าความต้าน

ไฟฟ้าจริงที่เป็นฟังก์ชันของความลึก ทำให้ภาพตัดขวางของโลก ถ้าเราทำ การวัดหลายๆ profile พร้อมๆ กันก็ จะทำให้ได้โครงสร้างของโลกแบบ 3 มิติ ดังรูปที่ 4 สีแดงหมายถึงพื้นที่ที่ นำไฟฟ้าได้ดีกว่าบริเวณที่เป็นสีน้ำ เงิน ซึ่งหมายถึงบริเวณที่เป็นแหล่ง สะสมตัวของแร่ยูเรเนียมใต้พื้นดิน บริเวณนี้



ร**ูปที่ 4** แสดงภาพตัดขวางที่แสดงโครงสร้างของโลกจากหลาย profile ข้อมูลจากบริเวณ McArthur River Mine, northern Saskatchewan (Canada)

ปัจจุบันมีนักวิทยาศาสตร์จากหลายประเทศได้ขอนำโปรแกรม WSINV3DMT ไปใช้ใน การสำรวจโครงสร้างความต้านทานไฟฟ้าโลก ได้แก่ ประเทศสหรัฐอเมริกา นิวซีแลนด์ สเปน ออสเตรเลีย บราซิล รัสเซีย แคนาดา สวีเดน ไอซ์แลนด์ อังกฤษ อินเดีย ยูเครน เยอรมัน จีน สวิสเซอร์แลนด์ เม็กซิโก ญี่ปุ่น อิตาลี ไอร์แลนด์ และในจีเรีย